

## ABSTRACT

Title of Thesis:

MOISTURE CONTENT EFFECTS ON  
ENERGY AND EMISSIONS RELEASED  
DURING COMBUSTION OF PYROPHYTIC  
VEGETATION

Nathaniel Andrew May, Master of Science,  
2017

Thesis Directed By:

Professor Michael J. Gollner  
Department of Fire Protection Engineering

A series of small-scale laboratory fires were conducted to study the influence of species type and moisture content (MC) on the burning of vegetative fuels common in wildland fires. The experimental results seek to understand the effects these have on the release of gaseous emissions, namely carbon dioxide and carbon monoxide, as well as particulate matter (PM<sub>2.5</sub>), and fire radiative energy (FRE). Current wildland fire emissions estimates rely on remote sensing techniques coupled with empirically-based linear relationships to relate FRE to biomass consumed, regardless of fuel type and moisture content. Emission factors (EF) are then applied to the estimated fuel consumption to estimate total emissions of specific combustion byproducts. In this study, we revisit these assumptions under the influence of moisture content for species containing volatile oils (pyrophytic species). Experimental results show that while the relationship between FRE and biomass consumed remains linear for dead, dry fuels,

pyrophytic species examined in this study failed to follow existing relationships when their moisture content was increased.

MOISTURE CONTENT EFFECTS ON ENERGY AND EMISSIONS  
RELEASED DURING COMBUSTION OF PYROPHYTIC VEGETATION

by

Nathaniel Andrew May

Thesis submitted to the Faculty of the Graduate School of the  
University of Maryland, College Park, in partial fulfillment  
of the requirements for the degree of  
Master of Science  
2017

Advisory Committee:  
Professor Michael J. Gollner, Chair  
Professor Evan Ellicott  
Professor Arnaud Trouvé

© Copyright by  
Nathaniel Andrew May  
2017

## Acknowledgements

I am grateful to Professor Michael Gollner for giving me this opportunity to explore a topic that has not been tackled within the Fire Protection Engineering Department before. I would like to thank him for his continued support and advising throughout the entire process. I truly could not have asked for a better advisor. Additionally, I would like to thank Evan Ellicott, whose knowledge in this field made him an invaluable asset and mentor.

Thank you to Professors Andre Marshall for allowing me to utilize his calorimetry setup for testing and Peter Sunderland for the use of the DustTrak. I would also like to thank Professor Arnaud Trouvé for being on my thesis committee. I must also express my extreme gratitude to Dr. James White for training me to use the calorimetry setup and for troubleshooting many issues even after having graduated.

Michael Gallagher from the US Forest Service was always extremely helpful with collecting and sending fuels to burn, as well as taking the time out of his day to show us around the Pine Barrens.

Thank you to Dave Robbins, Dawn Letts, and Sean Weaver from the Maryland DNR, as well as Jenny Willoughby from the City of Frederick for allowing me to pick fuels from park lands. Elyse Sanchez from the University of California, San Diego and Dave Proskow from Dynaletric, were extremely helpful in procuring 60 pounds of eucalyptus leaves.

To my fellow colleagues in the Department of Fire Protection Engineering, whether it was helping to pick through hundreds of pounds of leaves or simply being someone to talk to and get advice from, I could not have done it without you all.

Last but not least, I must thank my parents and my two brothers, my life-long friends I made at College Park and especially to my fiancé Caitlyn, for sitting with me for hours, picking leaves, for supporting me and making me do my work.

## Table of Contents

|   |      |
|---|------|
| Acknowledgements.....   | ii   |
| List of Tables .....  | vi   |
| List of Figures .....   | viii |
| Nomenclature .....  | xii  |
| 1. Introduction.....  | 1    |
| 1.1 The Problem.....  | 1    |
| 1.2 Research Objectives.....  | 5    |
| 2. Literature Review.....   | 8    |
| 2.1 Vegetative Burning .....  | 8    |
| 2.2 Pyrophytic Fuels .....  | 12   |
| 2.3 Emissions.....  | 15   |
| 2.4 Remote Sensing .....  | 26   |
| 3. Experimental Setup.....  | 31   |
| 3.1 Fuel Selection.....   | 31   |
| 3.2 Shipping, Storage, and Drying.....                                      | 36   |
| 3.3 Measurement Setup.....  | 43   |
| 4. Results.....   | 54   |
| 4.1 Overview of Results.....  | 54   |
| 4.2 Northern Bayberry .....   | 57   |
| 4.2.1 Dry Condition .....   | 57   |
| 4.2.2 Wet Condition.....  | 61   |
| 4.2.3 Comparison.....   | 65   |
| 4.3 Mountain Laurel.....  | 67   |
| 4.3.1 Dry Condition .....   | 67   |
| 4.3.2 Wet Condition.....  | 71   |
| 4.3.3 Comparison.....   | 73   |
| 4.4 Eucalyptus.....   | 76   |
| 4.4.1 Dry Condition .....   | 76   |
| 4.4.2 Wet Condition.....  | 79   |
| 4.4.3 Comparison.....   | 81   |
| 4.5 Elevated vs. Flat Configuration .....                                   | 83   |
| 4.6 Longleaf Pine.....  | 87   |
| 4.7 Results Summary .....   | 90   |
| 5. Discussion .....   | 97   |
| 5.1 Introduction.....   | 97   |
| 5.2 Emission Factors.....   | 97   |
| 5.2.1 Comparison of Pine Emissions .....                                    | 97   |
| 5.2.2 Review of Emission Factor Literature Values from Previous Studies ... | 100  |
| 5.2.3 Emission Correlations.....  | 101  |

|   |     |
|---|-----|
| 5.2.4 Emission Conclusions .....          | 105 |
| 5.3 Fire Behavior .....                   | 106 |
| 5.4 Fire Radiative Energy .....           | 106 |
| 5.4.1 Estimating Biomass Consumption..... | 106 |
| 5.4.2 Energy Density.....                 | 109 |
| 5.4.3 Emission Coefficient.....           | 113 |
| 6. Conclusion .....                       | 118 |
| Appendix A.....                           | 121 |
| Bibliography .....                        | 125 |

## List of Tables

|   |     |
|---|-----|
| Table 1: Options for obtaining inputs needed for prescribed fire emission inventories (adapted from [36]).....  | 20  |
| Table 2: List of experiments conducted based on species and drying conditions. Underlined and bold numbers refer to tests that are discussed during the following sections and used as representative tests for the particular series. .  | 56  |
| Table 3: Average emission factors and pertinent fire behavior metrics for the northern bayberry tests with the standard deviation included.....   | 66  |
| Table 4: Average emission factors and pertinent fire behavior metrics for the mountain laurel tests with the standard deviation included.....   | 75  |
| Table 5: Average emission factors and pertinent fire behavior metrics for the eucalyptus tests with the standard deviation included.....  | 82  |
| Table 6: List of experiments conducted based on setup conditions. Underlined and bolded numbers refer to tests that are discussed during the following section and used as representative tests for the particular series.....  | 84  |
| Table 7: Average emission factors and pertinent fire behavior metrics for the eucalyptus tests with the standard deviation included.....  | 85  |
| Table 8: Average emission factors and pertinent fire behavior metrics for the longleaf pine tests with the standard deviation included.....   | 89  |
| Table 9: Averaged emission factors for the six different conditions.....  | 91  |
| Table 10: Table of emission coefficients, EC, for CO, CO <sub>2</sub> , and PM <sub>2.5</sub> . The ECs were calculated and averaged for all six series of tests. Values from literature are included for comparison. ....  | 91  |
| Table 11: Averaged values of total and radiative energy densities (ED), radiative fraction ( $\chi_r$ ), and fuel combustion factor (CF) for the six different conditions   | 92  |
| Table 12: Table of emission factors and MCE, comparing values found in literature and those found during experimentation. Two tests were from prescribed and/or wildfire field measurements of pine forests in the Southeastern United State [7], [32]. One test is a field measurements of burning pine understory [48]. Three tests are laboratory tests, ponderosa pine [19], southern pine litter [39] and big sagebrush [55]. The experimental results are from burning longleaf pine .... | 99  |
| Table 13: Various literature emission factors shown for eucalyptus to be compared with those shown in Table 9.....  | 101 |
| Table 14: Literature values for total and radiative energy densities (ED), radiative fraction ( $\chi_r$ ), and fuel combustion factor (CF) to be compared with those shown in Table 11.....  | 112 |

Table 15: Table of emission coefficients, EC, for CO, CO<sub>2</sub>, and PM<sub>2.5</sub>. The ECs were calculated and averaged for all six series of tests. Values from literature are included for comparison. .... 114

Table A1: CE, EF<sub>CO</sub>, and EF<sub>PM<sub>2.5</sub></sub> values calculated using Equations (10), (11), and (12), based on the experimentally determined MCE ..... 121

Table A2: Emission factor, energy density, and MCE values for all of the tests ..... 122

Table A3: Emission coefficients, spread rates, flame height, and peak HRR values for all of the tests ..... 123

## List of Figures

|   |    |
|---|----|
| Figure 1: Diagram of the spectral radiant flux for varying temperatures. Based on the Planck function, the peak radiant flux for temperatures associated with fire (around 1000 K and denoted by the vertical red line on the plot) is several times greater than the flux associated with background ambient temperatures [53] | 28 |
| Figure 2: Flowering mountain laurel ( <i>kalmia latifolia</i> ), demonstrating the potential for extensive ground cover [58].....   | 32 |
| Figure 3: Mountain laurel collected from the Frederick Municipal Forest. The foliage shown up close (left) and a relatively small shrub (right) in an area recently mechanically thinned .....  | 34 |
| Figure 4: Northern bayberry collected from the Point Lookout State Park. The foliage is shown up close (left) and a medium sized shrub (right) alongside a park road .....  | 35 |
| Figure 5: Eucalyptus grove located on UCSD campus [61].....   | 36 |
| Figure 6: VWR drying oven with door open. Three aluminum trays with holes drilled for enhanced air circulation could be placed in the oven at one time.....   | 39 |
| Figure 7: (top) The moisture content analyzer with the lid open showing the sample tray. (bottom) Northern bayberry being tested for MC level via the halogen heating lamp. Note that the leaves were crushed prior testing .....   | 42 |
| Figure 8: Image of the experimental setup, showing 80/20 stand, balance, ceramic board and elevated platform, GoPro video camera, exhaust hood with 1.5 m hood rolled during setup. The air purge line heading to the radiometer can be partially seen .....  | 45 |
| Figure 9: (Top left) Exhaust hood with containment curtain rolled up. (Bottom left) Pitot tube, thermocouple. H <sub>2</sub> O analyzer, and gas sampling ports. (Right) Gas analysis rack, with CO/CO <sub>2</sub> sensor above and O <sub>2</sub> below.....  | 48 |
| Figure 10: Images of the dual-band thermopile radiometer (left) and the TSI DUSTTRAK 8250 Aerosol Monitor .....   | 49 |
| Figure 11: Schematic of the experimental setup.....   | 53 |
| Figure 12: Image of (left) northern bayberry leaves and twigs and (right) dried leaves in .25 m <sup>2</sup> mold.....  | 57 |
| Figure 13: Plots showing the HRR, MCE, FRP, and PM <sub>2.5</sub> production during NB-D1. Note that the vertical dashed line indicates the burnout time .....  | 58 |
| Figure 14: (left) Glowing embers post-flame extinction (right) ash remnants .....   | 59 |
| Figure 15: Plots of HRR, MCE, FRP, and Soot Production for the four different tests conducted during the Dry Northern Bayberry series. The colored lines correspond to the different tests as follows: Red ~ NB-D1, Blue ~ NB-D2,   |    |

|  |    |
|--|----|
| Yellow ~ NB-D3, Black ~ NB-D4. The dashed vertical lines denote burnout times.....   | 61 |
| Figure 16: Plots showing the HRR, MCE, FRP, and PM <sub>2.5</sub> production during NB-W4. Note that the vertical dashed line indicates the burnout time .....   | 63 |
| Figure 17: Still image from NB-W4 video showing self-extinction after 165 s. Note the large amount of smoke being produced. ....   | 63 |
| Figure 18: Plots of HRR, MCE, FRP, and Soot Production for the four different tests conducted during the Wet Northern Bayberry series. The colored lines correspond to the different tests as follows: Red ~ NB-W1, Blue ~ NB-W2, Yellow ~ NB-W3, Black ~ NB-W4. The dashed vertical lines denote burnout times..... | 64 |
| Figure 19: Time-lapse of both the dry (top) and wet (bottom) northern bayberry tests (NB-D1 and NB-W4), taken every 30 s for 2 minutes   | 65 |
| Figure 20: Comparison of NB-D1 (red), the dry northern bayberry condition, and NB-W4 (blue), the wet condition. HRR, MCE, FRP, and PM <sub>2.5</sub> are reported .....  | 66 |
| Figure 21: Leaves and twigs from undried mountain laurel ( <i>kalmia latifolia</i> ) .....   | 67 |
| Figure 22: Ash remaining after combustion of dry mountain laurel .....   | 68 |
| Figure 23: Plots showing the HRR, MCE, FRP, and PM <sub>2.5</sub> production during ML-D4. Note that the vertical dashed line indicates the burnout time .....   | 69 |
| Figure 24: Plots of HRR, MCE, FRP, and Soot Production for the five different tests conducted during the Dry Mountain Laurel series. The colored lines correspond to the different tests as follows: Red ~ ML-D1, Blue ~ ML-D2, Yellow ~ ML-D3, Black ~ ML-D4, Green ~ ML-D5.....                                    | 70 |
| Figure 25: Plots showing the HRR, MCE, FRP, and PM <sub>2.5</sub> production during ML-W1. Note that the vertical dashed line indicates the burnout time .....   | 71 |
| Figure 26: Plots of HRR, MCE, FRP, and Soot Production for the four different tests conducted during the Wet Mountain Laurel series. The colored lines correspond to the different tests as follows: Red ~ ML-W1, Blue ~ ML-W2, Yellow ~ ML-W3, Black ~ ML-W4.....   | 73 |
| Figure 27: High-speed image sequence of flame jet forming due to contained volatile oils.....  | 74 |
| Figure 28: Time-lapse of both the dry (top) and wet (bottom) mountain laurel tests..... (ML-D4 and ML-W1), taken every 30 s for 2 minutes  | 74 |
| Figure 29: Comparison of ML-D4 (red), the dry mountain laurel condition, and ML-W1 (blue), the wet condition. HRR, MCE, FRP, and PM <sub>2.5</sub> are reported .....  | 75 |
| Figure 30: Images of eucalyptus leaves prior to drying (left) and the fuel after burning, reduced to ash (right) .....   | 76 |
| Figure 31: Plots of HRR, MCE, FRP, and Soot Production for the five different tests conducted during the Dry Eucalyptus series. The colored lines correspond to  |    |

|   |    |
|---|----|
| the different tests as follows: Red ~ EU-D1, Blue ~ EU-D2, Yellow ~ EU-D3, Black ~ EU-D4, Green ~ EU-D5 .....   | 78 |
| Figure 32: Consecutive frames of intermittent burning of fuel behind main fire front during EU-D5.....  | 78 |
| Figure 33: Plots showing the HRR, MCE, FRP, and PM <sub>2.5</sub> production during EU-W1. Note that the vertical dashed line indicates the burnout time .....  | 80 |
| Figure 34: Plots of HRR, MCE, FRP, and Soot Production for the four different tests conducted during the Wet Eucalyptus series. The colored lines correspond to the different tests as follows: Red ~ EU-W1, Blue ~ EU-W2, Yellow ~ EU-W3, Black ~ EU-W4..... | 80 |
| Figure 35: Time-lapse of both the dry (top) and wet (bottom) eucalyptus tests (EU-D3 and EU-W1), taken every 30 s for 2 minutes.....  | 81 |
| Figure 36: Comparison of EU-D3 (red), the dry eucalyptus condition, and EU-W1 (blue), the wet condition. HRR, MCE, FRP, and PM <sub>2.5</sub> are reported .....  | 82 |
| Figure 37: Time-lapse of both the elevated (top) and flat (bottom) experimental setups (ML-D4 and ML-FL4), taken every 30 s for 2 minutes .....   | 84 |
| Figure 38: Comparison of ML-D4 (red), the elevated mountain laurel condition, and ML-FL4 (blue), the flat condition. HRR, MCE, FRP, and PM <sub>2.5</sub> are reported .....  | 85 |
| Figure 39: Dried longleaf pine needles .....  | 87 |
| Figure 40: Plots showing the HRR, MCE, FRP, and PM <sub>2.5</sub> production during LLP-4. Note that the vertical dashed line indicates the burnout time. ....  | 88 |
| Figure 41: Time-lapse of a longleaf pine experiment (LLP-4), taken every 30 s for 2 minutes.....  | 89 |
| Figure 42: Plots of HRR, MCE, FRP, and Soot Production for the four different tests conducted during the Longleaf pine series. The colored lines correspond to the different tests as follows: Red ~ LLP-1, Blue ~ LLP-2, Yellow ~ LLP-3, Black ~ LLP-4. .... | 90 |
| Figure 43: Column charts showing the average spread rate, flame height, and peak HRR for all of the test conditions. ....   | 93 |
| Figure 44: Column charts showing the average CO, CO <sub>2</sub> , and PM <sub>2.5</sub> EF, as well as MCE .....   | 94 |
| Figure 45: Column charts showing the average emission coefficients calculated for CO, CO <sub>2</sub> , and PM <sub>2.5</sub> . The EC's calculated using the FRE, as well as total energy are presented .....  | 95 |
| Figure 46: Column charts showing the average FRE and total energy produced, as well as the total energy and FRE ED.....   | 96 |

Figure 47: Plot of the CO emission factors against the experimentally derived MCE. The solid line represents a linear regression fit to the experimental data ( $EF_{CO} = 1906.5 - 1904.1 \times MCE$ ;  $R^2 = 0.88$ ). The dashed line is Equation (11)... 103

Figure 48: Plot of the  $PM_{2.5}$  emission factors against the experimentally derived MCE. The solid line represents a linear regression fit to the experimental data ( $EF_{PM_{2.5}} = 2924.1 - 3048.2 \times MCE$ ;  $R^2 = 0.80$ ). The dashed line is Equation (12)... 105

Figure 49: Plot of the measured FRE against the amount of dry biomass consumed. Equation (17) is shown as the dotted black line. Equation (18) is the dashed line. A linear regression, shown as Equation (19) below was fit to the data, shown by the solid line, with an  $R^2=0.71$  ..... 108

Figure 50: Plot of the radiative energy versus total energy. The radiative fraction can be ascertained from the slope of the applied linear regression. .... 113

Figure 51: Plot of the total  $CO_2$  produced against the FRE. A linear regression, Equation (23), with an  $R^2=0.88$  was applied to the data..... 116

Figure 52: Plot of the total  $PM_{2.5}$  produced against the FRE. An exponential regression, Equation (23), with an  $R^2=0.74$  was applied to the data..... 117

Figure A1: Plot of the total carbon monoxide production versus the FRE..... 121

# Nomenclature

## Acronyms and Symbols

|                   |  |          |
|-------------------|--|----------|
| ASTER             | Advanced Spaceborne Thermal Emission and Reflection Radiometer |          |
| BC                | Biomass consumed   | [kg]     |
| CE                | combustion efficiency  | % or 0–1 |
| CF                | Fuel combustion coefficient                                    | [kg/MJ]  |
| CO                | carbon monoxide  |          |
| CO <sub>2</sub>   | carbon dioxide   |          |
| CRDS              | cavity ring-down spectroscopy                                  |          |
| E                 | Total emissions produced                                       | [g]      |
| EC                | Emissions coefficient  | [g/MJ]   |
| ED <sub>FRE</sub> | energy density based on FRE                                    | [MJ/kg]  |
| ED <sub>HRR</sub> | energy density based on total energy                           | [MJ/kg]  |
| EPA               | Environmental Protection Agency                                |          |
| EU-D              | Dry eucalyptus tests   |          |
| EU-W              | Wet eucalyptus tests   |          |
| DWD               | Downed woody debris  |          |
| FRE               | fire radiative energy  | [MJ]     |
| FRP               | fire radiative power   | [W]      |
| FTIR              | Fourier transform infrared spectroscopy                        |          |
| HRR               | Heat release rate  | kW       |
| IR                | infrared   |          |
| LFL               | Lower flammability limit                                       | %        |
| LiDAR             | Light detection and ranging                                    |          |
| LLP               | Longleaf pine tests  |          |
| M <sub>D</sub>    | Dry mass   | [kg]     |
| M <sub>F</sub>    | Estimated final mass   | [kg]     |
| M <sub>W</sub>    | Wet mass   | [kg]     |
| MATLAB            | Matrix Lab, computer software                                  |          |

|                   |   |          |
|-------------------|---|----------|
| MC                | moisture content                                | % or 0–1 |
| MCE               | modified combustion efficiency                  | % or 0–1 |
| MC <sub>F</sub>   | desired final moisture content                  | % or 0–1 |
| ML-D              | Dry mountain laurel tests                       |          |
| ML-FL             | Flat mountain laurel tests                      |          |
| ML-W              | Wet mountain laurel tests                       |          |
| MODIS             | Moderate Resolution Imaging Spectroradiometer   |          |
| NB-D              | Dry northern bayberry tests                     |          |
| NB-W              | Wet northern bayberry tests                     |          |
| O <sub>2</sub>    | oxygen  |          |
| PAS               | photoacoustic spectroscopy                      |          |
| PM <sub>2.5</sub> | particulate matter less than 2.5 μm in diameter |          |
| Q                 | Total energy                                    | MJ       |
| RH                | Relative humidity                               |          |
| TEOM              | tapered element oscillating microbalance        |          |
| UCSD              | University of California, San Diego             |          |
| W <sub>C</sub>    | Water content                                   | 0–1      |
| χ <sub>r</sub>    | Radiative fraction                              |          |

# 1. Introduction

## 1.1 The Problem

Prior to the colonization of the Americas, the indigenous populations living in forested areas, as well as the grassy plains, had learned to live with wildland fires and harness them for their advantage. Early colonizers took note of the flourishing and abounding forests, where forest floors were free of the ground cover that is often observed in modern forests which makes navigation and travel difficult. The natives learned that by regularly burning the forests to remove leaf litter, deadfall, and small trees, they could more easily travel, gather plant foods, and hunt game [1]. As industrialization expanded, the economic impact of fire on the timber industry became a great concern and the idea of prescribed fires as a means of land management quickly fell out of favor. In fact, by the late 1800s and early 1900s, policies were put in place that required the immediate extinguishment of wildland fires [2]. The resulting stockpile of ground fuels increased over the ensuing decades, leading to forests being dangerously full of dry fuel, waiting for the right conditions to burn. Congruently, a growing body of research is showing that in certain ecosystems, fires are not only preferable, but necessary in order to maintain a healthy and balanced environment [2]. The lack of recurring fires resulted in unhealthy forests and shrublands waiting to burn. In recent decades the total number of wildland fires has decreased, however the total acreage of land burned as increased, largely due to more fires that demonstrate extreme fire behavior, defined as fire behavior characteristics that ordinarily precludes

methods of direct control action [3],[4]. A high rate of spread, prolific crowning and/or spotting, presence of fire whirls and a strong convection column are some characteristics of such fires. Predictability is difficult because these fires often exercise some degree of influence on their environment and behave erratically, sometimes dangerously [4]. This erratic nature makes predicting fire spread and smoke production quite difficult.

The increased prevalence of large wildfires exhibiting extreme fire behavior has necessitated the increased use of prescribed fires to reduce dangerous stockpiles of fuel. However, there are still hazards associated with prescribed fires. If not planned and orchestrated properly, a prescribed fire can quickly transition into an uncontrollable wildfire. Additionally, concerns over air pollution, particularly from prescribed burns, has created a sense of urgency within the wildland fire community to enhance predictive capabilities in regards to fire.

One of the largest contributions to advancing fire detection has been in the form of remote sensing. Remote sensing is simply a term used to describe observations and measurements made from a removed or “remote” location. This can be accomplished in the form of overhead planes and drones, or increasingly, space-based orbiting satellites. The applications for remote sensing in the wildfire community are abundant. Data provided from satellite-based sensors such as LANDSAT can inform ecologists of the vegetative makeup and health of given areas [5]. This allows researchers to not only know what type of fuels may comprise a given location, but if there is a dangerous amount of dead fuel and overgrowth. Remote sensing is great for pre and post-fire analysis regarding forest regrowth, burn severity, etc. However, one

of its greatest uses is with detecting and tracking ongoing incidents. MODIS is a satellite-based sensor that has the capabilities to detect certain infrared wavelengths synonymous with fire. This is extremely useful for detecting fires in remote areas and/or in incipient stages. These abilities also allow interested parties to determine the size of a fire, how much vegetation, or biomass, has burned, and increasing, how much emissions have been produced [6].

The use of remote sensing to estimate the amount of biomass burned during an incident, as well as the amount of emissions released into the atmosphere is of extreme importance. Air quality regulators have become increasingly vested in quantifying and reducing pollution due to health and environmental concerns. As mentioned above, remote sensing techniques for sensing fire typically operate by measuring increased infrared radiation within a specific band of wavelengths specific to fire. Correlations have also been drawn between the amount of radiation emitted and the amount of biomass burned. This predicted amount of consumed biomass can also be used to estimate the amount of specific species produced during combustion. This has vast applications to health and environmental safety.

On a global scale, biomass combustion is the largest source of fine carbonaceous particulate and second largest source of trace gases [7]. When released into the atmosphere, pollutants like carbon monoxide (CO) and carbon dioxide (CO<sub>2</sub>), as well as the particulate matter (PM), are capable of absorbing and/or scattering incoming light radiation, as well as outgoing. Many of the emitted species, due to photo-chemical processes, can breakdown and form secondary pollutants like ozone

(O<sub>3</sub>). This contributes to surface warming and climate change, which among other things, has an impact on wildfire prevalence [8].

Acute impacts from wildland fires on surrounding areas are also of concern [9]. Various pollutants contribute to the formation of haze, reducing visibility. Other than the environmental effects, certain effluents have alarming health implications. Particulate matter has long been known to have adverse health effects. A well-known condition related to fine particulate matter, black lung, is a pulmonary disease caused by chronic exposure to coal dust. Similarly, carbonaceous particulate matter produced during the combustion of organic fuels can have significant health concerns. Specifically, fine PM, those 2.5 μm or less, have been linked to several serious conditions. The particles effectively penetrate the deepest and smallest regions of the lungs, the alveoli, where air exchange with red blood cells occurs. Not only can these particles block alveoli, but they can cause DNA mutations that lead to cancer. The presence of PM<sub>2.5</sub> has also been shown to increase chances of developing cardiovascular diseases, increasing infant mortality, and exacerbating pulmonary conditions like asthma and emphysema [10].

The issue with the correlations currently used to calculate emissions from wildland fires results from the assumption that the biomass consumed is linearly related to the fire radiative energy (FRE) produced, regardless of fuel type and fuel moisture. There is also an assumption that the proportion of energy emitted via convection vs. radiation is constant [5]. There are two issues with these assumptions. One is that all species are not created equally. Certain species, like eucalyptus and those that make up chaparral, contain oils and resins that make them highly combustible. These are

termed pyrophytic plants. The concern is that these plant species may have a higher energy content than those without oils, making the correlations currently in use oversimplistic [11]. Similarly, the moisture content may have an effect on both the FRE, as well as the emissions. Studies have shown that higher moisture levels likely result in decreased CO<sub>2</sub> production and increases in CO and PM<sub>2.5</sub>. The total fire radiative power (FRP), analogous to the fire intensity, has also been observed as decreasing with higher MC levels [12]. These changes are all most likely due to an increase in smoldering and incomplete combustion brought on by the presence of water.

## 1.2 Research Objectives

The main goal of this research is to address the question of fuel type and moisture content and their effects on the emissions and energy output during combustion. A bulk of the scientific work currently available addresses only one aspect of this interrelated process at a time. Studies have shown the impact that moisture content has on the burning of live fuels [13]. These studies showed that higher moisture content levels significantly impact the time to ignition and required ignition temperatures for various fuels. Building on this, the influence of moisture on combustion product emissions has been investigated. These studies suggest that moisture has the effect of increasing the production of carbon monoxide, carbonaceous particulate, unburned hydrocarbons, as well as a decrease in carbon dioxide production and combustion efficiency [12]. Similarly, another study sought to examine the relationship between fuel moisture and the radiant emissions and the impact this could

have on established relationships between radiant emissions and biomass consumed [14]. The study showed that moisture content is an essential component in measuring fire radiative energy. However, no research has been done to combine these two, the question of moisture content on both combustion product emissions and emitted radiative energy.

There is also a lack of understanding of pyrophytic fuels and the influence they pose on emissions and radiative energy. Pyrophytes are plants that are particularly adapted to thrive in fire-prone ecosystems. There are both fire-promoting pyrophytic plant species and fire-adapted pyrophytes. Fire-adapted plants, like pitch pine (*Pinus rigida*), can have thick bark that protect the underlying flesh from being destroyed during a fire. They may also have epicormic shoots, buds that lay beneath the bark, that sprout after experiencing elevated temperatures. Even if the majority of the plant is killed off, these shoots allow for regrowth [1]. Some plants even display fire-induced serotiny, where seeds will only be released after experiencing elevated temperatures. These pyrophytes are adapted to live with a frequent fire regime, but do not directly promote fire [15]. However, plants like eucalyptus, mountain laurel, and some of those found in chaparral contain oils that are highly combustible. This is an adaptation that promotes fires to occur frequently, in the process removing competing plant species [16]. Species like mountain laurel, even though they will experience top-kill during a fire, can quickly resprout and outcompete less adapted species [17]. The pyrophytes of interest are the latter. Due the presence of volatile oils, they may have a higher energy content than non-pyrophytic fuels, like most deciduous species. This

higher energy content, like heat of combustion, could mean that pyrophytic fuel species may release higher levels of radiant energy per mass.

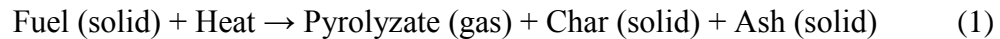
This research seeks to answer these questions regarding the influence moisture and volatile oils from pyrophytic species has on emitted FRE and produced PM<sub>2.5</sub>, CO, and CO<sub>2</sub>. Tests will be conducted on three pyrophytic species, mountain laurel (*Kalmia latifolia*), northern bayberry (*Myrica pensylvanica*), and sugar gum (*Eucalyptus cladocalyx*). Emission factors, EF, measured in the mass of effluent produced over the mass of dry consumed fuel, will be tabulated and compared against existing available data. Trends will also be drawn between the measured FRE and consumed mass to determine the viability of existing empirical correlations.

## 2. Literature Review

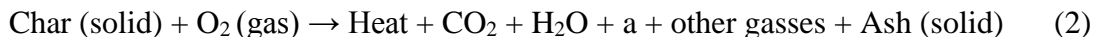
### 2.1 Vegetative Burning

Combustion is a chemical process involving a fuel and oxidizer resulting in a rapid release of energy, generally in the form of heat and light, as well as the production of various chemical byproducts. Solid fuel combustion involves a myriad of intermediate and elementary chemical reactions which govern the rate of release of volatile products that eventually burn in the gas phase (flaming combustion) or oxidize within the solid phase (smoldering combustion). While both processes typically occur with a myriad of intermediate steps and reactions, these two processes can be described simply by the following equations [18]:

#### Pyrolysis



#### Heterogeneous Oxidation (Smoldering)



#### Gas-phase Oxidation (Flaming)



For all combustion reactions within an oxygen-sufficient environment, an initial heat source must be applied to the fuel in order to stimulate oxidation or the release of flammable vapors to a critical concentration which initiates a sustained combustion

process. Whether it be a cigarette discarded out of a window, stray ember from a burning campfire, driptorches used by wildland firefighters and foresters, or lightening, heat sources are readily available within the wildland environment. Similarly, fuel is vastly abundant, particularly in those areas where stockpiling of unburned fuels have occurred. However, the mode of combustion, whether flaming or smoldering, is dependent on many factors.

While flaming combustion is the most visible and destructive mode of combustion in wildfires, with crown-fire flame heights reaching 100 meters above the tree line, the much slower and flameless mode of smoldering combustion can significantly contribute to atmospheric pollution. In many wildland fires, fuels can continue to smolder for days or weeks after the flame front has passed, producing large amounts of combustion products, as well as potentially reigniting unburned fuels. Smoldering travels on the order of 1mm/min, at least 10 orders of magnitude smaller than rates seen in flaming combustion. In wildland fires, after the passage of the flame front, smoldering is typically attributed to the burning of large (>7 cm) fuels like downed limbs, logs, and tree trunks. Duff is also a source, consisting of partially decomposed organic material that covers the ground floor encompassing of leaves, needles, and other decomposing vegetative materials.

Smoldering is a surface level oxidation reaction, where oxygen is drawn in through the porous fuel and supplied to the smoldering front [18]. During smoldering, pyrolysis still occurs, as shown in Eqn. (1), however, due to the low temperatures and emitted heat flux, much of the pyrolyzate goes unconsumed. This leads to comparatively larger amounts of unburned hydrocarbons, particulate matter, carbon

monoxide, and other toxic compounds that are produced in far less quantity during flaming combustion [19]. Although smoldering combustion is typically less of a concern when burning smaller fuels (<0.6 cm), such as those used in these experiments, the higher water content of some fuels may lead to an increased proportion of smoldering versus flaming. In fact, it has been stated that “moisture content is the single most important property governing the ignition and spread of smoldering wildfires” [18]. The presence of water in the fuels used during these experiments could drain enough energy from a propagating flame to cause local extinction. If this were to occur, a transition from flaming to smoldering combustion would be likely.

Combustion efficiency is the measure of completeness of fuel combustion. Under stoichiometric burning conditions, all of the carbon present within the fuel prior to burning is converted to carbon dioxide during oxidation. However, this does not occur outside of theory due to impurities in the fuel, such as the presence of water and other inorganic compounds, and inefficient mixing of air with vaporized fuel. For this reason, a ratio for combustion efficiency (CE)

$$CE = \frac{\Delta CO_2}{\Delta CO_2 + \Delta CO + \Delta CH_4 + \Delta C_{other}} \quad (4)$$

was developed to measure how far from ideal fuel is being consumed, where 1 is stoichiometric. However, this method necessitates measuring all of the carbon-containing compounds remaining and produced during combustion. This is difficult to achieve without costly gas analysis. Due to the difficulty in calculating CE, the modified combustion efficiency, based on the principle that a majority of the carbon-

containing compounds produced will consist of carbon dioxide and carbon monoxide when burning cellulosic fuels, is instead utilized [20],

$$\text{MCE} = \frac{\Delta\text{CO}_2}{\Delta\text{CO}_2 + \Delta\text{CO}} \quad (5)$$

This equation is more suitable for establishing combustion efficiency in a wide array of applications as measuring CO and CO<sub>2</sub> production is far easier and less costly.

It has been found that a transition from flaming to smoldering combustion can be determined by measuring the real-time MCE, where values below 0.9 typically signal that the less-efficient smoldering combustion is occurring [21]. This is of extreme value and may help explain results that are obtained during this research.

Intuitively, wet fuels don't burn well. For example, wet wood is incredibly difficult to ignite and if the fire does in fact start, the result is often a small and smoky fire. This is due to water's high specific heat and is one of the reasons it is the most common fire suppression agent. Water contained within a solid fuel like wood or leafy foliage acts as a heat sink, drawing heat away from vaporizing fuel. Because the vaporization temperature of water is less than that of cellulose, the substance within vegetation that is actively burning, it is often assumed all of the water must be evaporated prior to pyrolysis. This results in less energy being imparted into pyrolyzing and combusting the available fuel. The emitted water vapor can also dilute gaseous fuel mixtures, limiting available oxygen. A reduction in flame height, rate of spread, emitted heat flux, and heat release rate are all attributed to increased fuel water content [22].

Water also causes a change in the species produced during combustion and explains the lower combustion efficiency. Because of the reduction in heat feedback to the pyrolyzed fuel, unburned fuel is allowed to escape the combustion zone. As the fuel breaks down, it decomposes into other species like carbon monoxide. This is why wet fuel is marked by a higher production of CO, a product of incomplete combustion.

## 2.2 Pyrophytic Fuels

The amount of literature available on pyrophytic fuels is very limited. Specific species of pyrophytic fuels, especially in fire-prone areas like Southern California, have been tabulated. However, these lists often simply discuss the relative fire-hazard associated with the species and are meant largely as literature for landscaping and designing defensible spaces around homes and communities [23]. However, eucalyptus (sugar gum or *Eucalyptus cladocalyx*), is one of the best examples of fire-promoting pyrophytes and has been studied a fair amount. It will be discussed in more detail. For the purposes of this research, sugar gum, the species used during testing, will colloquially be referred to simply as eucalyptus. The other fuels that are used in this research, mountain laurel (*kalmia latifolia*) and northern bayberry (*myrica pensylvanica*) are known to be combustible, but very little literature is available on them. Unfortunately, chemical analysis was not performed on these plant species in order to determine the type and concentration of volatile oils they contain. However, the relative degree of oil content amongst the three species was determined based on plant characteristics and the limited literature available. Eucalyptus was determined to

be “highly flammable” based on evidence presented in the following paragraphs. Mountain laurel was also determined to be “highly flammable”, based on observations made wildland fires where areas with dense mountain laurel understories exhibited high intensity fires [24]. Northern bayberry is the only fuel to be said to have a “low flammability”, but this is based on catalogues of plant species for purposes of selecting plants that should or should not be placed near homes due to their propensity to ignite during wildfires [25], [23].

As discussed in Section 1.1, pyrophytic species, or pyrophytes, are plant species that have adapted to survive with regular fire frequency. Plants can either be fire resistant or fire promoting. Fire resistant species have adapted to survive through frequently occurring wildland fires. The giant sequoia, *Sequoiadendron giganteum*, can have bark up to nearly 1 m thick. The pine cones only drop from the tree and release seeds once they have been dried. This generally only occurs through fire [26]. Other species may not be resistant to fire at all, but have developed to quickly resprout after a fire, taking advantage of cleared understory to grow without competition for space and light [27]. Other species, those that promote fire, have compounds within them that make fires more prevalent and intense. From this point forward, when using the term pyrophytic fuels, this is referring to these *fire promoting pyrophytes*.

Essential or volatile oils are aromatic compounds contained within plants. Some of these compounds, like those found in pyrophytes, can be highly flammable. Eucalyptus oil is an extract that has long been used for a multitude of purposes. The oil has medicinal uses in relieving symptoms of influenza, as a

decongestant, as a mouth rinse for killing odor-causing bacteria, as an anti-inflammatory and topical pain reliever, and as a means to clean wounds due to its antibacterial properties. Eucalyptus oil can also be used as an insect repellent and pesticide, used as a fragrance in perfumes, soaps and sprays, as well as a flavoring in foods [28]. But most telling of its flammability, eucalyptus oil can be used as an additive in motor vehicle fuels, or even as a fuel on its own [29].

Eucalyptus oil, as with most essential oils, is largely constituted of various terpenoids and terpenes, which are hydrocarbons. These terpenes are what make volatile oil containing plants combustible. Some species of eucalyptus have been found to contain 22% or more of these energy-rich compounds by dry volume. [30] studied the effects of terpene containing plants on overall flammability of leaf litter and found that the fuels with higher levels of terpenes experienced greater flame heights and shorter total combustion times, leading the researchers to suggest that terpene levels do in fact have an impact on the overall intensity of burning fuels containing essential oils.

As previously stated, very few studies have focused on the combustion of volatile oil-containing wildland fuels, let alone research on the emissions and emitted radiation associated with these fuels. For the most part, research has been relegated to observations on the impact of pyrophytic species on the surrounding species within the ecosystems and is largely based on observations made during active wildland fires or areas where fires have occurred in the recent past. The fact that little research exists in this area justifies the need for further research on pyrophytic plant species.

## 2.3 Emissions

When wildland fires occur, the main focus of the public typically turns to the amount of area burned and the number of homes or buildings destroyed. Rarely is the topic of air pollution discussed. However, rising concerns over air quality and global climate change make studying the contribution of wildland fires to pollution an important area of research. Biomass burning, defined as the open burning of biomass due to wildfires and prescribed burns, as well as agricultural burning, attributes to an estimated 40% of carbon monoxide and 35% of carbonaceous particulate annually emitted into the atmosphere on a global scale. In the western United States, wildland fires, both prescribed and wildfires, account for 20% and CO emissions and 39% of  $PM_{2.5}$  annually [9]. Generally speaking, wildland fires are third in overall  $PM_{2.5}$  production, only behind utility fuel burning and residential wood burning[19]. If current trends persist, the amount of land burned due to wildfires will only continue to increase, releasing more emissions into the atmosphere. Regional pollution is of equal concern, as areas surrounding active burn sites can experience gaseous and aerosol air pollution several times larger than these global values, having significant health and economic impacts. Not only does exposure to the fine PM increase the likelihood of developing certain cardio-pulmonary diseases, but the decreased visibility associated with smoke plumes can shutdown traffic roads and ground air transportation, severing critical economic arteries [31].

Due to the impact wildland fires have on air quality, the need to estimate produced emissions has increased both for prescribed and uncontrolled burns. The

most common method for doing so is through the use of emission factors (EF). Measured in mass of emitted species over the dry mass of fuel consumed, emission factors provide a useful estimation of the total emissions of a particular species based on a known quantity of burned mass. The EF can also be calculated by the carbon mass-balance method [32],

$$EF_i = F_c \times \frac{MW_i}{12} \times \frac{C_i}{C_T} \text{ [g/kg]}, \quad (6)$$

where  $F_c$  is the carbon mass fraction of the fuel,  $MW_i$  is the molecular mass of the species in question, and  $\frac{C_i}{C_T}$  the number of moles of the emitted species divided by the total moles of carbon emitted,

$$\frac{C_i}{C_T} = \frac{\frac{\Delta C_i}{\Delta CO_2}}{\sum_{j=1}^n \left( NC_j \times \frac{\Delta C_j}{\Delta CO_2} \right)}. \quad (7)$$

In equation (7),  $\frac{\Delta C_i}{\Delta CO_2}$  is the fire-average ratio of compound  $i$  to  $CO_2$  and  $NC_i$  is the number of carbon atoms in compound  $j$ . The issue with this method is that the  $F_c$  for the fuel is empirically determined, and simply not enough plant species have been tested to make this a viable option for this research. For this reason, a simplified equation based on the definition of emission factor,

$$EF_i = \frac{M_i}{M_{fuel,dry}} \text{ [g/kg]} \quad (8)$$

with  $M_i$  is the mass of the desired pollutant species (g) and  $M_{fuel,dry}$  is the mass of the dried biomass consumed (kg), is instead used

As will be discussed in Section 2.4., remote sensing techniques are enabling researchers to estimate the biomass consumed, as well as various combustion products produced, via remote observations. By measuring the emitted radiation from a fire, the amount of combustion product emissions can be estimated by proxy of the estimated consumed mass. Instead of relying on this estimated biomass consumption, some have suggested directly relating the produced emissions to the emitted fire radiative energy (FRE). This value, coined the emission coefficient, EC,

$$EC_i = \frac{M_i}{FRE} \text{ [g/MJ]} \quad (9)$$

relates the total mass (g) of the combustion product in question to the fire radiative energy, FRE (MJ) [33], [34]. As will be discussed in Section 2.4, fire radiative energy is a time-integrated measure of the total energy emitted via radiation during a wildland fire. These measurements are gathered using remote sensing techniques, measured instantaneously as the fire radiative power, FRP (W). Emission coefficient values for carbonaceous particulates ranging from 2.7 g/MJ to 14.4 g/MJ, depending on the region and ecosystem (savanna, tropical, boreal) [34]. An energy-to-mass conversion factor of 0.41 kg/MJ is also provided as a means to convert between EC and EF for PM estimates.

The Clean Air Act, first implemented in 1970, was designed to regulate air pollution at a national level within the United States. In 1997, amendments were made to the act that began regulating PM<sub>2.5</sub>, a pollutant found to be a major contributor to atmospheric haze and of growing health concern [35]. Since then, amendments have been made calling for further reduction of PM<sub>2.5</sub> emissions. As part of these new

regulatory standards, PM<sub>2.5</sub> released during prescribed burning began to be of concern if regions were to meet federal attainment requirements. As a result, researchers from the Environmental Protection Agency, EPA, developed empirical correlations that could be used to estimate emission factors for not just PM<sub>2.5</sub>, but many other combustion products of note [36]. The governing principle behind these correlations stems from combustion efficiency. Because many of these pollutants, like CO and PM<sub>2.5</sub> are carbon-based and produced during incomplete combustion, emissions can be correlated to the combustion efficiency. Combustion efficiency is often difficult to derive. A correlation was developed,

$$CE = \frac{MCE - 0.15}{0.86} \quad (10)$$

to relate the easier to calculate modified combustion efficiency to the CE [37],[36].

Equation (10) can thus be used to calculate emission purely based on CE, as is such with the following two correlations.

$$EF_{CO} = 961 - 984 \times CE \text{ [g/kg]} \quad (11)$$

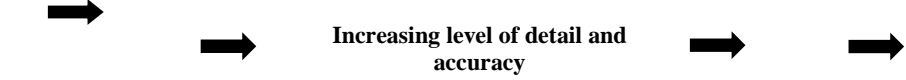
$$EF_{PM_{2.5}} = 67.4 - 66.8 \times CE \text{ [g/kg]} \quad (12)$$

The correlations shown in in equations (10), (11), and (12) were developed based on data collected from laboratory experiments, as well as field measurements from both prescribed and uncontrolled fires [36].

The EPA also created a methodology that land managers could use to create emission inventories for both wildfires and prescribed burns. Table 1 highlights the complexity in understanding the parameters related to emissions from wildland fires,

both wild and prescribed [36]. The far right column describes the actions that would lead to the most accurate emission inventories. However, to obtain this level of detail is unrealistic in many scenarios. Even if those parameters were to be fully evaluated, the associated errors are still appreciable.

Table 1: Options for obtaining inputs needed for prescribed fire emission inventories (adapted from [36])

| Parameter                                 | <div style="text-align: center;">  <p><b>Increasing level of detail and accuracy</b></p> </div> |   |   |  |   |   |
|---|---|---|---|--|---|---|
|   | <b>Area burned</b>  | Previous inventory estimates                            | State incident databases  | State incident databases with auditing and quality assurance | Survey land managers for different ownership categories | Satellite data with auditing and quality assurance      |
| <b>Vegetative cover</b>                   | Regional defaults   | Estimates from existing inventories                     | -----   | Satellite data   | Survey land managers                                    | Ground-truthing with land surveys, aerial surveys, etc. |
| <b>Fuel loading and characteristics</b>   | General estimates   | Land manager determination of NFDRS fuel classes        | Land manager determination of fuel type, with emission model defaults | Fuel characteristics classification system                   | Photo-series correlation                                | Transect measurements                                   |
| <b>Fuel consumption</b>                   | Regional defaults   | -----   | Vegetation-specific defaults  | Fuel consumption Models with default inputs                  | -----   | Models with input from land managers                    |
| <b>Emission factors</b>                   | General defaults  | Regional defaults                                       | Separate factors for flaming and smoldering                           | Emission models or correlation with CO or CE                 | Emission models with input from land managers           | Vegetation-specific emission data                       |
| <b>Impact of mitigation measures</b>      | Default emission factors for activity fuels   | Account for activity fuels in fuel consumption modeling | -----   | Account for impacts of fuel moisture                         | -----   | Situation-specific emission                             |
| <b>Temporal distribution of emissions</b> | Default seasonal and/or hourly profiles   | Allocation using actual seasonal fire                   | -----   | Fire-specific emission calculations                          | -----   | Fire-specific hourly modeling                           |

The methods for determining the emission factors largely depends on the equipment and environment in which sampling is performed. FTIR (Fourier transform infrared spectroscopy) allows for a detailed analysis of the many various species that constitute the smoke produced during combustion. FTIR operates by emitting a wide-spectrum light source through a sample and measuring the levels of infrared absorption. By performing a Fourier transform, the resulting data can be used to generate a spectrum, where individual species can be identified. FTIR has the ability to identify thousands of compounds produced during combustion [38], [39]. However, FTIR is a tool for analyzing the composition of the effluents, not the quantity. Secondly, CO, CO<sub>2</sub>, and CH<sub>4</sub> account for up to 99% of carbon mass produced, making the remaining thousands of compounds fairly irrelevant. Lastly, FTIR is an expensive and sensitive apparatus to operate outside of a laboratory setting, making it impractical for most.

A method similar to FTIR, photoacoustic spectroscopy (PAS) irradiates a sample with a light beam of a specific wavelength. Certain molecules within the sample chamber will absorb the light, causing them to vibrate, increasing the heat energy. This subsequently causes an increase in temperature and pressure, creating acoustic waves within the chamber which can be detected with a microphone. The resulting waves are can be transformed, creating a spectrum identifying species [40], [41].

Infrared absorption techniques, like those used in for this research CO and CO<sub>2</sub> measurements, seem to be a preferred method for obtaining gaseous species measurements, both in laboratory and field testing. The operating principle, similar to

FTIR, is that an infrared light beam of a specific wavelength is passed through a column of sample gas. Like a fingerprint, elements and compounds absorb infrared light at a specific wavelength. If a compound, for instance CO, is present in the sample and the emitted infrared beam is set to only produce a beam at the wavelength absorbed by CO molecules, then the detector will recognize the attenuation of the beam being received. The amount of attenuation corresponds to the concentration of the detected species in the sample [42], [19]. This method is valuable because it provides not only species recognition, but concentration as well. These devices can also be manufactured to be small and relatively portable, allowing for real-time field measurements.

Another species and concentration determining technique is cavity ring-down spectroscopy (CRDS). The underlying principle is that a precision light beam is allowed to enter a cavity containing several highly reflective mirrors. When the beam is turned off, the beam continues to bounce off the mirrors, decaying over time. When a gaseous sample enters this chamber, the molecules absorb and scatter the light beam, increasing the rate of decay. The time the beam takes to “ring-down” to  $1/e$  of the original light intensity correlates to a specific concentration [43], [44]. As discussed previously, the chosen beam wavelength used can be selected for specific species. This method is extremely precise, however, due to the need for precision mirrors, can be expensive and is typically not used outside of laboratory settings, although plane-mounted devices have been used.

The technique utilized in this research to measure oxygen ( $O_2$ ) involves the use of a paramagnetic analyzer. This device leverages oxygen’s high susceptibility to magnetic fields to make measurements. Within the sample chamber, two glass spheres

are balanced in a nonhomogeneous magnetic field, connected by a piece of metal. When the sample gases are flowed through the chambers, the oxygen is pulled towards the stronger magnetic field. This exerts a torsional force on the spheres, causing them to rotate. This rotation is detected by a change in light intensity reflected off the balancing spheres. The change in intensity is correlated to concentration of O<sub>2</sub> [42].

There exists several techniques for measuring carbonaceous PM emissions from wildland fuels. The simplest method involves flowing the combustion products through a Teflon filter. Multiple filters can be used in series to measure particulate of various sizes. The filters can then be weighed, providing a time-integrated value for particulate production. This crude method provides reliable data, especially when utilized in the field. This method also allows for precision analysis of the chemical makeup, through processes like thermal optical carbon analysis [41], [45]. However, gravimetric methods do not allow for instantaneous measurements.

As already discussed, FTIR could be used to determine the presence of particulate matter and its chemical composition, but does not provide concentrations. The tapered element oscillating microbalance (TEOM) is a method that has been used by several researchers to obtain real-time particulate concentrations. Effluents are continuously sampled via sampling ports that allow for specific particulate sizes to be measured. The sample passes through a tapered chamber that oscillates at a known frequency. As particles attach to this chamber, the rate of oscillation changes. The magnitude and rate of oscillation change can be correlated to concentration [41], [46].

Lastly, the technique used for particulate measurements used in this research are based on light-scattering photometry. This method involves emitting a beam of light into a detection chamber. The amount and angles at which of the light is scattered is used to determine the size and quantity of particles. This method requires the device to be calibrated to the expected particles being sampled since different compounds will scatter light to varying degrees. It also cannot differentiate the composition of the particulate matter [44].

Several issues have arisen with how emission factors have been and are currently being indexed. Due to differences in chemical makeup, geometry, and moisture, emission factors are highly variable and species dependent. Developing an index of all species involved in wildland fires would be a daunting and unrealistic endeavor. Variabilities both within the same species as well as seasonally would make this task more difficult. To avoid this issue, some researchers have simply developed emission factors for specific fuel inventories like grassland and forest understory, or even entire ecosystems like Southern California. This method removes the need to know the exact composition of plant species in a given area, but introduces a large degree of variability. Some have even suggested that environmental conditions like wind and topography may play just as important of a role in EF as the fuel type itself [47], [48].

Wildland fires are extremely difficult to gather useful data from. The safety concerns alone make placing personnel and equipment in close proximity difficult. The path of fires can unexpectedly deviate, making sensor placement a guessing game. Sensors can be utilized from safe distances, sometimes on the order of

kilometers, but issues of dilution and wind direction become apparent. Because of this, laboratory-scaled experiments often seek to replicate naturally occurring phenomena. However, the process of removing variables to ensure repeatability and enable trends to be drawn often leads to findings that deviate from nature. This is no different in determining emission factors. In wildland fires, both prescribed and naturally occurring, excluded laboratory variables likely add a significant amount of error to the tabulated EFs. Inhomogeneity in fuel types, moisture, and packing densities, as well as changes in fire behavior (weather, topography, etc.) can all affect emission outputs. This also translates to the issue of simultaneous smoldering and flaming combustion that occurs in nature. Generally, laboratory-scaled experiments operate in one or the other of these two combustion regimes. The inability to account for how much emissions are contributed to a type of combustion further compounds this problem.

Another complication is that emission factors that have been measured from prescribed fires may have significant deviations from wildfires. It has been postulated that the nature and amount of air pollutant emissions is directly related to the intensity and direction of a wildfire [49]. Oftentimes, fire intensity experienced during prescribed fires is less than wildfires. This is likely due to the fact that prescribed fires are often performed outside of wildfire season when fuels have higher moisture contents. Due to concerns over loss of containment, prescribed burns also don't typically occur in areas with heavy fuel loading. As previously discussed, this could impact the ratio of smoldering and flaming combustion.

## 2.4 Remote Sensing

Prior to the 1950s, monitoring active wildland fires was only possible via ground-based observations near the fire line or from fire towers. With the use of airplanes greatly expanding after WWII, monitoring and firefighting was able to expand into an aerial arena. This greatly enhanced the fire service's capabilities to track active fires, allowing for proactive measures to be taken. However, these techniques still required direct human involvement in order to make observations and measurements. It was not until the advent of space-borne imaging that remote sensing truly began to change how wildland fires could be monitored, and studied.

Despite advancements in airplane technology, remote sensing, the ability to make observations and obtain measurements off-site, was severely lacking. This was abundantly clear during the night. Nighttime flying is generally not allowed due to the increased chances of crashing. However, fires can travel miles and unpredictably change directions during the night without much warning. It was not until the advent of spaceborne imaging that remote sensing truly began to change how wildland fires could be predicted, monitored, and studied.

Within the wildland fire community, there are many different applications for remote sensing. Creating fuel inventories for a given ecosystem allows land managers to know the vegetative makeup of the land and potential fuel loading. One of the most detailed methods involves taking field observations utilizing the Brown's Planar Intercept Method. This technique looks to estimate the amount of duff, litter, downed woody debris (DWD), and herbaceous fuels by taking several onsite

measurements. The individual performing this method inventories the amount and type of fuels encountered along three ~18 m, 2 m tall intercepts, 90° apart. If repeated at an additional two or more locations, this method has been found to provide a statistically accurate inventory of the fuel expected to be found in a particular ecosystem [50]. Although very informative and often the most detailed type of fuel investigation, this method is time and labor intensive. Instead, LiDAR (Light Detection and Ranging) methods using aerial platforms can provide fairly resolved data on the fuel volume over large areas of forest.

LiDAR is an active form of remote sensing because the sensor emits its own source of light. The emitted beam travels to the surface and a topographical map of sort is created based on the time of flight. Although this technique does not provide insight on specific species, smaller amounts of ground sampling would be needed that could then be extrapolated to fit the LiDAR data to provide a more comprehensive fuel inventory [51]. This data allows land managers to know what areas may be prone to large fires, as well as assist in the planning of prescribed burns. In a similar fashion, LiDAR can be used to analyze natural recovery in post-fire regions. This can also be accomplished using satellite-based radiometers. A passive form of remote sensing, the radiometers measures incoming solar electromagnetic radiation that is reflected of the surface of a previously burned area. Charred remains do not reflect as much radiation as a green area, indicating the level of recovery.

Fire radiative power, FRP (W), is the measure of emitted radiation from an actively burning wildland fire. The underlying principle relies on the Planck function, where, at 1000 to 2000 K (temperatures expected during an active fire), the amount of

infrared radiation emitted in the mid-infrared band ( $\sim 3.9 \mu\text{m}$ ) is several times the background radiation [5], [51], [52]. This is demonstrated in Figure 1, where the peak radiant flux for 1000 K is several times larger than spectral radiant flux emitted for temperatures associated with ambient conditions, around 300 K.

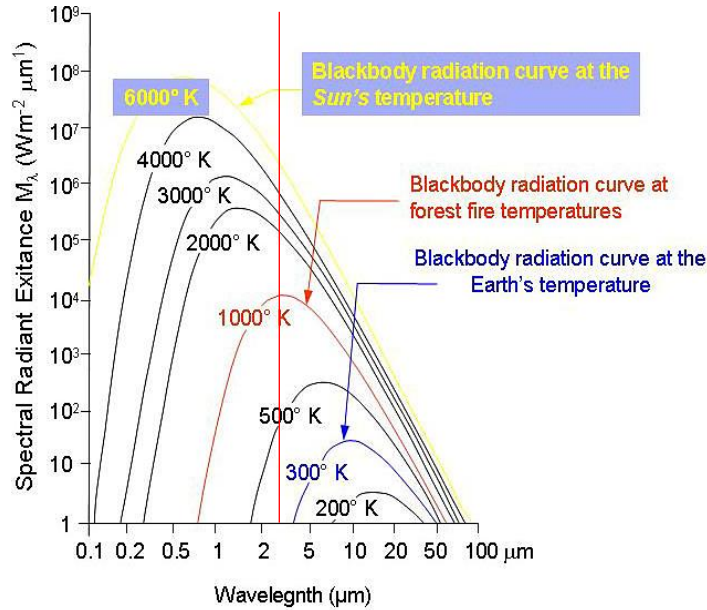


Figure 1: Diagram of the spectral radiant flux for varying temperatures. Based on the Planck function, the peak radiant flux for temperatures associated with fire (around 1000 K and denoted by the vertical red line on the plot) is several times greater than the flux associated with background ambient temperatures [53]

One such sensor capable of making these measurements is MODIS, Moderate Resolution Imaging Spectroradiometer. MODIS is a sensor onboard the Terra and Aqua satellites that orbit the poles in opposite directions. This allows the two sensors to image nearly the entire Earth four times daily [5]. MODIS provides some of the highest temporal resolution while being able to observe the entire Earth. Coupled with temporal resolution is spatial resolution. These sensors work by imaging slices of a given width of the Earth’s surface as the satellite orbits. The narrower the width of the scanned slice, generally the greater the spatial resolution, sometimes as little as 0.001

km<sup>2</sup>. However, there are associated temporal costs. The Advanced Spaceborne Thermal Emission and Reflection Radiometer, ASTER, has a spatial resolution of 0.015 - 0.09 km<sup>2</sup>, but a temporal resolution of 16 days [5]. This type of sensor package is great for post-fire investigations, but is of little use during active fires. Geostationary satellites, satellites that maintain an orbit directly above a given ground-based location, may be tasked with monitoring fires and can provide data on a more real-time like basis. However, being able to task satellites for this purpose can be extremely costly and is not always available depending of the location of the fire in relation to the satellite. The issue of temporal and spatial resolution is of much concern when considering wildland fire applications. Significant changes can occur in wildland fires within a matter of hours. Aerial platforms have been utilized for acquiring radiation data. The benefit is that the spatial and temporal resolution is vastly improved. However, the planes and helicopters used cannot fly at all times of the day, can be costly to operate, and may not be geographically available at all times for tasking [54].

The data provided by sensors like MODIS typically take the form of measured FRP. By integrating the FRP over the duration of a fire, the fire radiative energy (FRE), the total energy released radiatively, can be determined [55]. This value is important as it describes the size and intensity of the fire. Laboratory, as well as field experiments, have shown that there is a linear relationship between the amount of energy released and biomass consumed. This value alone is important, as it describes not only the burning process, can provides insight of post-fire recovery. Secondly, and directly applicable to this research, is that the amount of biomass consumed has been

linearly related to the amount of various gases and particulate matter produced. As previously discussed, this has extreme value in determining the environmental impact of wildland fires, both prescribed and wild. However, these methods rely on the assumption that the amount of radiant energy produced is proportional to the consumption of biomass of fuel. It is also assumed that the proportions of energy emitted as conductive, convective, and radiative are constant, the measure of the radiative energy released from burning biomass is indicative of the quantity of biomass combusted [5].

## 3. Experimental Setup

### 3.1 Fuel Selection

As discussed in Sections 1.2 and 2.2, pyrophytic plant species were chosen to study here due to the fire-promoting nature of the plants and the lack of research on the involvement of volatile oils on the energy and emissions output of these burning fuels. The three specific species tested, mountain laurel (*Kalmia latifolia*), northern bayberry (*Myrica pensylvanica*), and sugar gum (*Eucalyptus cladocalyx*) were chosen for several reasons described below, however, the general motivation for selecting these species is due their prevalence in fire-prone areas.

Mountain laurel and northern bayberry can both be found in the New Jersey Pine Barrens. Part of the Atlantic coastal pine barrens, the Pine Barrens is an ecoregion consisting largely of pitch pine, with shortleaf pine and loblolly pine present in varying amounts. Various species of oak can also be found in different parts of the region. The understory typically consists of mountain laurel, sheep laurel, black huckleberry, northern bayberry, to name a few [15].

The New Jersey Pine Barrens is known to experience frequent wildland fires, where prescribed burns may occur as often as every 5-8 years with a historic wildfire cycle of 15-40 years [56], [57]. This region has adapted to this short fire cycle. Pitch pine has epicormic shoots that allows the plant to resprout through the bark when damaged by fire. The cones are also serotinous, meaning the seeds are only released from the cone when heat is applied.

In areas with a high density of mountain laurel (86% ground cover), high-intensity fires with flame heights over 30 m have been observed [24]. This high density ground coverage is apparent in Figure 2. The extremely high flame heights is thought to due to the flammable oils found in the foliage and the abundance of 1-hour (<0.6 cm) fuels that make up the shrubs. This propensity to burn helps the species to grow and spread. While fire top-kills the plant (burning of the aboveground portion of the plant), rhizomes up to .75 m beneath the soil are able to regrow due to the insulating nature of the soil. This allows the species to quickly recover after a fire while competing vegetation is limited [15], [24].



Figure 2: Flowering mountain laurel (*kalmia latifolia*), demonstrating the potential for extensive ground cover [58]

Northern bayberry is less abundant in the Pine Barrens, but still constitutes roughly 5% of the ground cover. Its impact on fire spread and intensity is not widely understood, as well as the effects fire has on plant mortality. However, the foliage does

contain some amounts of flammable oils that may contribute to fire spread and thus are of interest to this study.

Eucalyptus is a genus of trees known to promote wildland fires and contain volatile oils. Some species of eucalyptus trees have even been known to explode due the heating and ignition of the combustible oils within the tree. Eucalyptus trees are found naturally throughout Australia, often times a propagator of bushfires frequently experienced in certain regions of the continent. Eucalyptus can also be found in the dry arid regions of the western United States, namely Southern California. Here, blue gum (*Eucalyptus globulus*) and sugar gum (*eucalyptus Eladocalyx*) eucalyptus are common species. In the Oakland Hills Firestorm, an estimated 70% of the energy released during the fire was a result of burning eucalyptus [59].

The other reason for the selection of these three plant species was the availability of the fuels. Like many of the pyrophytic species, these three species are largely evergreen, meaning the plants bear foliage year-round. However, depending on the latitude, northern bayberry and mountain laurel is prone to complete leaf drop during winter months. It was for this reason that fuels collected for experimentation were not from the New Jersey Pine Barrens. Instead, mountain laurel was collected from Frederick Municipal Forest, part of the Catoctin Mountain range in Frederick, Maryland. Here, the forests largely consist of deciduous trees like oak, hickory, and tulip poplar. The understory consists of mountain laurel, spicebush, lowbush blueberry, and more [60]. More importantly, at this latitude, mountain laurel is evergreen. The mountain laurel collected in the Frederick Municipal Forest is shown in Figure 3



Figure 3: Mountain laurel collected from the Frederick Municipal Forest. The foliage shown up close (left) and a relatively small shrub (right) in an area recently mechanically thinned

Similarly, northern bayberry was collected from Point Lookout State Park in Southern Maryland due to its year-round availability. Fortunately, the ecology of Southern Maryland more closely resembles that of the Pine Barrens, with sandy soil and tree cover constituted by various species of pine and oak. The species, shown in Figure 4, is similar in size and footprint as mountain laurel, but is typically less abundant.



Figure 4: Northern bayberry collected from the Point Lookout State Park. The foliage is shown up close (left) and a medium sized shrub (right) alongside a park road

Although the samples tested were not from the New Jersey Pine Barrens, it was assumed and shown through initial testing that the difference in emissions and energy outputs from the different regions was not appreciable.

The species of eucalyptus used for testing, *Eucalyptus cladocalyx*, came from the campus of the University of California, San Diego in La Jolla, California. San Diego, with its abundance of fire-promoting chaparral and eucalyptus, was an ideal location to gather fuel samples. Figure 5 shows some eucalyptus present on the campus.



Figure 5: Eucalyptus grove located on UCSD campus [61]

### 3.2 Shipping, Storage, and Drying

All fuels were picked with leaves still attached to branches to help preserve fuel moisture. They were subsequently packaged in plastic bags and cooled with cold packs during transportation. However, due to the large size of the eucalyptus shipment (30 kg), the packaging was not cooled while in transit. The mountain laurel and northern bayberry fuels were collected locally. Samples were clipped from shrubs that appeared healthy, devoid of spotting, insect damage, or obvious death. In order to protect the existing shrubs and to maximize collection storage, samples were collected as individual twigs typically containing 5-10 leaves.

Upon receiving shipments, the leaves were quickly removed from the branches and twigs and placed in sealed bags. The general rule was to remove any woody remnants of the branches, leaving only the fleshy blade and petiole (stem). These are the portions of the plants that contain the largest amount of the volatile oils that are of interest. These are also what would be classified as 1-hour fuels (<0.6cm in diameter), meaning they are the first portion of the plant to dried to the point where pyrolysis can effectively take place be consumed during a fire. After removing the leaves, the samples were placed in plastic bags and weighed. They were then placed in a refrigerator to stop chemical changes to the samples, i.e. decomposition, and to prevent moisture loss until the samples could be dried and burned.

Two different drying regiments were implemented in order to achieve the two desired moisture content conditions. The moisture content is defined in this work as

$$MC = \frac{(M_W - M_D)}{M_W} \quad (13)$$

where MC is the moisture content of the fresh, undried sample,  $M_W$  is the wet mass of the fuel (mass prior to drying) and  $M_D$  is the dry mass for a sample that was dried completely. This parameter is used by [14], but is called water content ( $W_C$ ) in his work. Other variations are also possible, such as dividing the change in mass by  $M_D$  rather than  $M_W$ , often termed the fuel moisture content (FMC), however in this work it was more straightforward to use a parameter that varied from 0 to 1. This means that if a fuel were to have a 0.25 MC, 25% of the fuel mass would result from the water held within. Note that the MC measured using this method only provides the moisture content of the undried samples. The MC of the dried sample prior to burning was found

using a moisture content analyzer that performs the same calculation as above, but with a much smaller sample size and higher heating temperature. A description of the apparatus used will be provided below.

Two different MC conditions were sought for the different plant species. This was achieved by placing the fuels in a VWR Forced Air Oven for varying times depending on the desired MC condition. The oven has a temperature sensitivity of  $\pm 1^{\circ}\text{C}$  and temperature uniformity of  $\pm 1.4^{\circ}\text{C}$ . Samples were placed in aluminum trays and placed on one of the three racks within the oven, as depicted in Figure 6. The trays had holes drilled into them to improve penetration of warm air throughout the samples. In total, the maximum drying capacity for the oven ranged from 1.8 to 2.5 kg of undried fuel depending on the fuel species.



Figure 6: VWR drying oven with door open. Three aluminum trays with holes drilled for enhanced air circulation could be placed in the oven at one time

One drying condition represented fuel samples devoid of moisture, a MC of 0.01 – 0.02. For this paper, this condition will be defined as the “dry” condition. This was accomplished by drying the samples at 70°C for 72 hours. Previous studies, as well as earlier preliminary tests, showed that after 24 hours of drying at this temperature, the mass of the samples remains fairly constant. 72 hours was chosen to ensure the fuel mass had stabilized prior to burning. However, it was not possible to remove all of the moisture from the samples. As was confirmed by the moisture analyzer, the leaves typically retain 1-2% of water even after 72 hours of drying [62]. The drying temperature was selected because it efficiently dries the foliage without causing thermal degradation of the fuels. The mass of the samples was

recorded before and after drying. The leaves were immediately burned after drying as to not allow ambient moisture from the air to be absorbed.

The second drying condition involved drying the samples to a final MC level of 0.1-0.15. This condition will be referred to as the “wet” condition. In order to achieve this condition, a predicted target mass needed to be found for the samples that would correspond to the desired final MC. The following equation was developed,

$$M_F = M_W - (M_W \times MC) + MC_F \text{ [g]} \quad (14)$$

where  $M_F$  is the predicted sample mass and  $MC_F$  is the desired final moisture-content level. This equation required a test sample of the fuel to be dried to completeness so that an original MC for the undried fuel could be determined [12]. This MC is what is used in equation (14). For the experiments, the dry condition tests were always done first in the series so that the MC could be determined. With the MC found, the target mass,  $M_F$ , could also be determined. Because the fuels were stored in sealed bags while in refrigeration, it was assumed that the MC did not change.

Some studies achieved the desired MC levels by drying the fuels completely, then allowing the samples to reabsorb ambient water vapor until the MC was reached [14]. Although this method is simple and reliable, there is a worry that, for example, a rehydrated sample with an ultimate MC of 0.2 may not have the same amount of volatile compounds as a sample that was dried directly from a fresh sample to a MC of 0.20. This is because, despite the low temperatures used, some compounds may be drawn out during heating. Additionally, by drying the samples using this method, it

more accurately replicates how lived fuels in the wildland would be dried and subsequently burned during a fire.

Having determined the target mass, fuels were placed into the metal trays and placed in the oven, still set to 70°C. However, smaller amounts of fuel placed in a thin layer was necessary to ensure even heating of the leaves. The maximum drying capacity was only 0.4 kg for this drying condition. Samples were weighed prior to entering the oven. Every 30-45 minutes, the fuels were stirred to ensure even heating and weighed. Once the samples reached the target weight they were removed from the oven and immediately placed in several layers of sealable plastic bags. This was required so that the fuels would not continue to dry or gain moisture from the air, depending on the relative humidity. Samples were also tested using the moisture analyzer to confirm the moisture content. Other studies have dried the samples at lower temperatures, typically 40°C for 24 hours, in order to achieve higher MC levels [30]. However, this proved to dry the fuels below 0.1 MC due to limited amount of fuel dried at a given time.

An A&D MF-50 Moisture Analyzer was utilized throughout testing to confirm the final MC of the dried samples. The analyzer consists of a 51 g capacity, 0.002 g resolution balance and a halogen heating lamp. 5 g samples are placed on an aluminum tray, raised to a constant 105°C, and heated until the mass loss rate drops below 0.1% per minute. The leaves being sampled were cut and/or crushed into small pieces to make certain that pieces were evenly distributed on the tray and were not too close to the heating bulb. The analyzer manufacturer states a moisture reading accuracy of

0.05%. Figure 7 depicts how the fuel samples were tested for moisture content using the A&D analyzer.

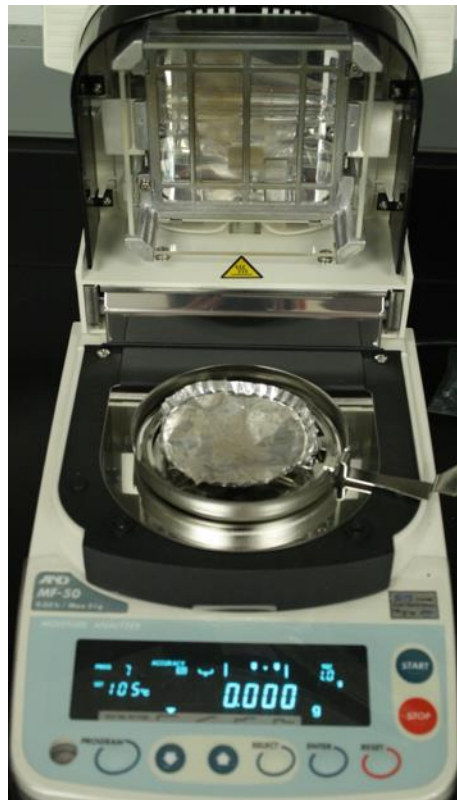


Figure 7: (top) The moisture content analyzer with the lid open showing the sample tray. (bottom) Northern bayberry being tested for MC level via the halogen heating lamp. Note that the leaves were crushed prior testing

Because of differences in packing, heating, initial moisture, and air circulation within the oven, the fuels, especially in the cases of the higher MC levels, experienced a degree of inhomogeneity. Due to this, leaves were thoroughly mixed inside the containment bags and multiple samples were tested with the moisture analyzer and averaged. For the driest samples, the actual MC likely only varied within  $\pm 0.5\%$ . However, with the higher MC levels, this could have varied  $\pm 2.5\%$ .

### 3.3 Measurement Setup

Tests conducted at the University of Maryland's Department of Fire Protection Engineering Fire Laboratory were performed in a manner that would as realistically as possible replicate burning conditions observed during prescribed fires, while remaining easy to conduct and highly repeatable.

All burns were conducted underneath a 2 m by 2 m wide exhaust hood with an average ambient volumetric flow rate of  $0.78 \text{ m}^3/\text{s}$ . The hood is capable of handling a 200 kW fire, but with the temperature limitations of the added instrumentation, this drops to 100 kW. The hood hangs 2.2 m above the floor. Fiberglass curtains 1.5m tall hung from the hood. These were installed to ensure total collection of all effluents produced during combustion.

A movable structure made of 80/20 aluminum t-slot beams was constructed to raise the top of the fuel bed 1 m below the exhaust hood. A Mettler Toledo MS32001L balance was placed on top of the structure and used to provide mass data. The balance output data at 1 Hz, with a 0.1 g resolution. The data was collected using Mettler Toledo's BalanceLink software. A layer of OSB plywood was placed on top of the

balance to provide a stable platform for the insulation board used. Two layers of ceramic fiberboard were then placed on top of the OSB board, to reduce conductive and radiative losses below the burning fuel, as well as to protect the balance. The fiberboard was cut to roughly 0.6 m by 0.6 m, large enough to retain the fuel without leaves falling off, but small enough to limit upward draft effects caused by the entrained air. As is typically required with this particular brand of fiberboard, the insulation was baked using a butane torch prior to conducting experiments. This was done to burn off the binding agent which holds the ceramic together. If not performed prior to testing, the binder would be vaporized, contributing to the overall mass loss, potentially contaminating results.

Initially, experiments were performed directly on top of the fiberboard. This was done to recreate an environment seen in nature, where fuels collect in layers on the ground. However, initial tests proved that at this scale, complete combustion of the fuel samples was difficult, even under very dry conditions. The amount of convective and radiative heat released during burning was often not adequate to allow for sustained flame propagation. To combat this issue, a 1 cm by 1 cm steel-mesh platform was constructed, placed 2.5 cm above the fiberboard. This allowed for enhanced airflow to both the top and bottom of the fuel layer. This perhaps simulates conditions observed in nature, where leaves in the canopy would be exposed to available air in all directions. Figure 8 provides a visualization of the burning platform and the exhaust hood with the attached containment curtain. A steel-mesh containment apparatus has been used in other studies, but has consisted of a mesh basket and cylinder used to contain the fuel [63].

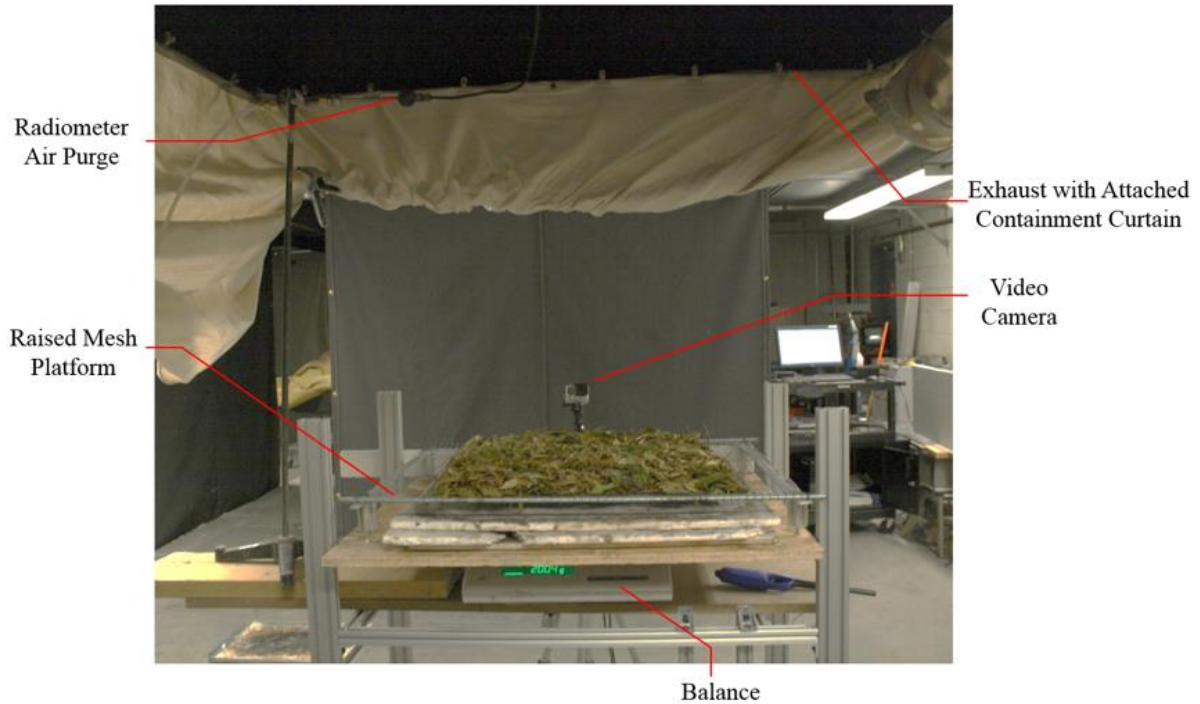


Figure 8: Image of the experimental setup, showing 80/20 stand, balance, ceramic board and elevated platform, GoPro video camera, exhaust hood with 1.5 m hood rolled during setup. The air purge line heading to the radiometer can be partially seen

Utilizing a wooden template, 200 g,  $\pm 1.5$  g, of fuel were placed on top of the mesh platform. The template allowed for the fuel to be formed into a 0.5 m by 0.5 m square layer of leaves. The template also included measurement markings to ensure an even distribution of leaves, as well as provide the fuel depth in order to calculate the bulk density, measured in the mass of fuel over volume of fuel [14]. For the purposes of these experiments, the bulk density is calculated using the “wet” mass. The fuels were evenly poured into the mold and allowed to settle naturally, i.e. without any packing. This was done, as opposed to creating a standard fuel volume across all tests, to minimize fuel breakage and ensure complete combustion. Initial tests found that, especially in the case of northern bayberry, that forcing the fuel bed into a denser layer made it difficult for the flame front to propagate across the entire bed. Secondly, by

allowing gravity to naturally settle the fuels, the bulk density more closely replicates what would be experienced in the wildland.

To mimic realistic burning, the leaf pile was ignited along one edge and allowed to spread laterally as a line fire. This recreates how a wildland fire would spread, as a line with a smoldering region produced behind the head fire. 10 mL of methanol was applied to the edge of the fuel bed prior to ignition as a pilot. For the dry testing condition, this pilot was not necessary as the fuel bed would easily ignite and propagate by simply using a butane lighter to start. However, testing under the wet conditions required a pilot. For consistency across all tests, the methanol pilot was used in all tests. The methanol pilot was tested independently so its influence on emissions and energy release could be determined. It was found that the emissions produced, as well as radiation, was small enough ( $< 3\%$ ) that it could be neglected in the data results.

A GoPro HERO4 Silver was used to track the flame spread and flame height during the experiments. The camera was set to record video at 1080p and 60 fps with a wide field of view. This did lead to warping of the images in the near-field, but was necessary due to the confining nature of the curtain that was hung from the exhaust hood. A meter stick was used to provide a reference measurement so that spread rates and flame heights could be calculated.

Gas sampling techniques were employed as a means to quantify the carbon dioxide, carbon monoxide, and particulate emissions released during the combustion of the different fuel species under different drying conditions. All gas measurements were sampled from within a 3 m long, 0.28 m diameter straight section of round steel exhaust ducting. The sampling ports were roughly 5.2m downstream of the exhaust

entrance from the collection exhaust hood, a distance such that sufficiently full-developed and well-mixed flow can be assumed [64].

A sampling probe consisting of a 4.5 mm stainless-steel tube with 1.5 mm holes spaced 1.27 cm apart along the length ran through the diameter of the exhaust duct. Employing an Air Cadet Dual-head Vacuum pump, the effluents were drawn from both ends of the sampling probe, via 3.2 mm tubing, to the instrumentation rack. A K-type thermocouple also allowed exhaust gases to be sent to the particulate analyzer through 4.7 mm copper tubing via the analyzers onboard pump.

At the same location as the gas sampling ports, a Veris Verabar V100 pitot tube connected to a Setra Model 264 differential pressure transducer was used to ascertain the flow rate of the exhaust with a  $\pm 1\%$  uncertainty.

As part of the calorimetry instrumentation, a Michell Instruments PCMini52 relative humidity sensor is used to measure water content in the exhaust gases, with a  $\pm 1\%$  uncertainty and response time of 10 s. A K-type thermocouple with a response time of 3 s and uncertainty of  $\pm 2$  K was also placed in the duct as part of the required inputs for the calorimetry data processing, both of these devices are referenced in Figure 9 in regards to duct placement.

The gas measurement devices of interest are a Siemens ULTRAMAT 23 infrared CO and CO<sub>2</sub> analyzer and Rosemont Model 755 paramagnetic O<sub>2</sub> analyzer. The analyzers both have a response time of 5 s and uncertainties of  $\pm 100$  ppm for CO<sub>2</sub>  $\pm 1000$  ppm for CO<sub>2</sub>, and  $\pm 1250$  ppm for O<sub>2</sub> [64]. A 2  $\mu$ m particulate filter, two sections of Drierite™ desiccant, and an additional 2  $\mu$ m particulate filter were used to remove particulate and moisture prior to the gas analyzers. Reference gases of

known composition were utilized to calibrate the two sensors. Ambient gases were also measured to secure a baseline reading for the tests and were assumed to remain constant throughout each test. The instrumentation rack is shown in Figure 9 below.



Figure 9: (Top left) Exhaust hood with containment curtain rolled up. (Bottom left) Pitot tube, thermocouple, H<sub>2</sub>O analyzer, and gas sampling ports. (Right) Gas analysis rack, with CO/CO<sub>2</sub> sensor above and O<sub>2</sub> below.

A TSI DUSTTRAK 8520 Aerosol Monitor (Figure 10) was used to quantify the particulate, namely the respirable PM<sub>2.5</sub> (particulate at or below 2.5  $\mu\text{m}$  in diameter). The analyzer uses 90° light scattering measurements to size and count particles. Based on literature, it can be assumed that a majority of this particulate is carbonaceous (soot) [45]. The analyzer had a sampling rate of 1 Hz and uncertainty of  $\pm 0.001 \text{ mg/m}^3$ . Per manufacturer recommendations, the analyzer was kept within 1.2 m of the sampling port to avoid soot deposition along the inner wall of the copper tube.

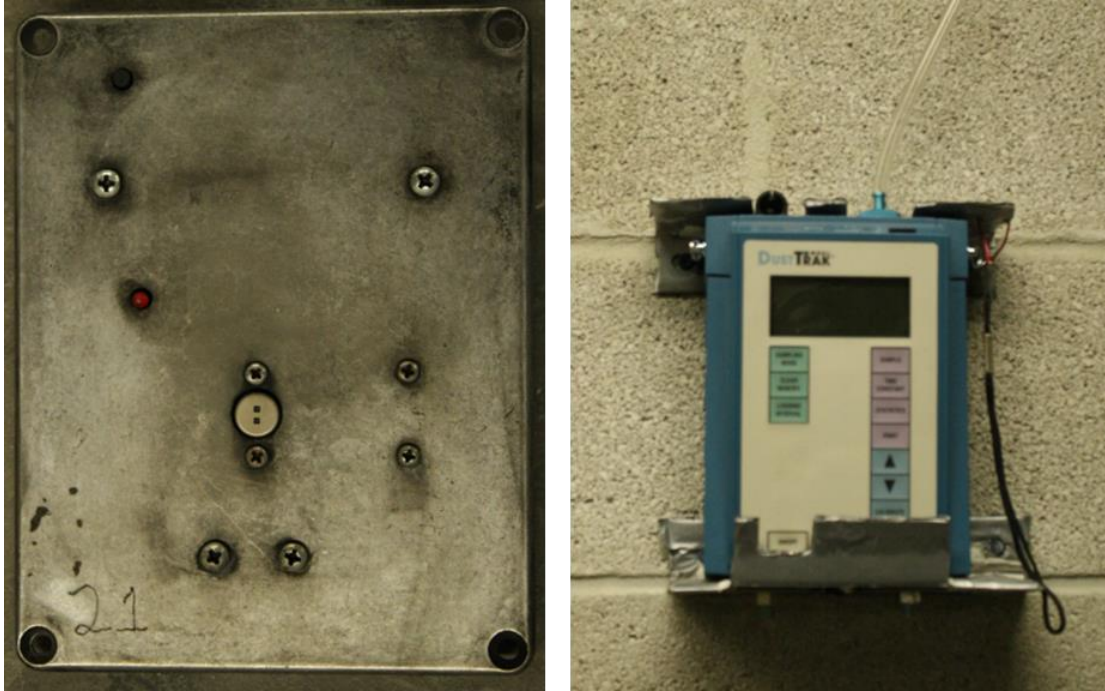


Figure 10: Images of the dual-band thermopile radiometer (left) and the TSI DUSTTRAK 8250 Aerosol Monitor

This particular analyzer was chosen over other measurement techniques largely due to its ease of implementation, as well as its cited use in several other field and laboratory emission investigations. Some of these papers discussed the need for correction factors because measured measurements overestimated  $PM_{2.5}$  values by up to a factor of 2. This was due to the optical measurement technique employed by the device. The analyzer is factory calibrated using an aerosol with particles of known size and refractive index. However, size and refractivity is a material dependent property. Because of this, the device needs to be calibrated to the environment being tested in. This calibration process would typically involve data collection of  $PM_{2.5}$  produced during burning. Simultaneously, particulate would be collected by placing a  $PM_{2.5}$  Teflon-glass filter in the exhaust flow. After a set elapsed time, the filter would be removed and DUSTTRAK stopped. The filter would be weighed and a time-

integrated average of PM<sub>2.5</sub> production calculated. The data from the analyzer would also be averaged over the same time. The percentage in difference between the known mass using the filter and the analyzer would be the correction factor for the analyzer. However, due to the existing laboratory facilities and available equipment, gravimetric measurements utilizing filters was not practical. Instead, correction values used in previous studies were evaluated and a value of 1.6 was chosen for all experiments. The two studies cited used five different correction factors, .91 for grass and 1.9 for forest burns [44], and 1.43, 1.59, and 1.70 for wood smoke [65]

The gas species analyzers were sought not only because they could provide near real time sampling of emitted gaseous emissions, but because CO<sub>2</sub> production calorimetry could be performed, providing insight into the fire intensity, as well as a comparison to the emitted radiation, or FRP (fire radiative power), measured with the overhead radiometer (Figure 10). The calorimetry setup and data processing techniques were developed by White for his research on suppression effects in buoyant turbulent line fires [64]. Traditional species-based calorimetry methods often utilized for small to large-scale testing works well for simple control volume systems, like that seen in these experiments. However, in White's experiments, the introduction of diluted oxidizers and water-mist into the system presented a challenge to these standard methods. To combat this, White developed a comprehensive derivation of previous assumptions and simplifications regarding the physical principles underlying species-based calorimetry. A more in-depth review of the calorimetry methods employed by White are provided in [64]. One assumption not made during White's research is in regards to two fuel properties. Two enthalpy parameters,  $\Delta h_{O_2}$  and  $\Delta h_{CO_2}$ , that were

ascertained by averaging values of many known fuel types. These average values were employed because exact values could not be found for the vegetative fuels. However, this only affects the calorimetry results, not the individual species mass flow measurements, and the effect is seen to be minimal.

One of the motivations behind this research was to compare radiometer and mass loss data collected by Ellicott. Part of his research seeks to determine the influence volatile oils contained in pyrophytic fuels have on the emitted radiation during wildland fires. The radiometers used for both small laboratory burns and large prescribed burns in Ellicott's research were utilized for this research. A dual-band infrared thermopile radiometer, developed by the Rochester Institute of Technology, was placed 1 m above the fuel bed for all tests. The radiometer works by measuring the thermal radiation emitted in the 0.1-7.0  $\mu\text{m}$  and 8.0-14.0  $\mu\text{m}$  infrared bands. Dual-band thermometry employs the principle that for black and grey-body radiation sources, the ratio between two infrared bands allows the kinetic temperature of the source to be estimated via a two-point fit to the Planck function [14], [52], [66]. The benefits of this system is that environmental background noise can be clearly identified and accounted for. The radiometer sampled at a rate of 1 Hz. With a viewing window of  $47^\circ$ , the sensor was more than capable of viewing the entire  $.25 \text{ m}^2$  fuel bed from 1 m above the bed. A continuous stream of dry air via an air compressor was blown across the viewing lens to avoid particulate deposition. The lens was also routinely cleaned to remove any soot that could foul measurements.

Due to the variability associated with burning vegetation, a standardized test length could not be determined for these experiments. In lieu of this, data was collected

until gas and particulate reading returned to ambient levels. For the dry samples, this times typically amounted to 5 minutes. However, tests involving wet samples could last for more than 10 minutes.

A diagram of the complete setup is provided in Figure 11.

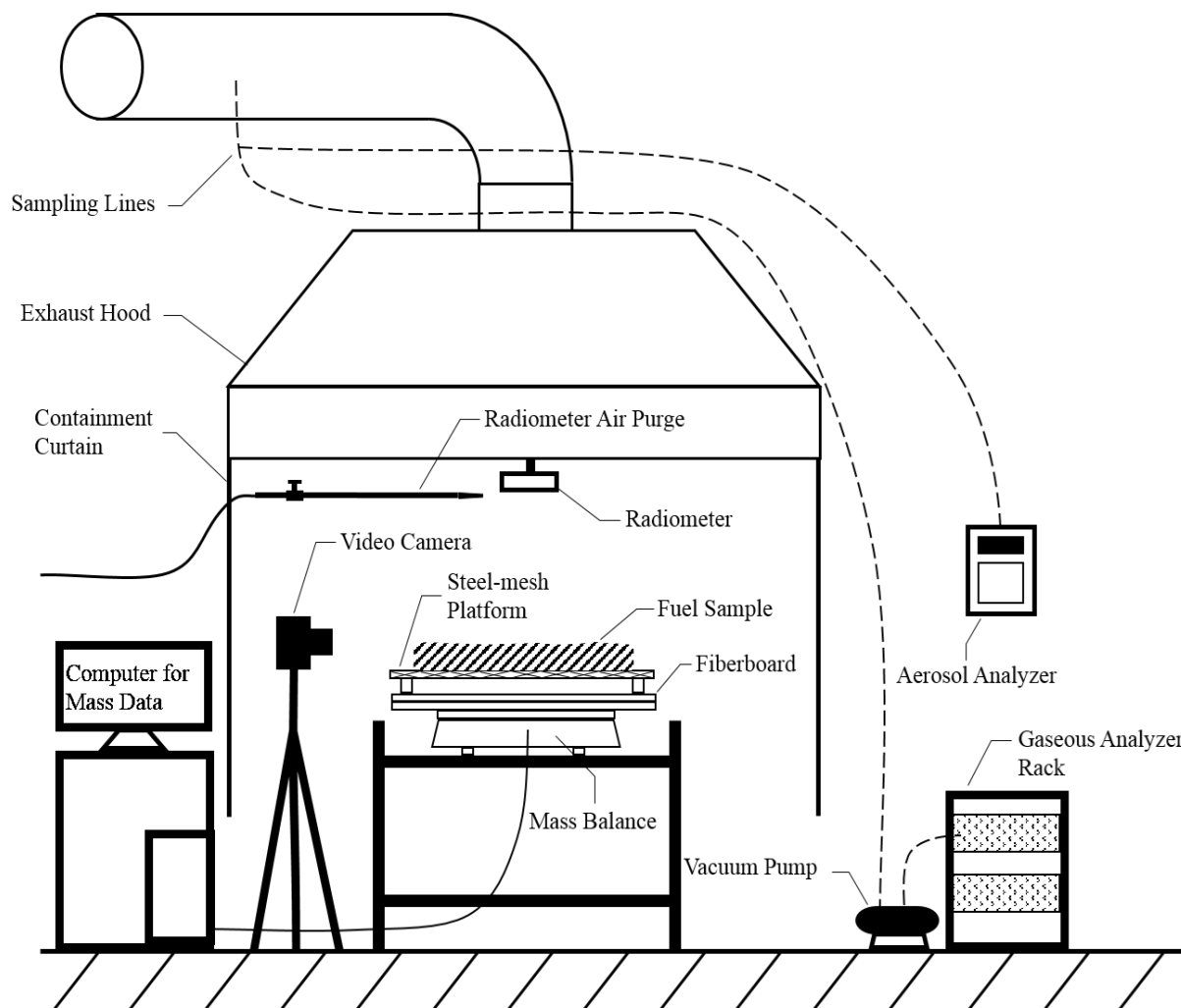


Figure 11: Schematic of the experimental setup

## 4. Results

### 4.1 Overview of Results

The main objective of this research is to quantify the influence of volatile oils and moisture contained within wildland fuels on the emissions and radiant energy output during a spreading fire. Initial expectations were that the experiments on the fuels with lower moisture content would produce lower amounts of carbon monoxide and particulate matter, with greater amounts of carbon dioxide and energy output. Similarly, the fuels with qualitatively higher amounts of volatile oils were expected to have increased energy output.

Based on observations and initial results, it was found that the moisture content plays a key role in not only governing emissions and energy output, but fire behavior in general. As the moisture content increases, smoldering combustion begins to influence behavior. Although the pyrophytic nature of the fuel does seem to influence how great of an impact moisture has on emissions and energy release, its influence on energy release itself is less telling.

As part of the observations for each testing condition, the flame height and spread rate were found in order to evaluate the effects of moisture and volatile oils on burning behavior. A MATLAB program, developed by Overholt, was used to ascertain these two values from video recordings of the burn [67]. The program operates by first measuring a known reference distance, in this case a meter stick. Individual frames are then displayed at a set interval, typically every 5 seconds. The flame is tracked simply

by clicking on the flame tip or flame front in each frame. A minimum of 16 points were collected and averaged during steady burning for the flame height. A similar process was applied to calculate the spread rate, but instead a linear regression was applied to the data points and the slope was used as the spread rate.

The radiometer data was processed using a custom made Excel macro developed by Kremens [52]. The macro converts the raw voltage data into instantaneous FRP. This data was then input into a MATLAB script for further processing. The TSI DUSTTRAK 8520 aerosol analyzer measured particulate in mg of particulate over m<sup>3</sup> of air. Multiplying this value by the volumetric flow rate of the exhaust system provided the mass flow of PM<sub>2.5</sub>. This data could then be input into a MATLAB script for processing as well.

A MATLAB program was created, based on White's original program for heat release rate (HRR), to compile all of the chemical data and calculate emission factors [64]. The original code allowed for the HRR to be found based on several calorimetry methods. Most useful for this research is carbon dioxide production calorimetry due to the increased sensitivity of the sensor compared to others used. Any reference to heat release rates or total energy will stem from this CO<sub>2</sub> production calorimetry method.

The gas analyzers measure molar concentration. With the pressure data provided by the Pitot tube, the mass flow for each species could be determined. By integrating the species mass flow over the duration of the test, with ambient levels subtracted, the total mass for each species could be calculated. Dividing the total masses by the amount of dry biomass consumed provided the emission factors.

For the following seven subsections, plots of experimental data will be shown to help describe burning behavior during the tests. For each species and burning condition, a single test was selected to be representative of all tests conducted during that particular series. The selected test was the one that most closely reflected the averaged value, rather than smoothing tests together into an averaged curve. This more clearly demonstrates the temporal variability observed during experiments. Table 2 provides a breakdown of the testing conditions and associated fuels. One test series is included that utilized longleaf pine (*Pinus palustris*) as a comparative fuel type to those found in the literature. This was done because the three fuels being investigated have not been extensively researched. A fuel was needed that was more representative of previous work.

As a note, the axis ranges for the provided figures change from one test series to another. This is due to the varying burn times and amount of produced effluents.

Table 2: List of experiments conducted based on species and drying conditions. Underlined and bold numbers refer to tests that are discussed during the following sections and used as representative tests for the particular series.

| <b>Name</b> | <b>Test #</b>         | <b>Species</b>    | <b>Drying Condition</b> |
|-------------|-----------------------|-------------------|-------------------------|
| NB-D        | <u>1</u> , 2, 3, 4    | Northern Bayberry | Dry                     |
| NB-W        | 1, 2, 3, <b>4</b>     | Northern Bayberry | Wet                     |
| ML-D        | 1, 2, 3, <b>4</b> , 5 | Mountain Laurel   | Dry                     |
| ML-W        | <u>1</u> , 2, 3, 4    | Mountain Laurel   | Wet                     |
| EU-D        | 1, 2, <b>3</b> , 4, 5 | Eucalyptus        | Dry                     |
| EU-W        | <u>1</u> , 2, 3, 4    | Eucalyptus        | Wet                     |
| LLP         | 1, 2, 3, <b>4</b>     | Longleaf Pine     | Ambient                 |

## 4.2 Northern Bayberry

### 4.2.1 Dry Condition

Northern bayberry (*Myrica pensylvanica*) has long and slender foliage that is typically 3 to 7 cm in length and 2 cm in width (Figure 12) The leaves are slightly aromatic when broken, hinting at the slightly pyrophytic nature of the species. When 200 g of the dried leaves were placed on the burning platform, the fuel bed was an average of 3 cm deep with a bulk density of 26.8 kg/m<sup>3</sup>.



Figure 12: Image of (left) northern bayberry leaves and twigs and (right) dried leaves in .25 m<sup>2</sup> mold

Upon ignition of the methanol pilot, the flaming front propagated easily and steadily across the fuel bed at an average rate of 0.29 cm/s. The flames were at a fairly consistent height of 25.2 cm.

The steadiness of these burns is apparent by observing the heat release rate measurements, as shown in Figure 13 from test NB-D1. The fire reaches steady-state burning 40 s after ignition and remains so for approximately 160 s, at which point the flame front reaches the end of the fuel bed and begins to decay. Each subplot has a

vertical line that denotes the time of flame extinction. A decline in HRR and FRP is seen before this point because new fuel is no longer available to pyrolyze once the flame front reaches the end of the bed. Immediately before complete flame extinction, there was a noticeably sharp increase in smoke production. This is confirmed by the spike in  $PM_{2.2}$  and a sharp decrease in the modified combustion efficiency. The most likely cause of this is the reduction in flame height and thus, reduction in emitted heat flux. With less heating, the remaining fuel is burned more incompletely. A small

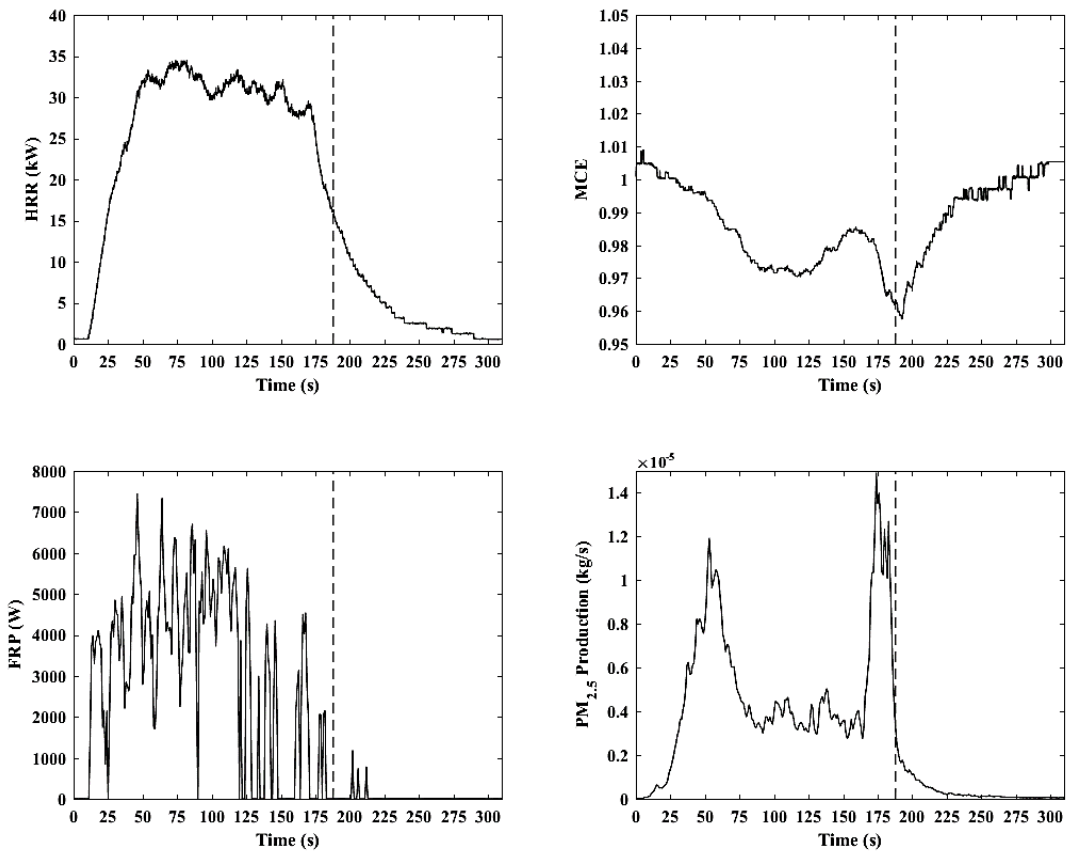


Figure 13: Plots showing the HRR, MCE, FRP, and  $PM_{2.5}$  production during NB-D1. Note that the vertical dashed line indicates the burnout time

amount of FRP is still recorded after burnout. This is mostly likely due to small amounts of glowing embers (Figure 14) that remain after extinction. However, this

quickly dissipates. Figure 14 also shows the ash that remained after the tests. All of the tests burned the fuel completely to ash, no charred remains of the fuel could be found. The final mass averaged to be 9.5 g.

The same plots shown in Figure 13 were plotted in Figure 15, however all four tests conducted during this series are shown. All four tests were run consecutively during the same day. There appears to be a trend that as the tests progressed through the series, the spread rate and intensity noticeably decreased. Initially, one may be inclined to question whether the calibration of the gas analyzers were being to drift from initial values. However, after each test the ambient levels were checked to ensure that this was not the case. Second, this would only explain why peak values were decreasing and not the increased burn time, i.e. a decreased spread rate. This could potentially be explained if the fuel were absorbing moisture from the air, as higher MC levels are expected to decrease spread rates and flame height. However, the moisture



Figure 14: (left) Glowing embers post-flame extinction (right) ash remnants

content levels of the fuels were tested throughout the experiments and found to remain constant. All of the fuel samples came from the same batch of vegetation and were dried at the same time. More densely packed fuels are known to have slower spread rates due to an overall lower surface area to volume ratio. This may have been a factor, as more densely packed piles of leaves could have occurred in the fuel bed, hampering flame spread. However, this too is doubtful. This could explain why a single test would have longer burn time, but why the all of the tests took longer to burn in a sequential order.

Despite inconsistencies in the total burn time, the time averaged emission factors, as shown in Table A2 and Table A3, are very similar. This means that instantaneous measurements can vary substantially, but bulk yields remain consistent.

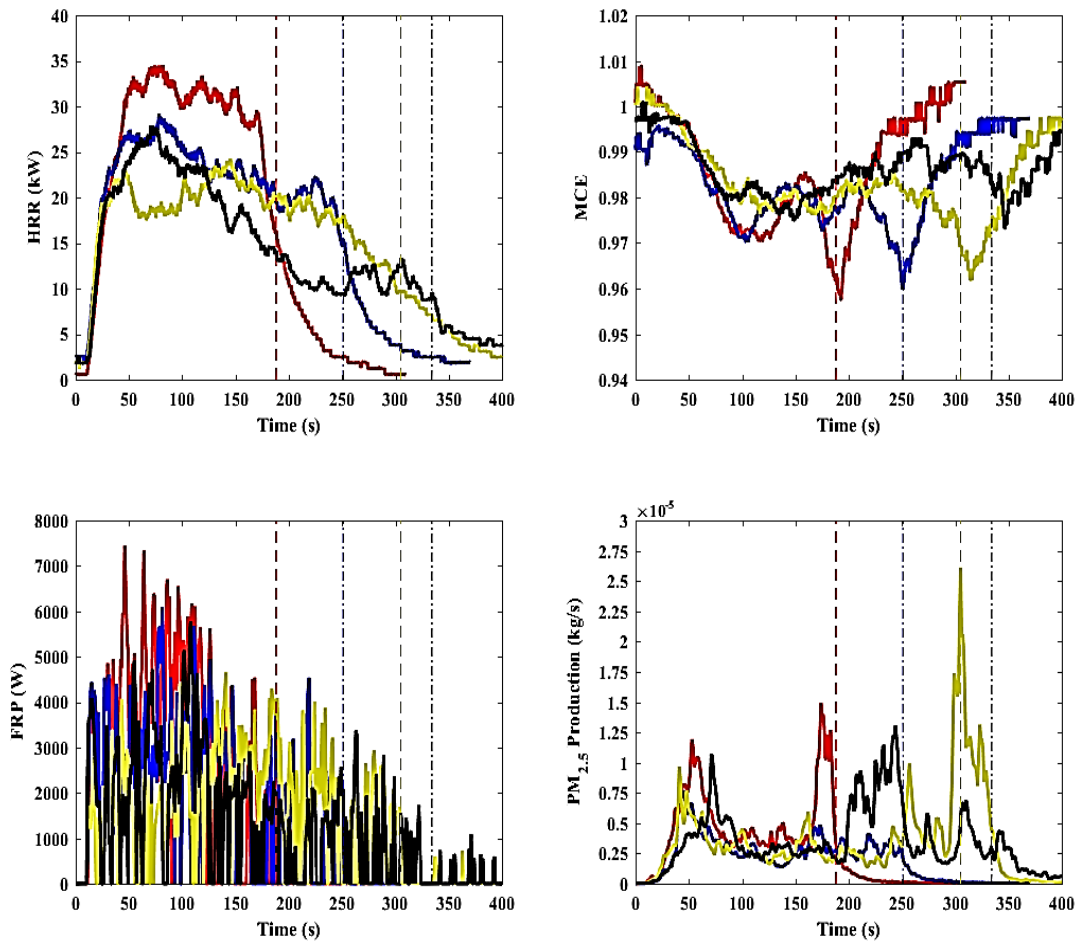


Figure 15: Plots of HRR, MCE, FRP, and Soot Production for the four different tests conducted during the Dry Northern Bayberry series. The colored lines correspond to the different tests as follows: Red ~ NB-D1, Blue ~ NB-D2, Yellow ~ NB-D3, Black ~ NB-D4. The dashed vertical lines denote burnout times

#### 4.2.2 Wet Condition

Like the dry testing condition, the wet condition (MC of 0.135) tests had bulk densities of 26.7 kg/m<sup>3</sup>. However, essentially every metric used to describe the fire behavior during the four wet tests differed from their dry counterparts. The flame spread rate was on average 0.12 cm/s with an average flame height of 16.4 cm. However, these values were more difficult to calculate, as they were far from steady during the

experiments. This also apparent in Figure 16, where the HRR reaches an initial peak, drops to almost zero and then rises again until burnout is reached. The video of the test, NB-W4, with a still frame shown in Figure 17, shows that at the time of the lowest HRR, auto extinction occurred. Also evident in the image is a large amount of smoke. This corresponds to a rise in  $PM_{2.5}$  around the 210 s mark. Within 15 seconds, the fuel bed is reignited from the smoldering combustion that continued. This type of intermittency accurately describes how these tests behaved and, perhaps the limiting spread conditions that occur during prescribed burning of wet fuels. The fire initially spread as a line, but would break off into smaller sections that would burn for some time, die out, and then another pocket would flare up. This process continued until the entire fuel bed was consumed. NB-W4 managed to burn nearly all of the fuel, with only approximately 5 g of charred fuel remaining. The rest of the fuel had been turned to ash like that found in Figure 14. However, the other three remaining tests for the series had varying degrees of completeness. NB-W2 only burned half of the fuel bed. The fire self-extinguished after about 165 s, but continued to smolder for another 325 s. This can be seen in Figure 18, where the HRR drops precipitously to zero, but  $PM_{2.5}$  continues to be produced until the 500 s mark. Additionally, this test had a carbon monoxide emission factor nearly double that of the other three tests. The other three tests were within  $\pm 5.0$  g/kg of each other. This discrepancy is likely due to the fact that the flame auto-extinguished halfway through the fuel bed. This changed the fire behavior from flaming to smoldering, a change that drastically affected the emissions output [21]. Table A2 and Table A3 provides all of the test data collected during this research.

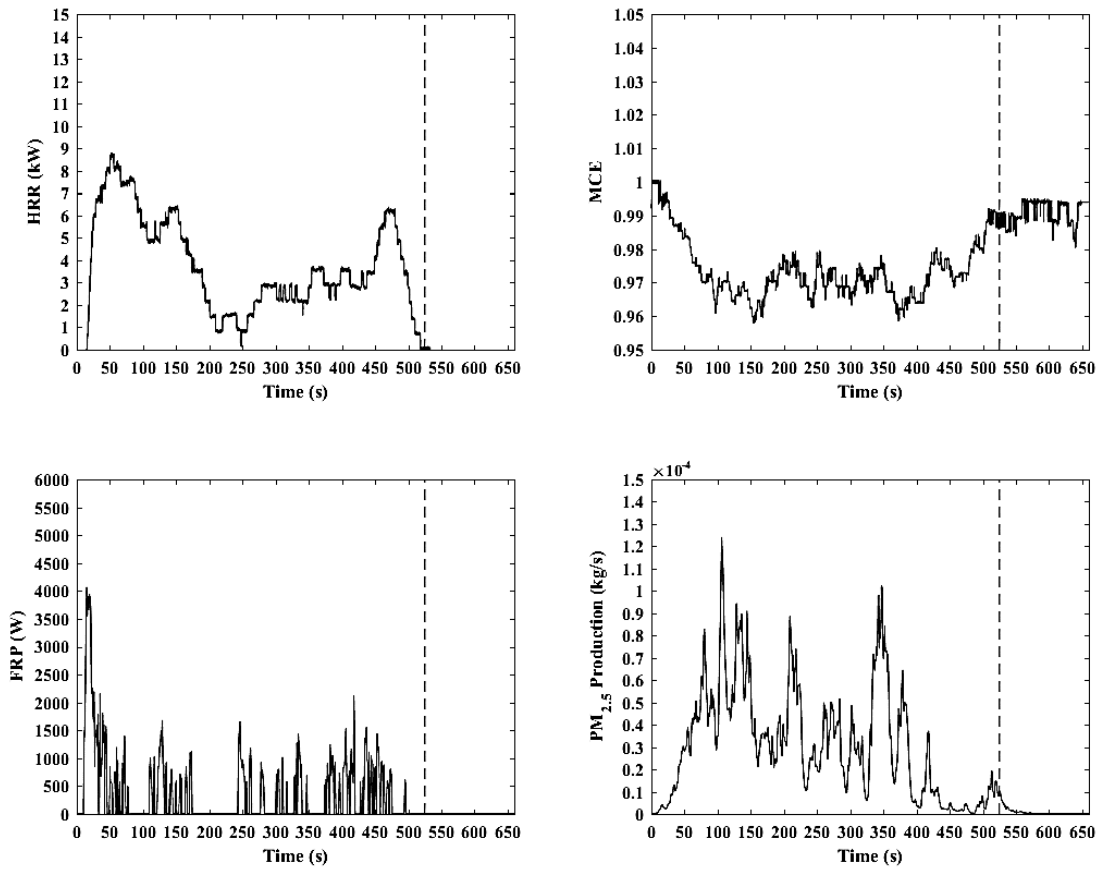


Figure 16: Plots showing the HRR, MCE, FRP, and PM<sub>2.5</sub> production during NB-W4. Note that the vertical dashed line indicates the burnout time



Figure 17: Still image from NB-W4 video showing self-extinction after 165 s. Note the large amount of smoke being produced.

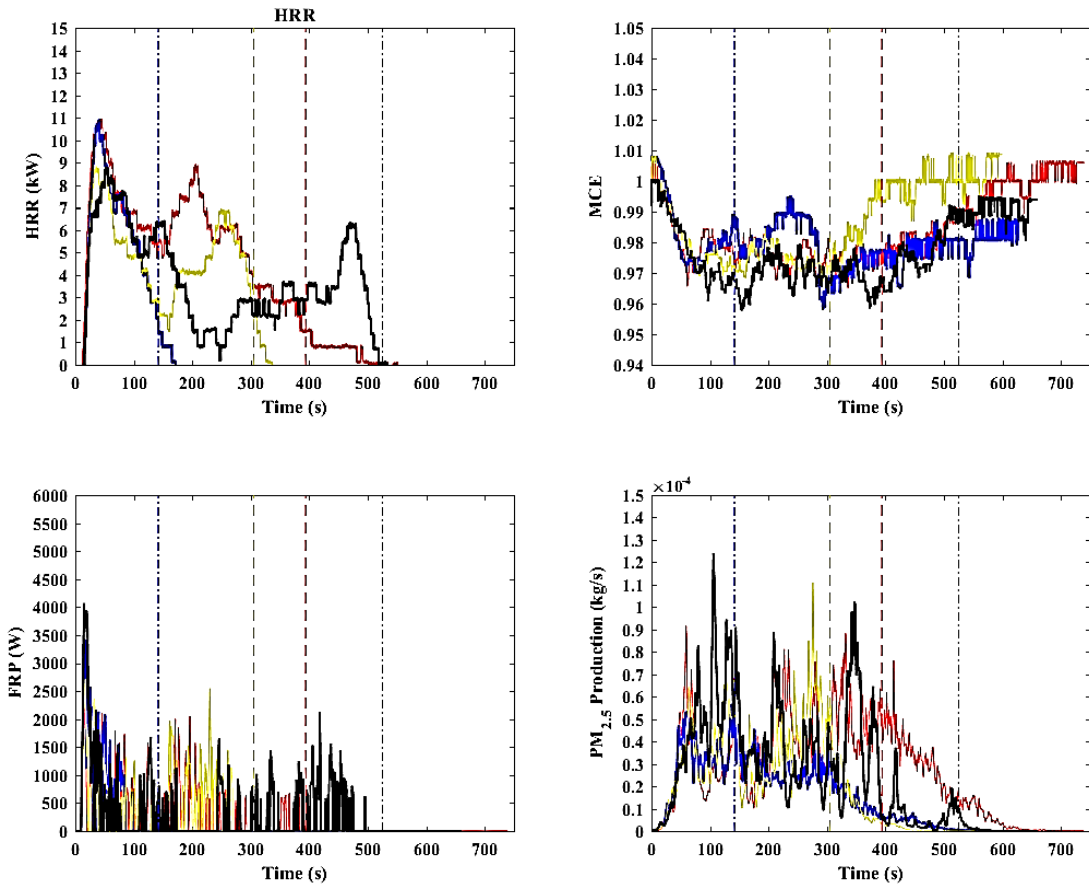


Figure 18: Plots of HRR, MCE, FRP, and Soot Production for the four different tests conducted during the Wet Northern Bayberry series. The colored lines correspond to the different tests as follows: Red ~ NB-W1, Blue ~ NB-W2, Yellow ~ NB-W3, Black ~ NB-W4. The dashed vertical lines denote burnout times

### 4.2.3 Comparison

One of the most telling indicators of the influence of moisture content on fire behavior is the flame height and spread rate. Figure 19 provides a time-lapse view of the first 120 s of NB-D1 and NB-W4, the dry and wet northern bayberry tests. The images show that the dry fuel burns more readily with less visible smoke production.

Another

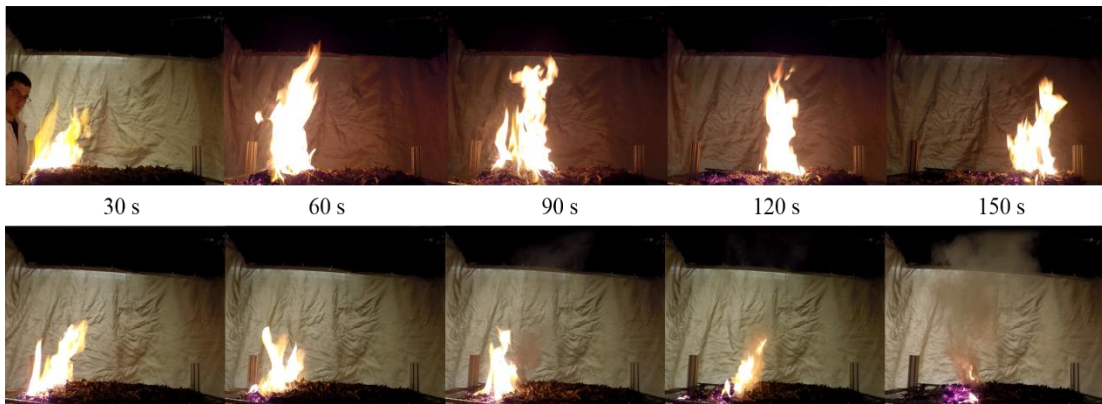


Figure 19: Time-lapse of both the dry (top) and wet (bottom) northern bayberry tests (NB-D1 and NB-W4), taken every 30 s for 2 minutes

stark difference is observed by directly comparing Figure 13 and Figure 16, as shown in Figure 20. The peak value for  $PM_{2.5}$  production for NB-W4 is an order of magnitude larger than that of NB-D1. The amount of FRP detected by the radiometer for NB-W4 is also markedly lower, which is consistent with the lower flame heights. This is also indicative of smoldering combustion. Reported in Table 3 are the averaged emission factors and other relevant parameters. The FRE is presented as the energy density of the fuel,  $ED_{FRE}$  in units of  $MJ/kg_{fuel}$ . Freeborn refers to this value simply as FRE, but  $ED_{FRE}$  is used to delineate between the true FRE, measured in MJ [55]. This value provides a description of total energy content for the given fuel type.

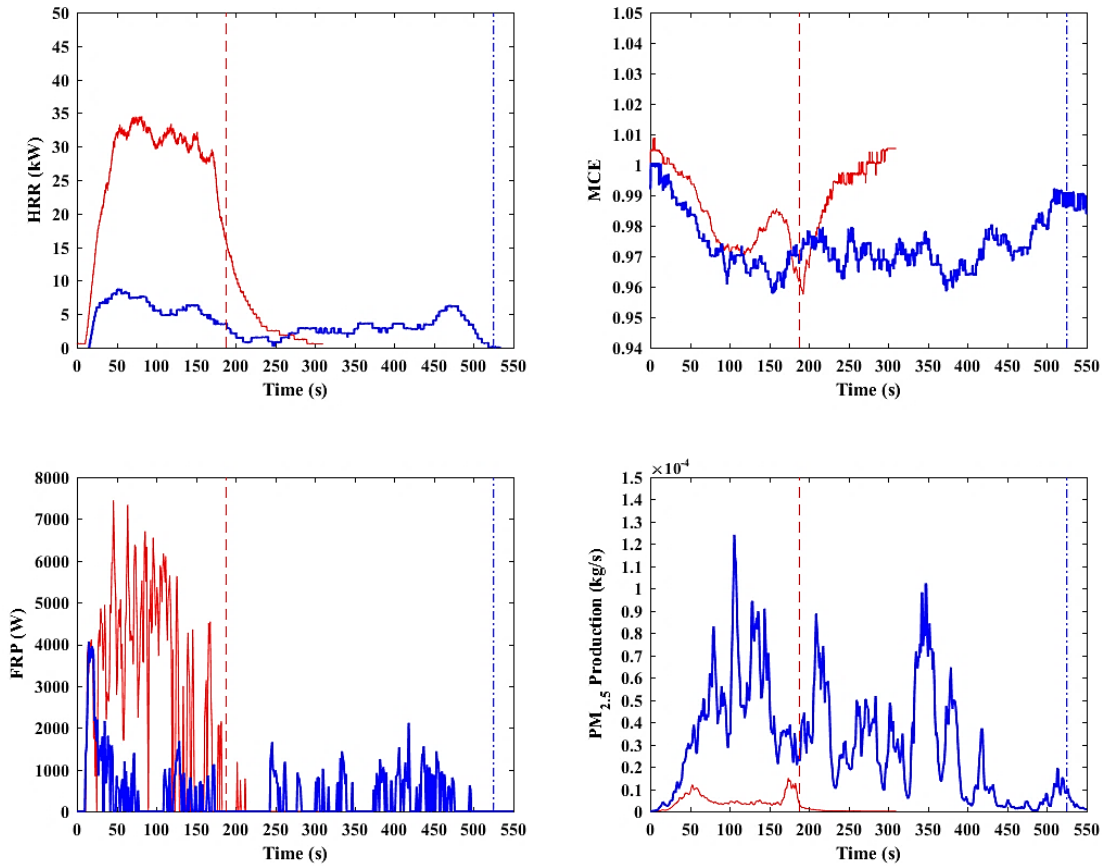


Figure 20: Comparison of NB-D1 (red), the dry northern bayberry condition, and NB-W4 (blue), the wet condition. HRR, MCE, FRP, and PM<sub>2.5</sub> are reported

Table 3: Average emission factors and pertinent fire behavior metrics for the northern bayberry tests with the standard deviation included

| Test Condition | EF <sub>CO2</sub> [g/kg] | EF <sub>CO</sub> [g/kg] | EF <sub>PM2.5</sub> [g/kg] | ED <sub>FRE</sub> [MJ/kg] | Spread Rate [cm/s] | Flame Height [cm] | Peak HRR [kW] | MCE            |
|----------------|--------------------------|-------------------------|----------------------------|---------------------------|--------------------|-------------------|---------------|----------------|
| Dry            | 1962 ± (59.6)            | 57.3 ± (7.38)           | 6.0 ± (1.86)               | 2.85 ± (0.16)             | 0.29 ± (0.05)      | 25.2 ± (3.33)     | 29.0 ± (4.26) | 0.97 ± (0.003) |
| Wet            | 1719 ± (275)             | 100.5 ± (35.6)          | 120.6 ± (22.7)             | 1.18 ± (0.18)             | 0.12 ± (0.02)      | 16.4 ± (1.75)     | 9.9 ± (1.22)  | 0.95 ± (0.01)  |

## 4.3 Mountain Laurel

### 4.3.1 Dry Condition

Mountain laurel, *kalmia latifolia*, has foliage that is typically 3 to 9 cm in length and 2 to 5 cm in width (Figure 21). Like northern bayberry, the 200 g of leaves would settle to create a 3 cm deep fuel bed with a bulk density of 26.7 kg/m<sup>3</sup>. Compared to the northern bayberry leaves, the mountain laurel leaves have a slight leathery feel, but are not very aromatic, even when broken.



Figure 21: Leaves and twigs from undried mountain laurel (*kalmia latifolia*)

All five tests burned very consistently based on flame spread rates, flame heights, and peak heat release rates. The fire front spread at an average rate of 0.45 cm/s with a flame height of 32.6 cm. The entire fuel bed was consumed in all occasions leaving only an average of 6.8 g of ash. An image of the ash remnants is shown in Figure 22.



Figure 22: Ash remaining after combustion of dry mountain laurel

Figure 23 provides measurements for ML-D4. The HRR is fairly steady, taking approximately 50 s to reach this point and burning for 90 s until the front reaches the end of the bed. This is observed in the FRP readings as well, but less steady. This is likely due to the intermittent nature of burning vegetation, where inhomogeneity in the fuel and packing will cause the flame height to fluctuate, decreasing radiant emissions sensed by the radiometer. Interestingly, unlike the northern bayberry tests, there was not a large production of smoke produced immediately before burnout. Instead, this test experienced a peak towards the middle of the fuel bed.

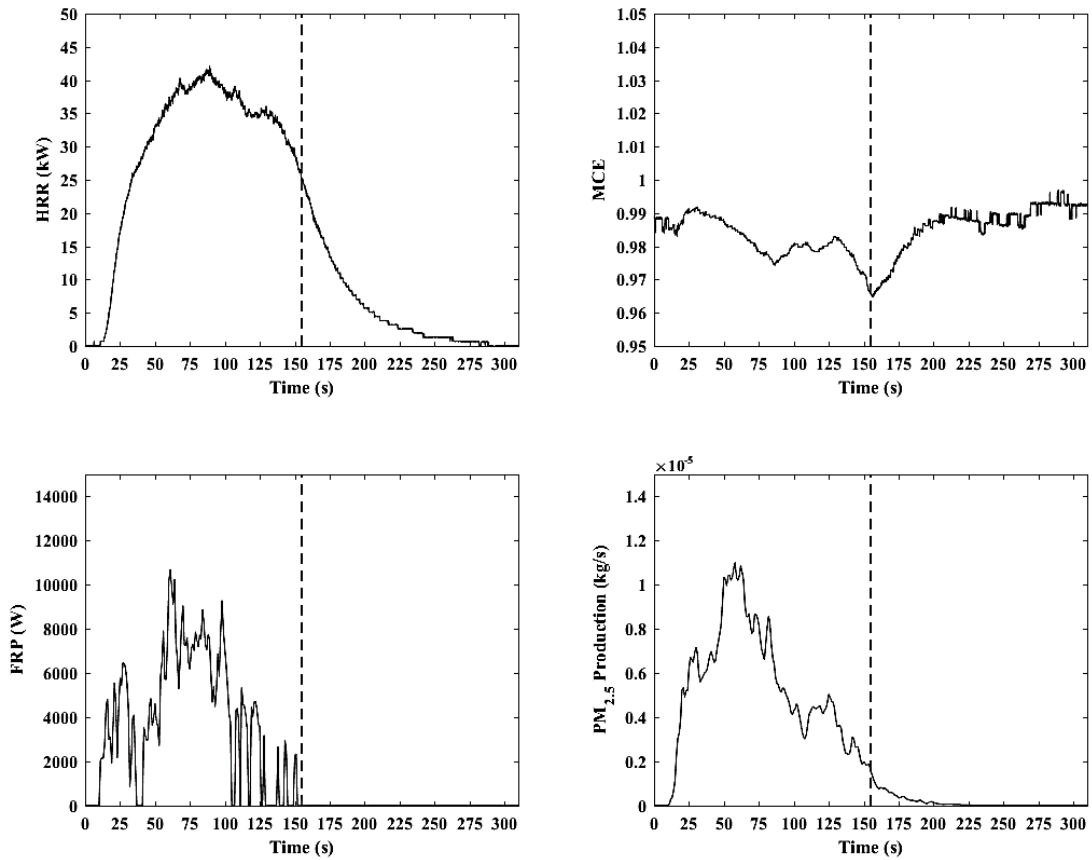


Figure 23: Plots showing the HRR, MCE, FRP, and PM<sub>2.5</sub> production during ML-D4. Note that the vertical dashed line indicates the burnout time

Upon analysis of the test video, it was observed that there was large production of pyrolyzate ahead of the flaming front that went unburned, which could be responsible for the spike in PM measured. This could possibly be caused by air entrainment due to the exhaust hood. The pyrolyzate may be drawn away from the flame front, going unconsumed.

Figure 24 is a comparison of all five tests completed for this series. The other tests do seem to have somewhat of a peak in PM<sub>2.5</sub> prior to extinction, however, the peak is equal or less to the peak seen towards the beginning of the tests. This differs

from the northern bayberry tests, shown Figure 15, where all tests had a significant increase in soot production prior to extinction.

The five different tests agree very well with each other. The burnout times occur within approximately 20 s of each other and the heat release rate curves match very well.

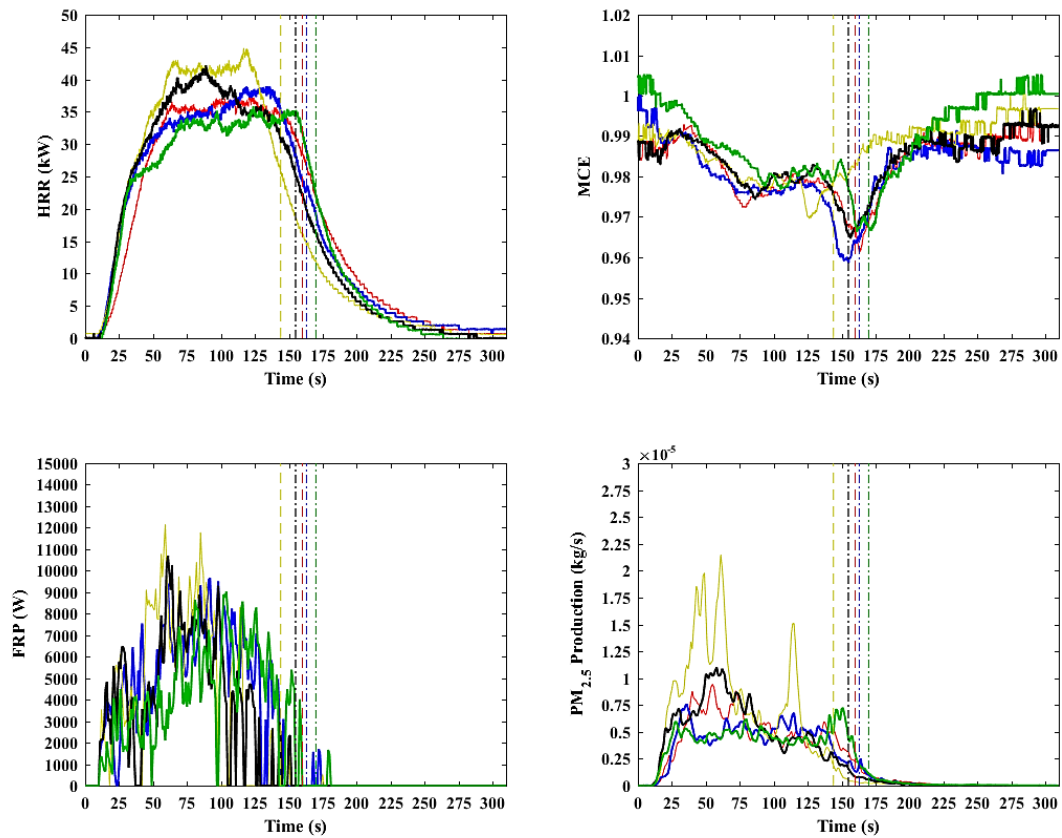


Figure 24: Plots of HRR, MCE, FRP, and Soot Production for the five different tests conducted during the Dry Mountain Laurel series. The colored lines correspond to the different tests as follows: Red ~ ML-D1, Blue ~ ML-D2, Yellow ~ ML-D3, Black ~ ML-D4, Green ~ ML-D5.

### 4.3.2 Wet Condition

Similar to the northern bayberry wet test series, the burning behavior for the wet mountain laurel test series (MC of 0.1207) differed substantially from their dry counterparts. The bulk density was the same at  $26.7 \text{ kg/m}^3$ . The flame spread rate was on average  $0.13 \text{ cm/s}$  with an average flame height of  $13.1 \text{ cm}$ . The average peak HRR was just  $15.1 \text{ kW}$ . As is apparent by the HRR and soot production curves provided in Figure 25, the burning was not steady across the fuel bed.

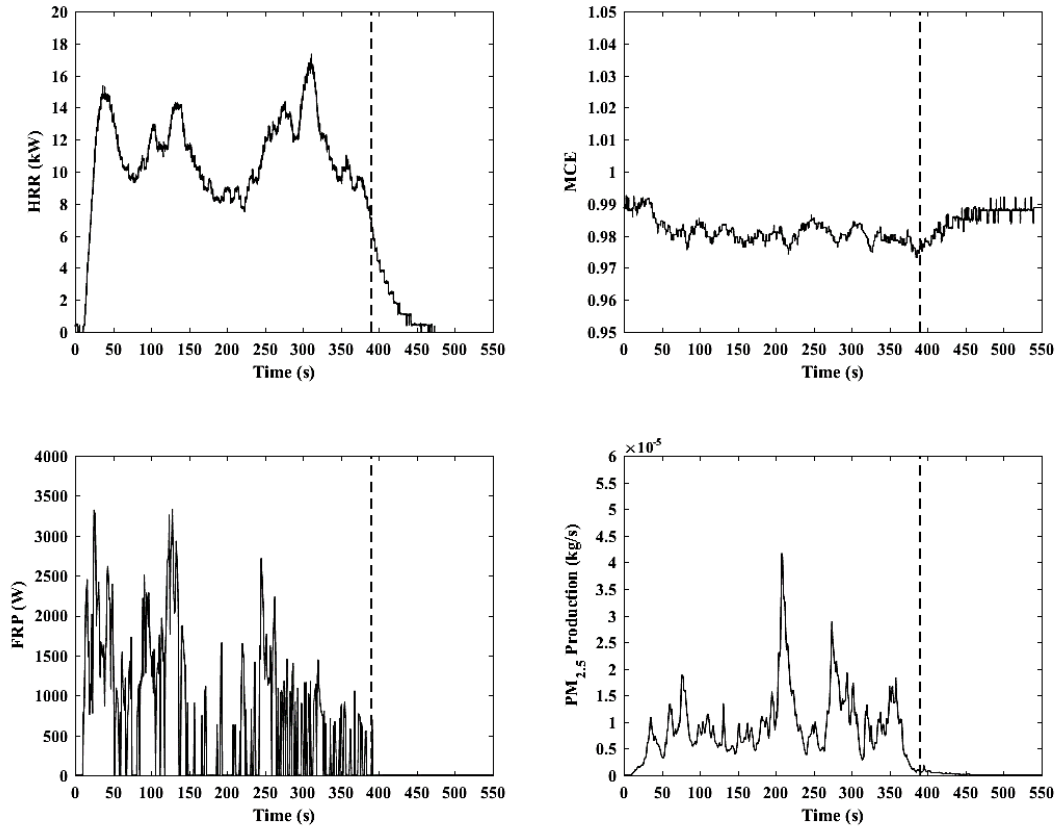


Figure 25: Plots showing the HRR, MCE, FRP, and PM<sub>2.5</sub> production during ML-W1. Note that the vertical dashed line indicates the burnout time

Both the HRR curve and  $PM_{2.5}$  show a reoccurring cycle of growth and decay. The flame front initiates as a continuous line-fire spanning the width of the fuel bed. However, as the front progresses, the line splits into smaller pockets of fire. Due to the reduction in flaming area, the HRR drops. At the same time, the previously burning regions begin to smolder, increasing the amount of  $PM_{2.5}$  produced. Once these smaller pockets reconverge, the HRR rises and soot production falls.

This trend continues for all of the four tests, as seen in Figure 26. The  $PM_{2.5}$  production has fairly even and continuous peaks throughout the tests. This is due to the same fluctuations seen in the HRR. Similar to the dry test of mountain laurel, these wet tests are consistent in behavior across all of the tests. There is minor variability in-between test results, but this is expected when burning organic material.

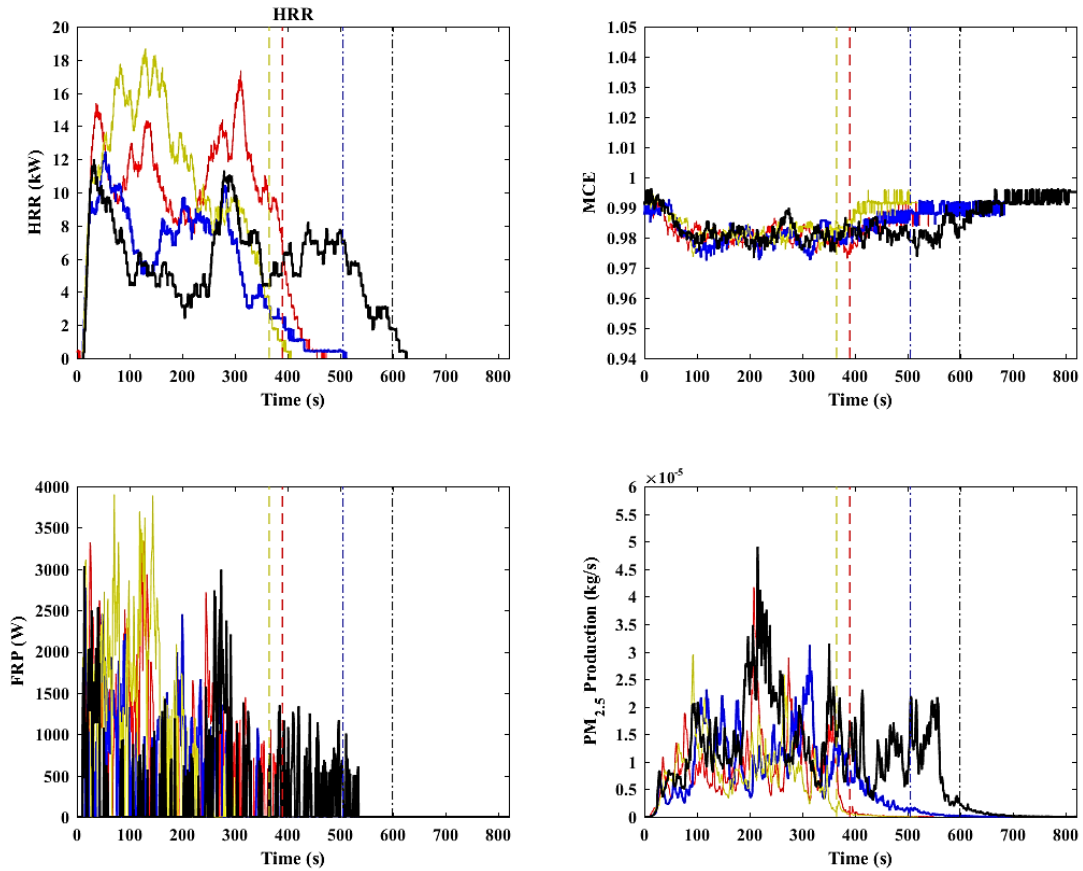


Figure 26: Plots of HRR, MCE, FRP, and Soot Production for the four different tests conducted during the Wet Mountain Laurel series. The colored lines correspond to the different tests as follows: Red ~ ML-W1, Blue ~ ML-W2, Yellow ~ ML-W3, Black ~ ML-W4.

### 4.3.3 Comparison

An interesting observation made during both rounds of testing is in regards to how the mountain laurel burns. When the leaves are ignited, small flame jets appear all over the leaves. Figure 27 highlights one of these jets forming. This is likely due to the volatile oils within the leaf vaporizing, increasing the internal pressure until cell wall failure. The escaping gases are then quickly ignited, forming the jet. This simply emphasizes the effect that these oils may have on burning behavior.



Figure 27: High-speed image sequence of flame jet forming due to contained volatile oils

Without analyzing the emission factors or FRE, it is quite apparent that the moisture content of a fuel has a strong influence on burning behavior. Figure 28, shown below, provides a time-lapse view of the 120 s of burning in 30 s intervals, with the ML-D4 above and ML-W1 below. The average spread rate and flame height for the wet series is nearly 3.5 and 2.5 times less than the dry series, respectively.

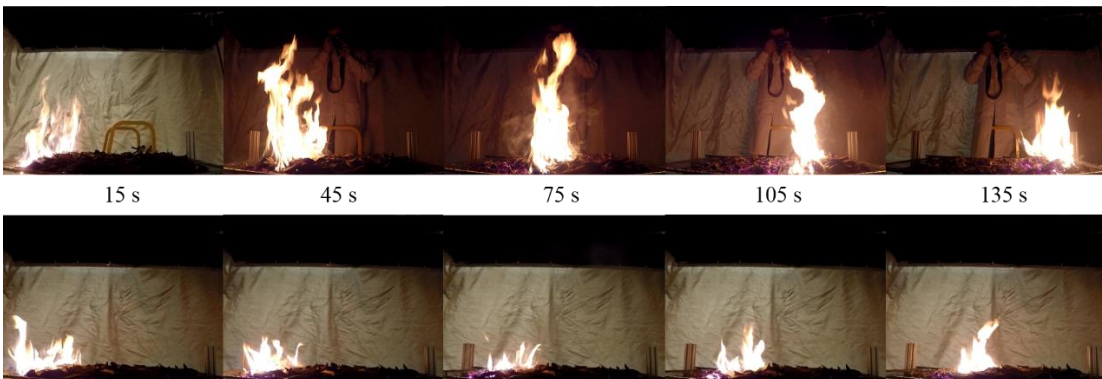


Figure 28: Time-lapse of both the dry (top) and wet (bottom) mountain laurel tests (ML-D4 and ML-W1), taken every 30 s for 2 minutes

The visual observations made during the tests are confirmed by the plots shown in Figure 29. The heat release rate for the dry tests is over two times that of the wet tests and nearly four times for the measured FRP. The amount of  $PM_{2.5}$  produced for the dry tests is also significantly less than that seen in the wet tests. Table 4 provides the averaged emission factors, FRE, and fire behavior values for the two different drying conditions. All values show trends in the direction that would be expected, with  $CO_2$ , FRE, spread rate, flame height, HRR, and MCE decreasing for the wet tests compared to the dry, and CO and  $PM_{2.5}$  increasing.

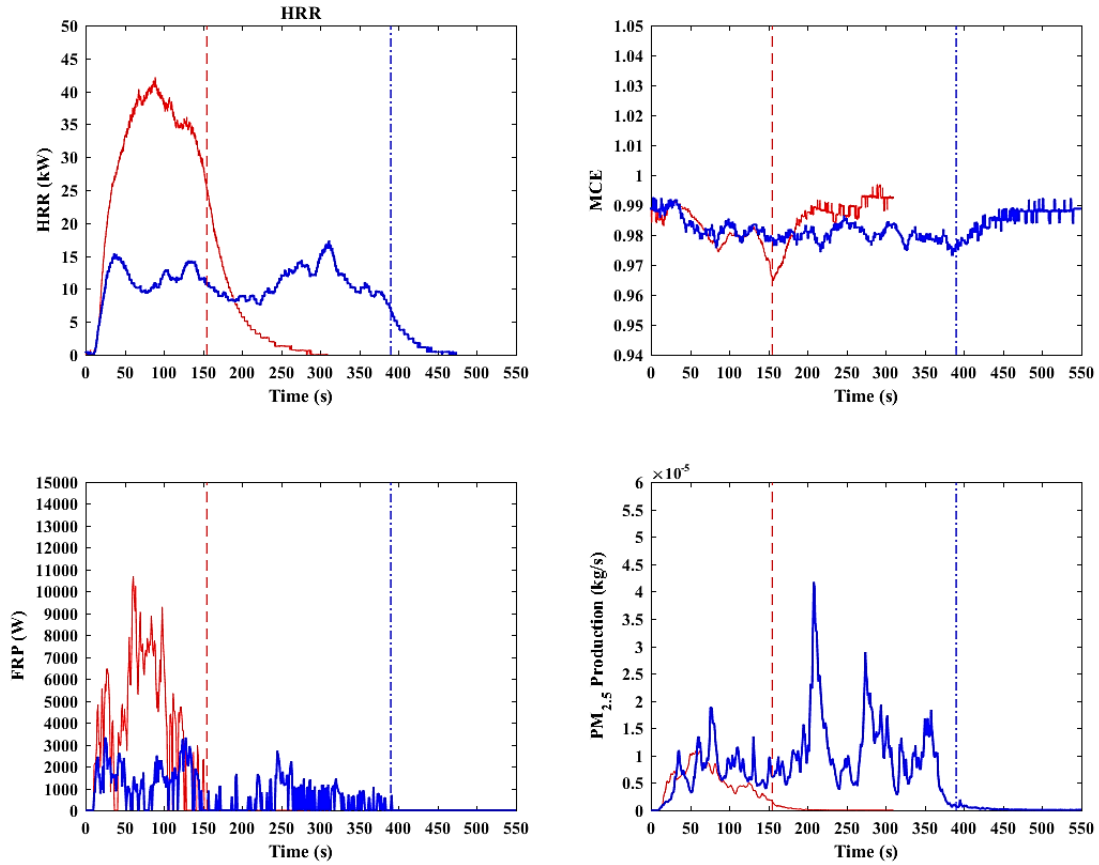


Figure 29: Comparison of ML-D4 (red), the dry mountain laurel condition, and ML-W1 (blue), the wet condition. HRR, MCE, FRP, and PM<sub>2.5</sub> are reported

Table 4: Average emission factors and pertinent fire behavior metrics for the mountain laurel tests with the standard deviation included

| Test Condition | EF <sub>CO2</sub> [g/kg] | EF <sub>CO</sub> [g/kg] | EF <sub>PM2.5</sub> [g/kg] | ED <sub>FRE</sub> [MJ/kg] | Spread Rate [cm/s] | Flame Height [cm] | Peak HRR [kW] | MCE            |
|----------------|--------------------------|-------------------------|----------------------------|---------------------------|--------------------|-------------------|---------------|----------------|
| Dry            | 2036 ± (30.5)            | 50.7 ± (8.38)           | 4.3 ± (0.93)               | 3.46 ± (0.34)             | 0.45 ± (0.04)      | 32.6 ± (1.81)     | 39.9 ± (3.58) | 0.98 ± (0.004) |
| Wet            | 1793 ± (41.1)            | 55.3 ± (5.02)           | 34.6 ± (12.2)              | 1.71 ± (0.31)             | 0.13 ± (0.04)      | 13.3 ± (1.11)     | 15.1 ± (3.38) | 0.97 ± (0.003) |

## 4.4 Eucalyptus

### 4.4.1 Dry Condition

Sugar gum, *eucalyptus cladocalyx*, or simply eucalyptus, is a species of tree indigenous to Australia, having been introduced to Southern California in 1878 [68]. The tree, reaching 35 m in height, has long, slender leaves approximately 8 to 15 cm in length and 2 to 3 cm in width (Figure 30). Unlike the other two fuels used, the average bulk density for the dry tests was greater than other species tested,  $32.2 \text{ kg/m}^3$ . This was likely due to the fact that leaves remained flat as they dried, allowing them to naturally pack more densely when poured into the wooden template. A similar behavior might happen in nature on the forest floor. The leaves had a very strong citronella-like scent, even when dried completely.



Figure 30: Images of eucalyptus leaves prior to drying (left) and the fuel after burning, reduced to ash (right)

In all five dry condition tests, the fuel bed burned completely through, leaving an average of 8.1 g of ash remaining, as shown in Figure 30. The first two tests of this series, EU-D1 and EU-D2, have significantly different heat release rate curves compared to the remaining three tests (Figure 31). This may be due to the fact that the

bulk densities for these two tests were much higher than the remaining three tests. One would expect that with a higher bulk density, the flame height and spread rates would be less. This is the case for these first two tests. The average flame height for EU-D1 and EU-D2 was 29.0 cm with a spread rate of 0.41 cm/s. This is in contrast to average values of 45.8 cm for flame height and 0.72 cm/s for the spread rate for tests EU-D3, EU-D4, and EU-D5. The exact reason for the higher bulk density is unclear. It may have been attributed to higher amounts of fragmented leaves. Leaves were seen to be very brittle when dried and could lay flat. Smaller fuel pieces could lead to a higher density. This also affected other measured values for the tests.

The computed FRE for EU-D1 and EU-D2 was greater than the other three tests despite lower peak FRP values. This is due to significantly longer burn times, allowing for more radiation over time to be emitted. With the exception of EU-D5, the other four had similar PM<sub>2.5</sub> emissions. An analysis of video taken of EU-D5 found that a pocket of fuel roughly 10 to 15 cm from the initial edge of the fuel bed continued to produce visible smoke and intermittently burn behind the main fire front. This can be seen in Figure 32. This may have been due to a pocket of more densely packed fuel. This is supported by the video, showing this region of the fuel bed continuing to produce visible smoke longer than any other region, despite having been the ignited towards the beginning of the test.

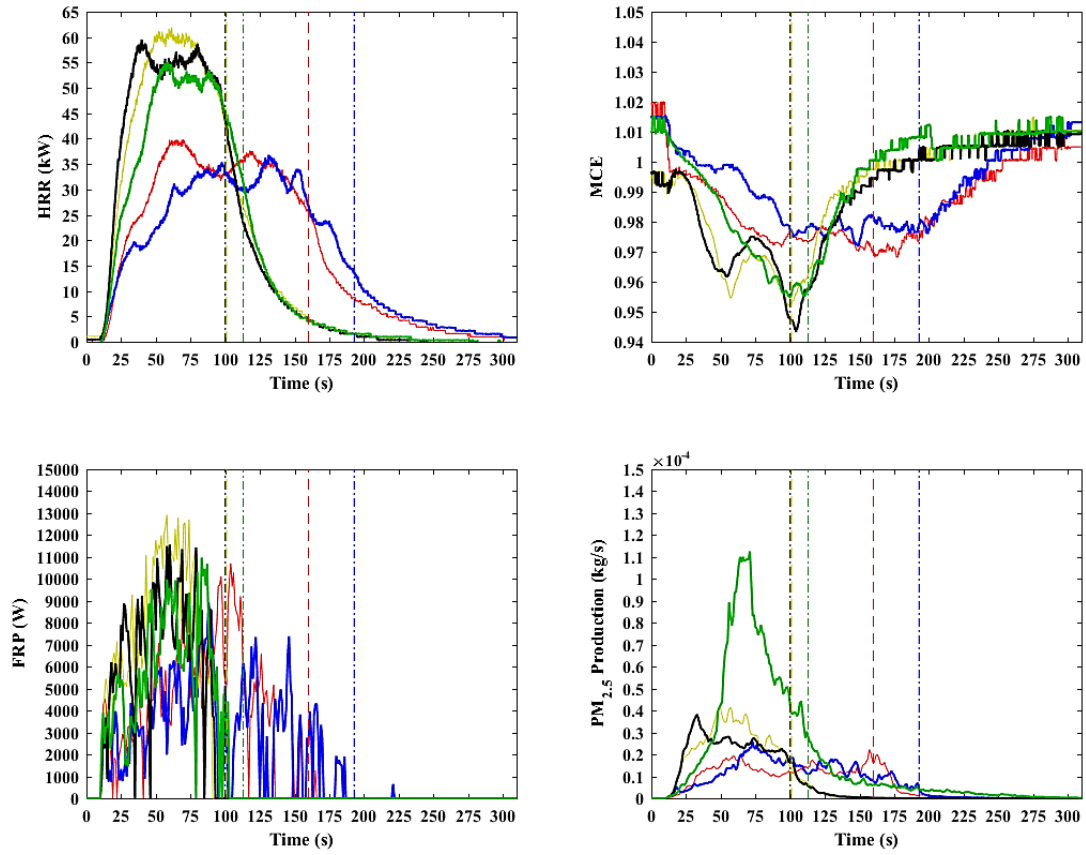


Figure 31: Plots of HRR, MCE, FRP, and Soot Production for the five different tests conducted during the Dry Eucalyptus series. The colored lines correspond to the different tests as follows: Red ~ EU-D1, Blue ~ EU-D2, Yellow ~ EU-D3, Black ~ EU-D4, Green ~ EU-D5



Figure 32: Consecutive frames of intermittent burning of fuel behind main fire front during EU-D5

#### 4.4.2 Wet Condition

For the four wet condition tests, the bulk density was much lower than the dry tests. This was most likely due to the drying method implemented in order to achieve a higher MC level. For the dry tests, at least 600 g of leaves were placed in each drying tray. As the samples dried, the mass of the pile kept the leaves from curling. However, the drying method used to achieve the higher MC required that much less fuel be placed in a tray at a given time to allow for even heating. This likely led to curling of the leaves. When the leaves were then poured into the wooden fuel bed mold, the curled leaves created a “fluffier” pile. This resulted in an increased volume and thus lower bulk density. This could be one explanation for the unexpected high flame height (44.8 cm), spread rate (0.51 cm/s), and peak HRR (40.9 kW). As shown by Figure 33, the tests were very steady, as evident by the heat release curve. The decreased bulk density could allow for better air penetration within the fuel bed, creating a more optimal fuel-to-air ratio.

Another explanation for the limited impact of the higher MC level could be due to the high amount of volatile oils within eucalyptus. The fragrance alone would suggest that these oil could have a significant impact on burning.

Figure 34 shows that there is good agreement between all of the tests with no single tests standing out as abnormal.

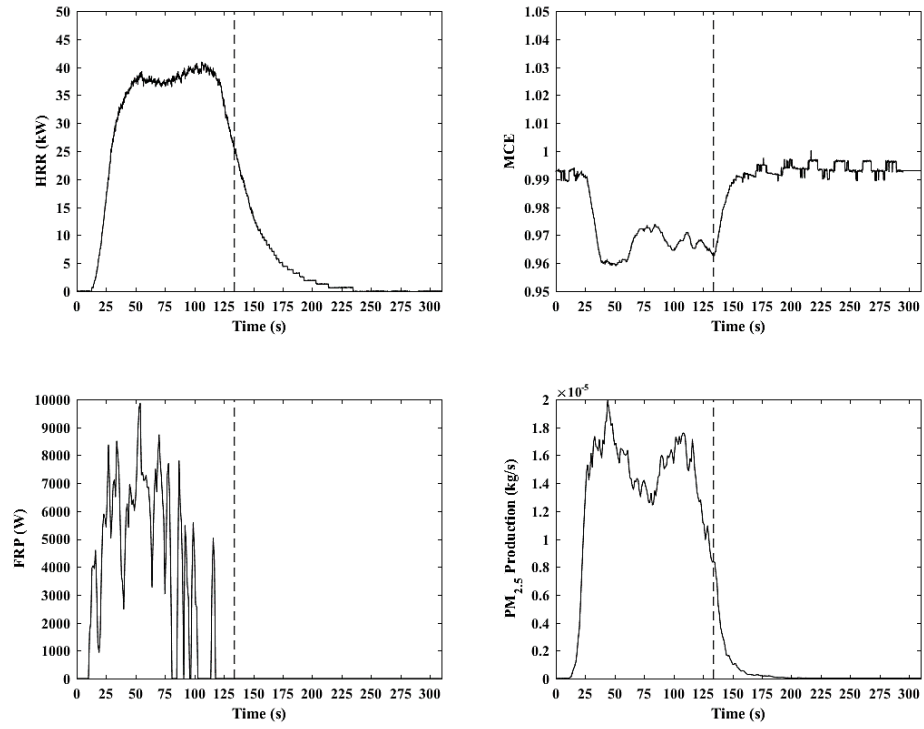


Figure 33: Plots showing the HRR, MCE, FRP, and PM<sub>2.5</sub> production during EU-W1. Note that the vertical dashed line indicates the burnout time

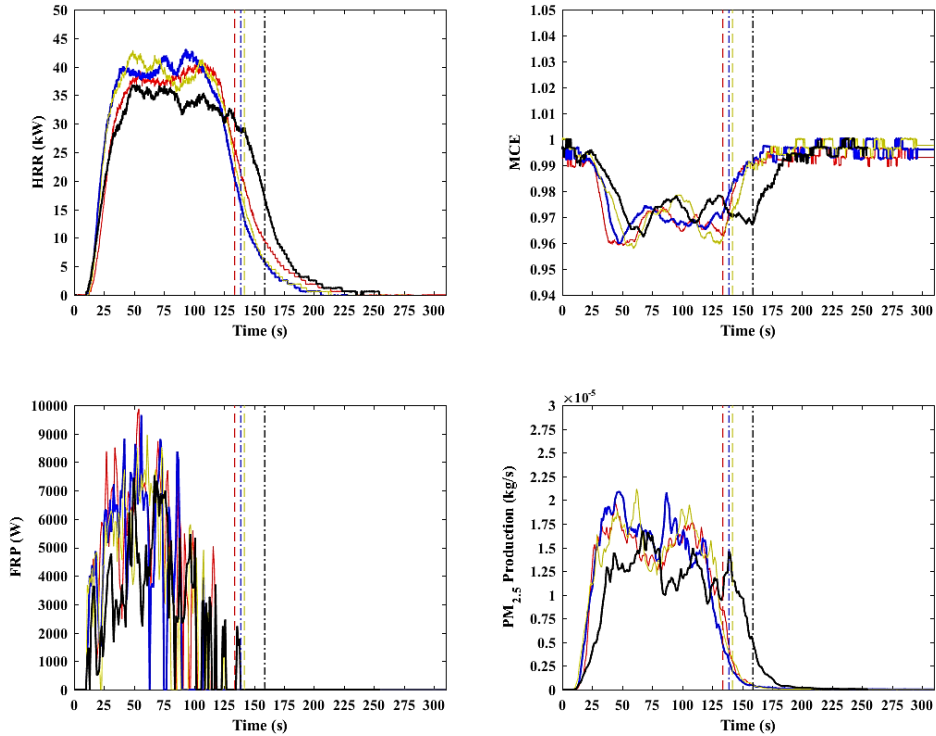


Figure 34: Plots of HRR, MCE, FRP, and Soot Production for the four different tests conducted during the Wet Eucalyptus series. The colored lines correspond to the different tests as follows: Red ~ EU-W1, Blue ~ EU-W2, Yellow ~ EU-W3, Black ~ EU-W4.

#### 4.4.3 Comparison

The eucalyptus tests were interesting due to the apparent lack of influence that the elevated moisture content in the wet series had on observations and collected data. Figure 35 shows how the wet tests did spread slightly slower than the dry cases, but not significantly.

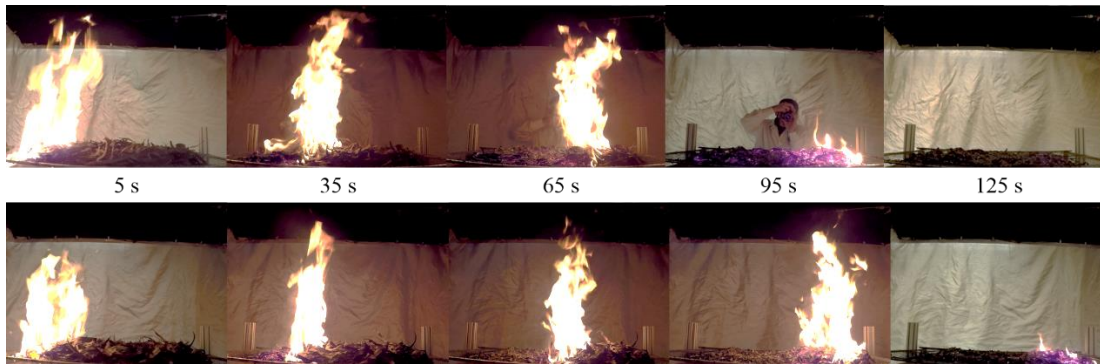


Figure 35: Time-lapse of both the dry (top) and wet (bottom) eucalyptus tests (EU-D3 and EU-W1), taken every 30 s for 2 minutes

One measurement that stands out is  $PM_{2.5}$  production. The comparison made in Figure 36 shows that wet tests produced less soot than the dry cases. In fact, every wet test performed better in terms of soot production than their dry counterparts (Table 5). As previously discussed, this may have been due to the difference in packing densities. Although most of the other measurements do trend in the expected directions, the differences are not as pronounced as would be expected. This may highlight the influence volatile oils can have on the burning behavior and emission output of some pyrophytic species.

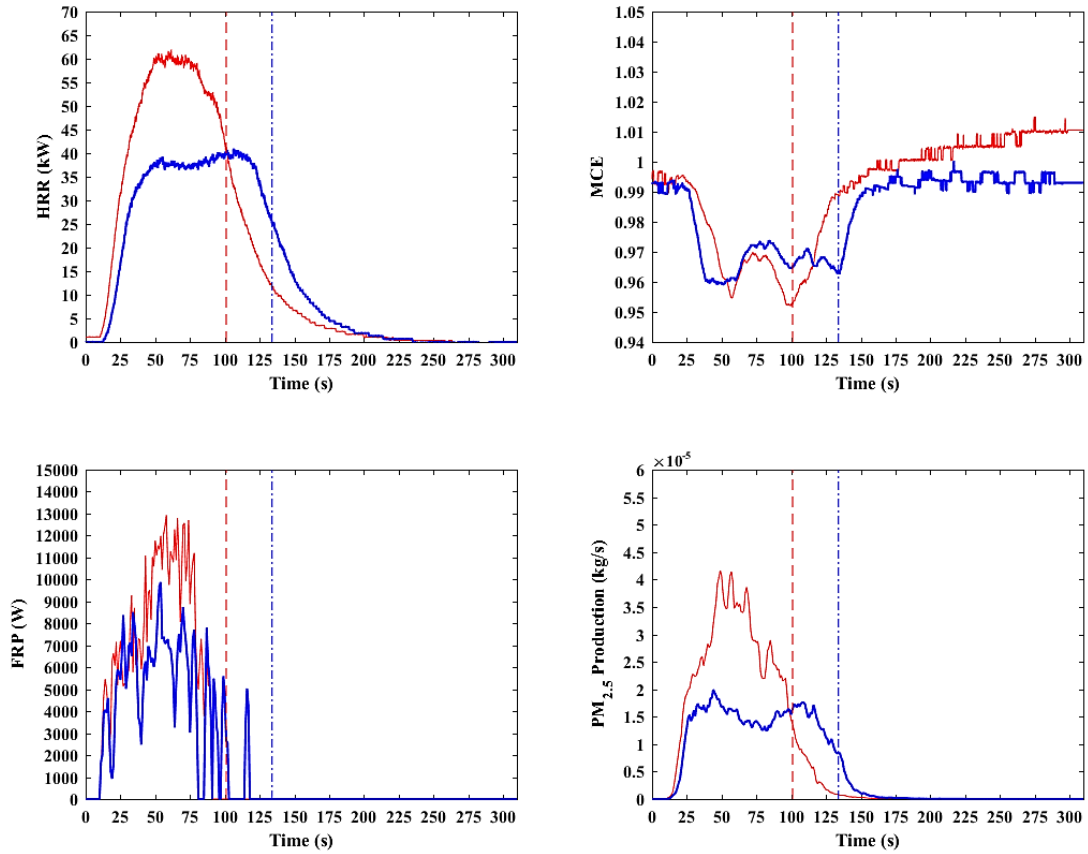


Figure 36: Comparison of EU-D3 (red), the dry eucalyptus condition, and EU-W1 (blue), the wet condition. HRR, MCE, FRP, and PM<sub>2.5</sub> are reported

Table 5: Average emission factors and pertinent fire behavior metrics for the eucalyptus tests with the standard deviation included

| Test Condition | EF <sub>CO2</sub> [g/kg] | EF <sub>CO</sub> [g/kg] | EF <sub>PM2.5</sub> [g/kg] | ED <sub>FRE</sub> [MJ/kg] | Spread Rate [cm/s] | Flame Height [cm] | Peak HRR [kW]  | MCE            |
|----------------|--------------------------|-------------------------|----------------------------|---------------------------|--------------------|-------------------|----------------|----------------|
| Dry            | 1986 ± (66.9)            | 65.9 ± (8.15)           | 15.6 ± (8.4)               | 3.12 ± (0.26)             | 0.59 ± (0.18)      | 39.1 ± (9.32)     | 50.6 ± (11.55) | 0.97 ± (0.004) |
| Wet            | 1983 ± (38.1)            | 72.0 ± (2.87)           | 10.3 ± (0.48)              | 2.53 ± (0.24)             | 0.51 ± (0.03)      | 44.8 ± (6.27)     | 40.9 ± (2.88)  | 0.96 ± (0.001) |

## 4.5 Elevated vs. Flat Configuration

As part of the original test setup, the burning surface was a flat piece of insulating ceramic fiberboard. This was chosen as it would simulate conditions experienced during surface fuel fires. However, after preliminary tests, there was a fairly significant degree of variability between dry tests for the same species. It was also extremely difficult to combust the wet species. In all of the tests conducted with final moisture content levels between 0.1 to 0.15, the fuels failed to burn much beyond the line of methanol used as a pilot. Once the methanol burned off, the leaves transitioned to smoldering and eventually combustion halted. Because of the significant amount of unburned fuel remaining, almost 75%, this method was not seen as viable. Due to these reasons, the test setup was redesigned to incorporate a raised, mesh platform. The platform sits just 2.5 cm above the previously used fiberboard. This small gap allows for improved air entrainment to the bottom of the pile, improving the air-to-fuel ratio and making complete combustion of the fuel bed more feasible. Of the twelve wet tests conducted, eleven burned at least 70% of the fuel bed.

To ensure that results obtained through the elevated mesh platform method were reasonable, a comparison between four flat surface tests and five elevated tests is provided. Both of these groups of tests were considered part of the dry MC condition, with the flat tests at 0.0135 and the elevated at 0.0155. The fuels used in all tests came from the same batch of mountain laurel collected from Frederick Municipal Forest. Table 6 describes the test types and names.

Table 6: List of experiments conducted based on setup conditions. Underlined and bolded numbers refer to tests that are discussed during the following section and used as representative tests for the particular series.

| Name  | Test #                       | Species         | Setup Condition |
|-------|------------------------------|-----------------|-----------------|
| ML-D  | 1, 2, 3, <u><b>4</b></u> , 5 | Mountain Laurel | Elevated        |
| ML-FL | 1, 2, 3, <u><b>4</b></u>     | Mountain Laurel | Flat            |

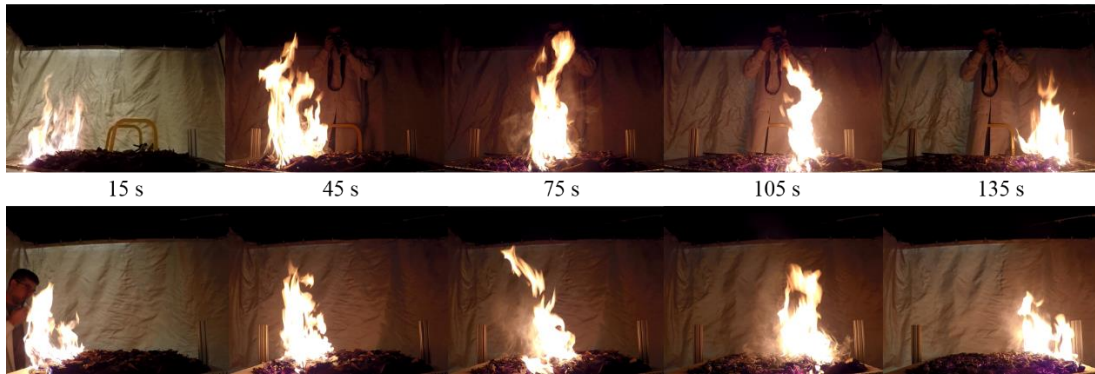


Figure 37: Time-lapse of both the elevated (top) and flat (bottom) experimental setups (ML-D4 and ML-FL4), taken every 30 s for 2 minutes

The comparison of images shown in Figure 37 perfectly highlights that there is not a significant difference in burning behavior between the two different setups. The spread rate and flame height for the elevated tests was 0.45 cm/s and 32.6 cm respectively, and 0.40 cm/s and 29.9 cm for the flat tests. However, it would be expected that the elevated tests would likely burn the fuel more efficiently than the flat case due to the improved air flow. This is reflected in the curves provided in Figure 38 and results in Table 7. The heat release rate and FRP is higher for the elevated tests. The FRP is particularly interesting, as the curve for ML-D4 drops rapidly to zero at burnout. However, ML-FL4 steadily declines over a longer period of time. Upon examining video from both tests, it was found that the embers from ML-FL4 continued to glow throughout the entire fuel bed, not just immediately behind the fire front. This

is indicative of smoldering combustion, a process that occurs after flaming where unburned fuels are still left. This is why the  $PM_{2.5}$  is still very minimal at this point, but

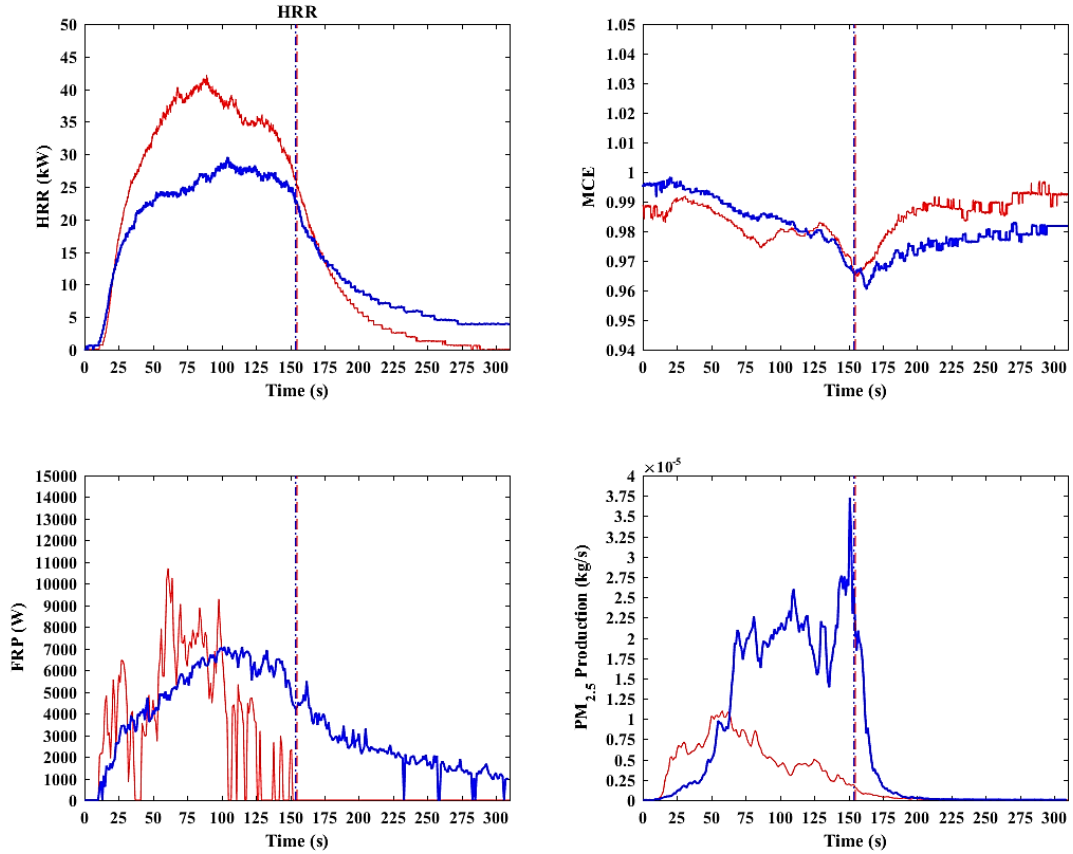


Figure 38: Comparison of ML-D4 (red), the elevated mountain laurel condition, and ML-FL4 (blue), the flat condition. HRR, MCE, FRP, and  $PM_{2.5}$  are reported

Table 7: Average emission factors and pertinent fire behavior metrics for the eucalyptus tests with the standard deviation included

| Test Condition | EF <sub>CO2</sub> [g/kg] | EF <sub>CO</sub> [g/kg] | EF <sub>PM2.5</sub> [g/kg] | ED <sub>FRE</sub> [MJ/kg] | Spread Rate [cm/s] | Flame Height [cm] | Peak HRR [kW] | MCE            |
|----------------|--------------------------|-------------------------|----------------------------|---------------------------|--------------------|-------------------|---------------|----------------|
| Elevated       | 2036 ± (30.5)            | 50.7 ± (8.38)           | 4.3 ± (0.93)               | 3.46 ± (0.34)             | 0.45 ± (0.04)      | 32.6 ± (1.81)     | 39.9 ± (3.58) | 0.98 ± (0.004) |
| Flat           | 1799 ± (62.9)            | 53.6 ± (3.7)            | 11.3 ± (1.9)               | 5.92 ± (0.27)             | 0.40 ± (0.04)      | 29.2 ± (4.48)     | 29.9 ± (3.58) | 0.97 ± (0.001) |

the radiometer is measuring radiation from the glowing area. This did not occur in the elevated setup because the entrained air from below the fuel quickly cooled the remaining embers below temperatures required to sustain smoldering combustion, whereas the fiberboard in the flat case insulated the embers. Interestingly, despite a higher amount of fire radiative energy, the total energy, found by integrating the heat release rate curves, was lower for the flat test setup. This means that the amount of radiation emitted from a fuel can vary and may not be representative of the overall energy output. This will be discussed further in the discussion section.

The PM<sub>2.5</sub> production is markedly larger for the flat scenario compared to elevated, at least double the amount. Again, this would be expected due to reduced airflow into the fuel bed. Similarly, the CO<sub>2</sub> levels for flat test were lower than the elevated for the same reason as the PM<sub>2.5</sub> levels. In fact, all of the values reported in Table 7 trended in the direction that was expected.

The change from burning on a flat, nonporous surface to an elevated mesh platform did affect the emissions and energy outputs in an appreciable manner. However, these differences can be explained and be anticipated. In essence, the elevated burns will provide data for burning under optimal conditions.

## 4.6 Longleaf Pine

The three pyrophytic species being tested as part of this research have previously gone unstudied, making comparisons with existing data difficult. In order to ensure that values being reported are within reasonable expectation, a surrogate fuel was utilized that could in turn be compared to more widely available data. *Pinus palustris*, known as longleaf pine, is conifer species with foliage consisting of needles 15 to 30 cm long and 2 or 2 mm in diameter, shown in Figure 39. The fuel was acquired through a commercial supplier of pine straw. Pine straw consists of dead needles collected from underneath longleaf pine trees that is used for ground cover. These trees are typically found on plantations, meaning contamination from other species is unlikely. Unlike the other three fuels tested, there was no need to refrigerate and subsequently dry the needles as they were already dried under ambient conditions underneath the trees.

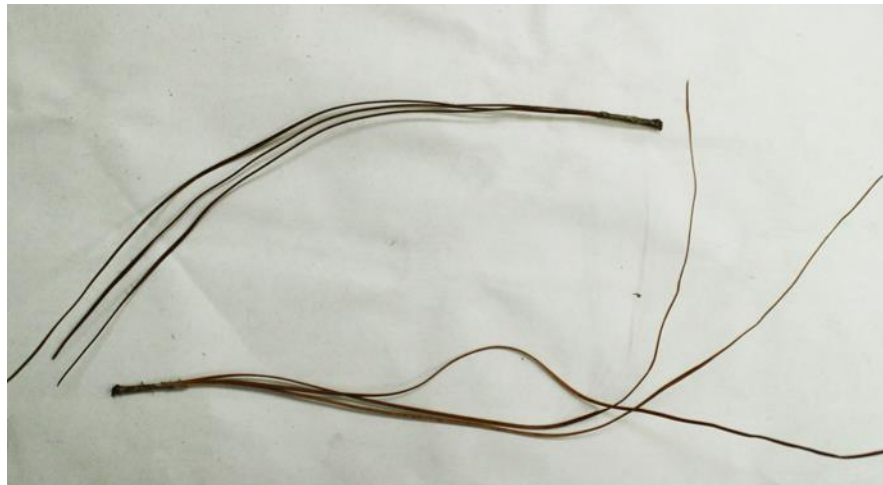


Figure 39: Dried longleaf pine needles

When the longleaf pine was placed in the wooden template, the fuel bed thickness reached 7 cm with a bulk density of 11.46 kg/m<sup>3</sup>. This is significantly less

than with the other fuels, as the needles have a much greater surface area to volume ratio. The sample also had a moisture content of 0.068. Although this value is in-between the two moisture condition sought during the various tests, it ultimately had little impact on the emissions produced and observed fire behavior, as will be discussed.

As with the previous sections, a single test from the longleaf pine series is used to discuss burning behavior for the fuel type. Figure 40 provides the plots of the instantaneous HRR, MCE, FRP, and  $PM_{2.5}$ . The behavior observed for the four pine straw tests were very similar to the mountain laurel and eucalyptus dry tests. Very little visible smoke was produced throughout the entirety of the test. This is confirmed by the PM plot and emission factor measurements, with an averaged  $EF_{PM_{2.5}}$  of 4.62 g/kg.

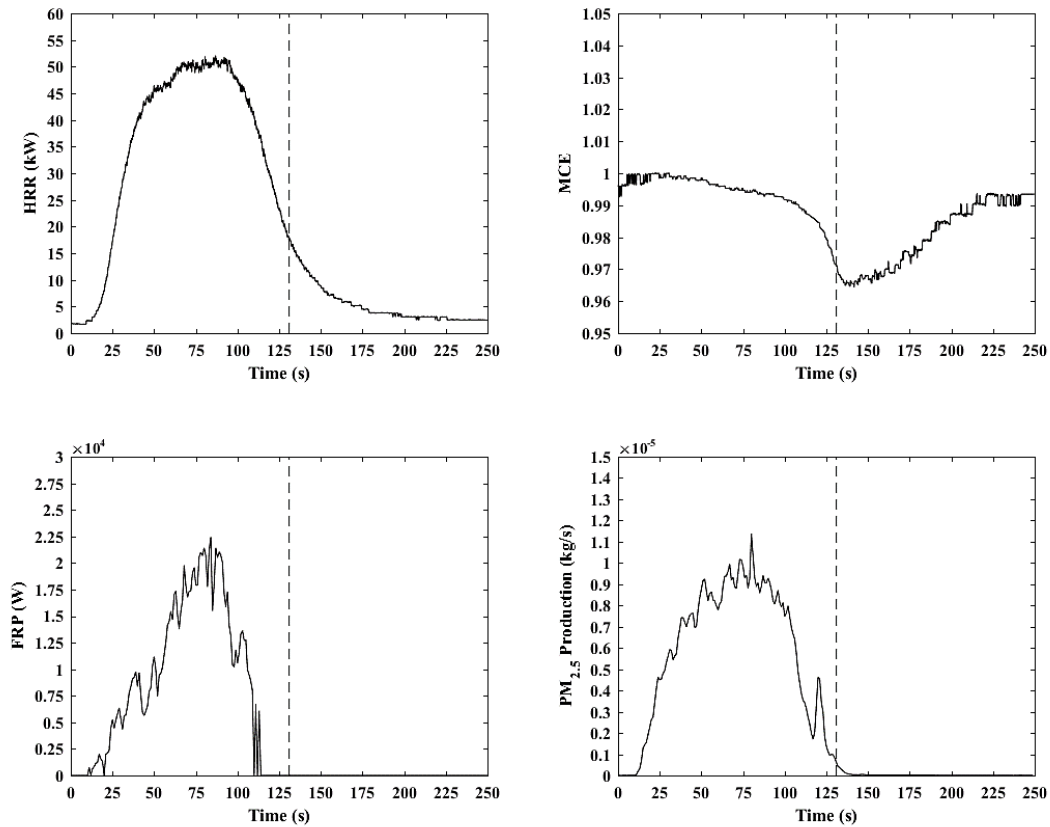


Figure 40: Plots showing the HRR, MCE, FRP, and  $PM_{2.5}$  production during LLP-4. Note that the vertical dashed line indicates the burnout time.

The flame spread rate and flame height were 0.53 cm/s and 37.1 cm, respectively. The heat release rate peaked at 50.2 kW, roughly 80 seconds after ignition. Based on the HRR curve, the flaming front reached steady state after around 45 s of burning. Flame height and general spread rate can be observed in Figure 41, a time-lapse composite of five images taken in 30 second intervals.



Figure 41: Time-lapse of a longleaf pine experiment (LLP-4), taken every 30 s for 2 minutes

A composite of the four different longleaf pine tests is provided by Figure 42. By and large, all four tests were consistent with one another. The first test, LLP-1, experienced a lower overall heat release rate, as well as a slightly longer burn time. However, this was really the only parameter that varied an appreciable amount.

The parameters that measured during the four tests were averaged and provided in Table 12. A comparison with literature values for emissions and energy will be discussed further in Section 5.2.1

Table 8: Average emission factors and pertinent fire behavior metrics for the longleaf pine tests with the standard deviation included

| Test Condition | EF <sub>CO2</sub><br>[g/kg] | EF <sub>CO</sub><br>[g/kg] | EF <sub>PM2.5</sub><br>[g/kg] | ED <sub>FRE</sub><br>[MJ/kg] | Spread Rate<br>[cm/s] | Flame Height<br>[cm] | Peak HRR<br>[kW] | MCE               |
|----------------|-----------------------------|----------------------------|-------------------------------|------------------------------|-----------------------|----------------------|------------------|-------------------|
| Longleaf Pine  | 1926 ±<br>(97.0)            | 33.0 ±<br>(4.2)            | 4.62 ±<br>(0.38)              | 5.75 ±<br>(0.65)             | 0.53 ±<br>(0.025)     | 37.1 ±<br>(1.4)      | 50.2 ±<br>(5.4)  | 0.98 ±<br>(0.002) |

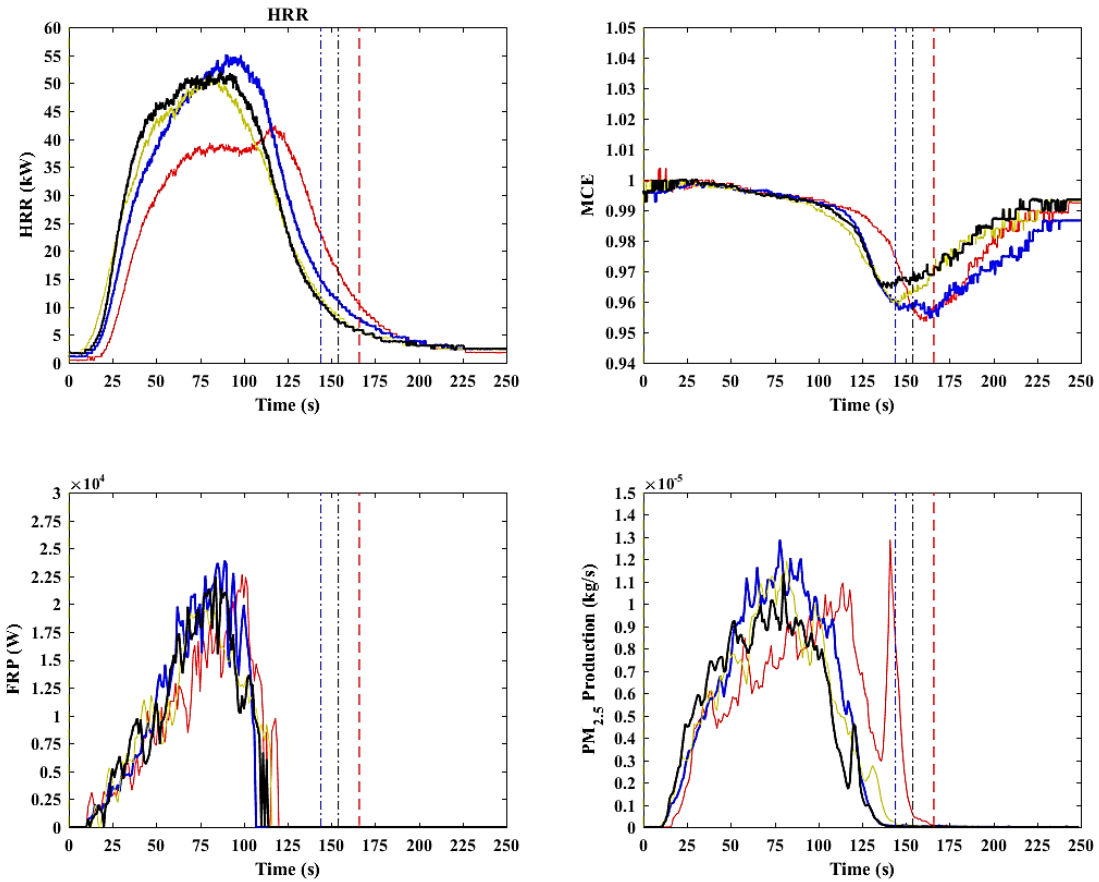


Figure 42: Plots of HRR, MCE, FRP, and Soot Production for the four different tests conducted during the Longleaf pine series. The colored lines correspond to the different tests as follows: Red ~ LLP-1, Blue ~ LLP-2, Yellow ~ LLP-3, Black ~ LLP-4.

## 4.7 Summary of Results

Provided are the tables and figures summarizing the data collected. These will be referred to in the discussion session when comparing results with existing literature values, as well as a means to describe trends that have implications on existing assumptions in regards to remote sensing and emissions inventorying.

Table 9: Averaged emission factors for the six different conditions

| <b>Tests</b> | <b>EF<sub>CO2</sub></b><br>[g/kg] | <b>EF<sub>CO</sub></b><br>[g/kg] | <b>EF<sub>PM2.5</sub></b><br>[g/kg] | <b>MCE</b>        |
|--------------|-----------------------------------|----------------------------------|-------------------------------------|-------------------|
| NB-D         | 1962 ±<br>(59.6)                  | 57.3 ±<br>(7.38)                 | 6.0 ±<br>(1.86)                     | 0.97 ±<br>(0.003) |
| ML-D         | 2036 ±<br>(30.5)                  | 50.7 ±<br>(8.38)                 | 4.3 ±<br>(0.93)                     | 0.98 ±<br>(0.004) |
| EU-D         | 1986 ±<br>(66.9)                  | 65.9 ±<br>(8.15)                 | 15.6 ±<br>(8.4)                     | 0.97 ±<br>(0.004) |
| NB-W         | 1719 ±<br>(275)                   | 100.5 ±<br>(35.6)                | 120.6 ±<br>(22.7)                   | 0.95 ±<br>(0.01)  |
| ML-W         | 1793 ±<br>(41.1)                  | 55.3 ±<br>(5.02)                 | 34.6 ±<br>(12.2)                    | 0.97 ±<br>(0.003) |
| EU-W         | 1983 ±<br>(38.1)                  | 72.0 ±<br>(2.87)                 | 10.3 ±<br>(0.48)                    | 0.96 ±<br>(0.001) |

Table 10: Table of emission coefficients, EC, for CO, CO<sub>2</sub>, and PM<sub>2.5</sub>. The ECs were calculated and averaged for all six series of tests. Values from literature are included for comparison.

| <b>Tests</b> | <b>EC<sub>CO2</sub></b><br>[g/MJ] | <b>EC<sub>CO</sub></b><br>[MJ/kg] | <b>EC<sub>PM2.5</sub></b><br>[MJ/kg] |
|--------------|-----------------------------------|-----------------------------------|--------------------------------------|
| NB-D         | 689 ±<br>(20.4)                   | 20.0 ±<br>(1.4)                   | 2.09 ±<br>(0.66)                     |
| ML-D         | 593 ±<br>(52.6)                   | 14.6 ±<br>(1.6)                   | 1.27 ±<br>(0.35)                     |
| EU-D         | 642 ±<br>(51.1)                   | 21.2 ±<br>(2.3)                   | 5.16 ±<br>(3.18)                     |
| NB-W         | 1588 ±<br>(289)                   | 93.5 ±<br>(36.0)                  | 114.0 ±<br>(36.5)                    |
| ML-W         | 1113 ±<br>(223)                   | 34.8 ±<br>(10.7)                  | 23.2 ±<br>(12.1)                     |
| EU-W         | 788 ±<br>(81.2)                   | 28.5 ±<br>(2.1)                   | 4.06 ±<br>(0.30)                     |

Table 11: Averaged values of total and radiative energy densities (ED), radiative fraction ( $\chi_r$ ), and fuel combustion factor (CF) for the six different conditions

| Tests | ED <sub>FRE</sub><br>[MJ/kg] | ED <sub>HRR</sub><br>[MJ/kg] | $\chi_r$           | CF<br>[kg/MJ]     |
|-------|------------------------------|------------------------------|--------------------|-------------------|
| NB-D  | 2.85 ±<br>(0.016)            | 27.0 ±<br>(0.95)             | 0.106 ±<br>(0.003) | 0.35 ±<br>(0.021) |
| ML-D  | 3.46 ±<br>(0.34)             | 27.9 ±<br>(0.48)             | 0.124 ±<br>(0.011) | 0.29 ±<br>(0.029) |
| EU-D  | 3.12 ±<br>(0.26)             | 27.4 ±<br>(0.96)             | 0.113 ±<br>(0.010) | 0.32 ±<br>(0.028) |
| NB-W  | 1.18 ±<br>(0.18)             | 24.0 ±<br>(4.03)             | 0.050 ±<br>(0.007) | 0.93 ±<br>(0.157) |
| ML-W  | 1.71 ±<br>(0.31)             | 24.7 ±<br>(0.58)             | 0.068 ±<br>(0.012) | 0.62 ±<br>(0.136) |
| EU-W  | 2.53 ±<br>(0.24)             | 27.5 ±<br>(0.49)             | 0.093 ±<br>(0.010) | 0.40 ±<br>(0.037) |

Table 11 provides four different parameters used to describe the energy released during the combustion process. These parameters will be briefly defined, but will be discussed in further detail in the following referring sections.

The energy density, ED, (MJ/kg) is a term used to describe the amount of energy contained within the fuel. ED<sub>FRE</sub> describes the amount of energy released via radiation, whereas ED<sub>HRR</sub> refers to the total emitted energy calculated using the calorimetry setup. This term is reported instead of the FRE and total energy because it provides a normalized value based on mass that is comparable to an emission factor.  $\chi_r$  is radiative fraction, the percentage of the emitted energy in the form of radiation. CF is the fuel combustion factor (kg/MJ), a factor describing how much fuel is required

to emit 1 MJ of radiative energy. This term is the inverse of the energy density, but is used as a comparison with existing data.

The following column charts (Figure 43-46) are used to visualize the various calculated fire behavior, emission, and FRE parameters provided in the previous section. This allows for trends to be more clearly observed and will be referenced as they are discussed in the following section.

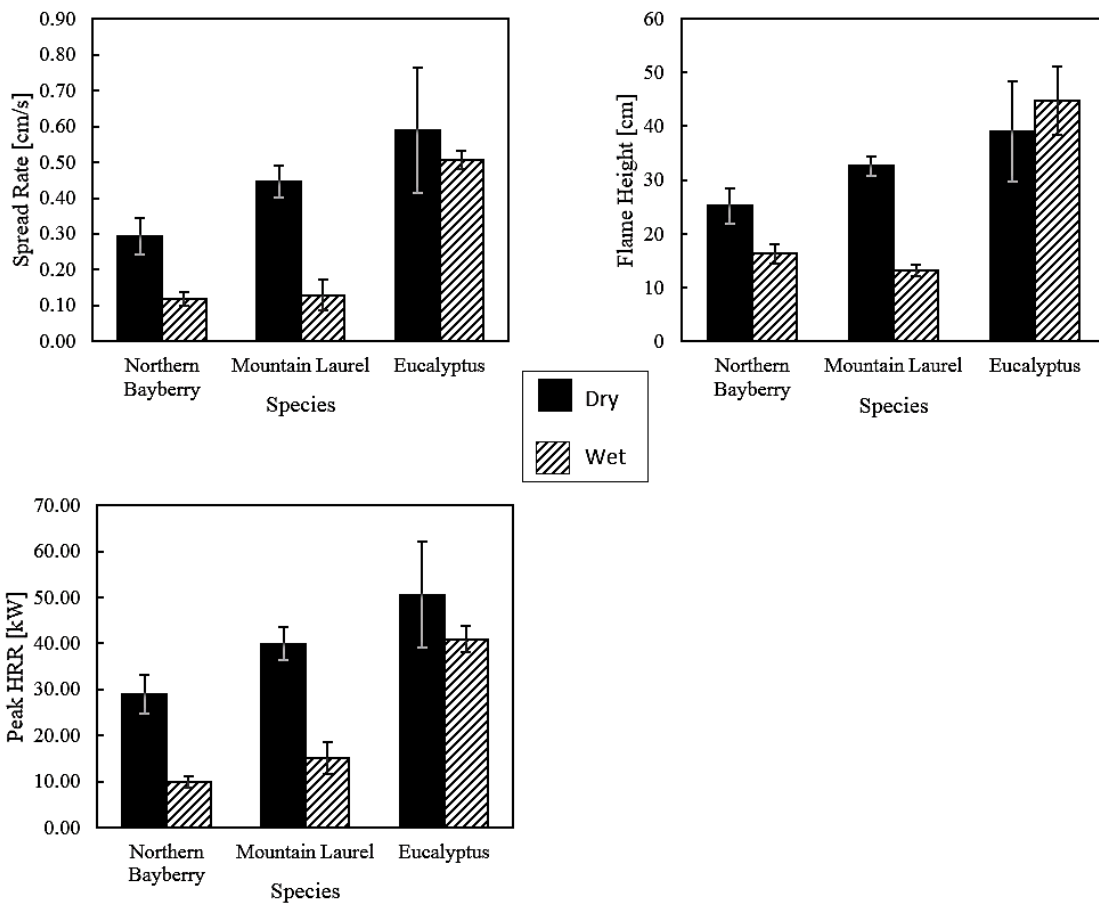


Figure 43: Column charts showing the average spread rate, flame height, and peak HRR for all of the test conditions.

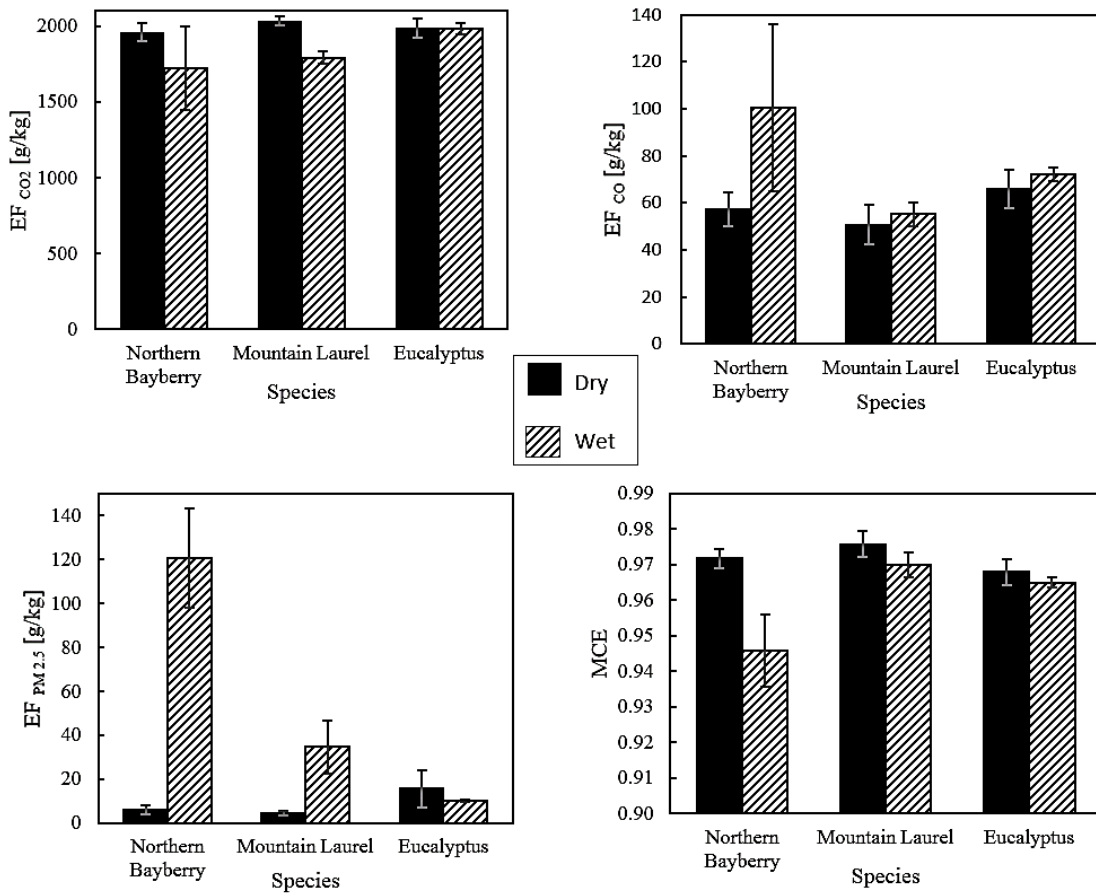


Figure 44: Column charts showing the average CO, CO<sub>2</sub>, and PM<sub>2.5</sub> EF, as well as MCE

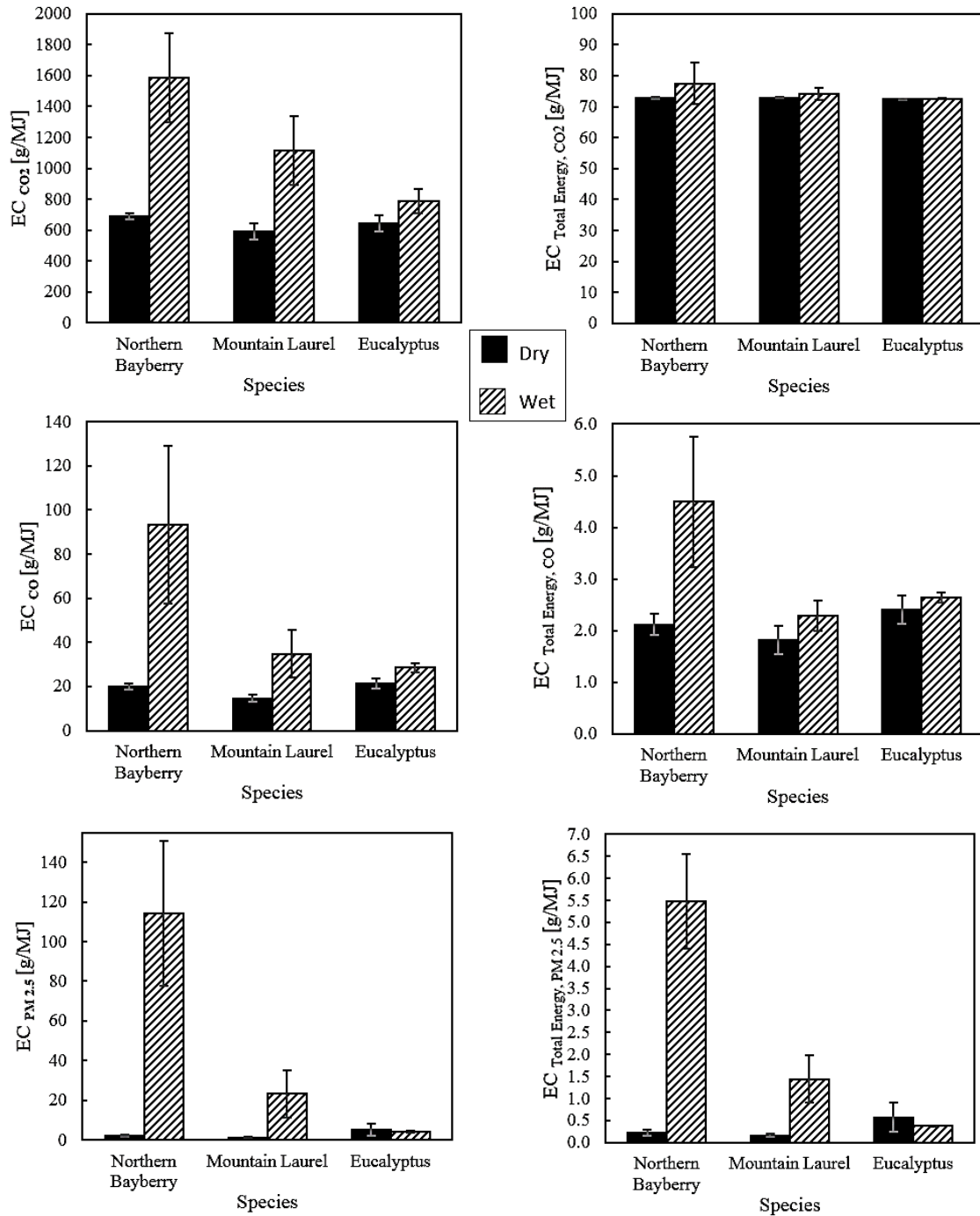


Figure 45: Column charts showing the average emission coefficients calculated for CO, CO<sub>2</sub>, and PM<sub>2.5</sub>. The EC's calculated using the FRE, as well as total energy are presented

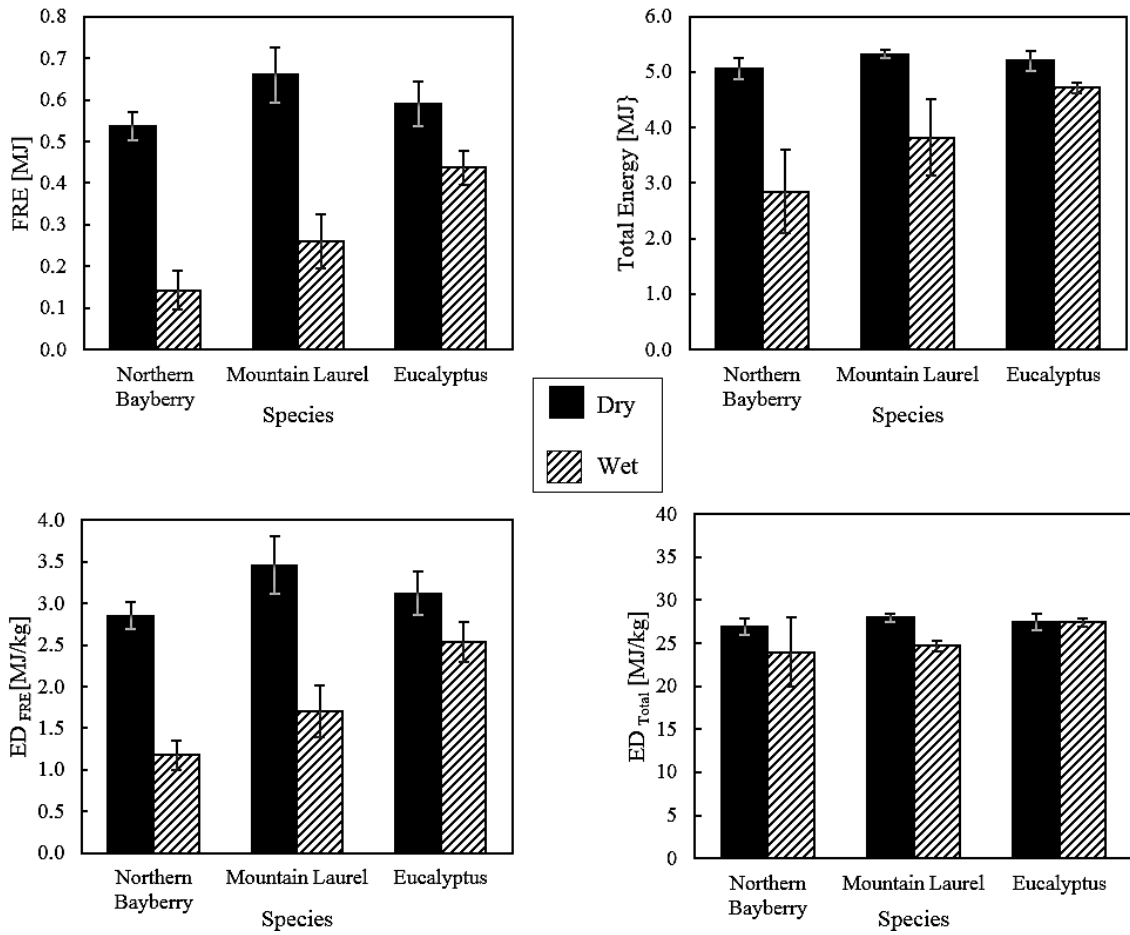


Figure 46: Column charts showing the average FRE and total energy produced, as well as the total energy and FRE ED

## 5. Discussion

### 5.1 Introduction

The following chapter provides an in-depth discussion of the key parameters, namely moisture content and volatility, which affect the emissions and energy output for the three different fuels. The chapter is broken into three sections, Emission Factors, Moisture Density, and Fire Radiative Energy. Within the EF and FRE sections, the experimental values are directly compared to values from the literature and/or compared to existing correlations. Correlations are then drawn from this study's data to describe behavior. Moisture density, a new term devised by ongoing research being conducted at the University of Maryland, is a parameter involving the moisture and volume of the fuel, appears to explain burning behavior and emissions well. Any experimental-based correlations using data collected as part of this research are not provided as alternative formulations to existing correlations, but purely to highlight critical differences.

### 5.2 Emission Factors

#### 5.2.1 Comparison of Pine Emissions

The three fuels being tested here have not been thoroughly studied in the literature, meaning emission factors have not been tabulated. A surrogate fuel, longleaf pine (*Pinus palustris*) was used instead as a large percentage of emissions studies have

specifically focused on pine species or at least the regions where pine is a significant percentage of biomass [69]. Table 12 provides emission values from six different papers. Three of these studies made field-based measurements taken from both prescribed and wildfires in the Southeastern United States [7],[32],[48]. These measurements were taken using various methods, from both ground and aerial-based sensors. Others provide values from laboratory studies of fuels from the Western United States [19],[39],[55]. The values from the field measurements do have noticeable differences when compared both to the laboratory derived values from the literature, as well as those found as part of this research. However, this is not unexpected; complexities such as variations in fuel types and packing, greater fire intensity, the interaction between underlying moist soil, simultaneous combustion phases, etc., mean that small-scale laboratory tests are simply going to be different [19]. However, trends can certainly be developed from laboratory studies and applied to real-world scenarios.

The values most similar to the experimental data gathered as part of this research come from a laboratory study burning ponderosa pine [19]. Both the comparison and these tests utilized air-dried pine needles (left in ambient conditions for several months to achieve MC of  $< 0,1$ ). The comparison test burned 250 g of fuel, similar to the 200 g used during this research's experiments. Both experiments were performed on flat surfaces, although the exact area and bulk density of the fuel bed is unknown for the comparison. The values reported from a similar study using big sagebrush are similar as well [55]. The CO and CO<sub>2</sub> emission factors agree very well

with the experimental data. The PM<sub>2.5</sub> emission factor is quite high in comparison to this study, but this is likely due to differences in fuel type

Table 12: Table of emission factors and MCE, comparing values found in literature and those found during experimentation. Two tests were from prescribed and/or wildfire field measurements of pine forests in the Southeastern United State [7], [32]. One test is a field measurements of burning pine understory [48]. Three tests are laboratory tests, ponderosa pine [19], southern pine litter [39] and big sagebrush [55]. The experimental results are from burning longleaf pine

| Source                      | EF <sub>CO2</sub><br>[g/kg] | EF <sub>CO</sub><br>[g/kg] | EF <sub>PM2.5</sub><br>[g/kg] | MCE             |
|-----------------------------|-----------------------------|----------------------------|-------------------------------|-----------------|
| <b>Experimental</b>         | 1926 ± (97.0)               | 32.5 ± (4.2)               | 4.62 ±(0.4)                   | 0.98 ± (0.002)  |
| [7] Field Measurement       | 1637 ± (71)                 | 89 ± (32)                  | 12.7 ± (7.5)                  | -----           |
| [19] Lab Measurement        | 1781.9 ± (8.7)              | 19.9 ± (4.3)               | 4.0 ± (0.5)                   | 0.98 ± (0.00)   |
| [32] Field Measurement      | 1671<br>1682                | 84.0<br>87.8               | -----                         | 0.927<br>0.925  |
| [39] Laboratory Measurement | 1710 ± (39)                 | 128.6 ± (19.8)             | -----                         | 0.894 ± (0.017) |
| [48] Field Measurement      | 1668                        | 72.1                       |                               | 0.936           |
| [55] Lab Measurement        | 1956.33 ± (325.45)          | 35.91 ± (10.8)             | 36.18 ± (0.08)                | -----           |

Despite some variation between measurements conducted as part of this research and those found in literature, this study shows that the methods and instrumentation utilized during this research provide results that are reasonable. When burning vegetation, there is always a large assumed degree of variability simply due to the nature of organic materials.

### 5.2.2 Review of Emission Factor Literature Values from Previous Studies

The three species selected for this study: northern bayberry, mountain laurel, and sugar gum, were chosen due to their existence in wildland fire prone areas, as well as their pyrophytic nature. However, very little research, if any, exists on the emissions from these fuels. Eucalyptus is a well-known pyrophytic species, yet only a few studies provide data on the emissions [12],[70],[71],[72]. Four studies, with values reported in Table 13, have sought to quantify some emissions. These values can be compared with the results provided in Table 9 from this research. However, the methods used in one of the referenced studies calls into question the validity of the reported values [70]. This study burned the different eucalyptus species in a commercially available woodstove. Woodstoves are designed to burn fuels more efficiently and produce less CO and PM<sub>2.5</sub> emissions than the open burning seen in wildland fires. Another study utilized a cone calorimeter, which enabled them to investigate the effects of fuel moisture on combustion of eucalyptus [12]. However, the small sample size, typically 100 cm<sup>2</sup>, and applied heat flux is not representative of real-world conditions [73]. The remaining two studies provide values found from field measurements [71],[72]. Even these can have large degrees of variability due to the complexity of the fire behavior, as well as the inability to discern emissions being produced by specific species.

For northern bayberry and mountain laurel, there is currently no other data that could be found for direct comparison. While these fuels do exist in regions where emission factors have been tabulated (Pine Barrens), these EFs are focused on the more dominate species.

Table 13: Various literature emission factors shown for eucalyptus to be compared with those shown in Table 9

| <b>Literature</b>            | EF <sub>CO2</sub><br>[g/kg] | EF <sub>CO</sub><br>[g/kg] | EF <sub>PM2.5</sub><br>[g/kg] | MCE   |
|------------------------------|-----------------------------|----------------------------|-------------------------------|-------|
| [12] Laboratory Measurements | 1350 ± (200)                | 25.0 ± (5.0)               | -----                         | 0.97  |
| [70] Laboratory Measurements | -----                       | -----                      | 1.8 ± (0.7)                   | ----- |
| [71] Field Measurements      | 1640 ± (160)                | 112 ± (18.0)               | -----                         | ----- |
| [72] Field Measurements      | 1558                        | 106                        | -----                         | ----- |

### 5.2.3 Emission Correlations

Section 2.4 introduced the idea of using correlations based on combustion efficiency to determine emissions production [36]. In stoichiometric combustion chemistry, carbon dioxide is the only carbon-containing compound produced when burning hydrocarbons. The presence of additional carbon-based products implies a deviation from stoichiometric conditions. The combustion efficiency is a measure of the emitted carbon dioxide versus all of carbon-containing compounds emitted, where stoichiometric burning is given a value of 1.0

Equations (10), (11), and (12) were developed by the EPA to aid forest managers and those parties involved with prescribed burning in predicting the total amount of a particular species emitted. Because the combustion efficiency is based on carbon-containing species, correlations can be used to calculate emissions based purely on the CE [36].

Using the three equations, CO and PM<sub>2.5</sub> emission factors were found, based on the average MCE calculated for the different experimental conditions and displayed in Table A1.

Equations (11) and (12) were plotted along with CO and PM<sub>2.5</sub> values calculated from the experimental data to establish if any trends existed.

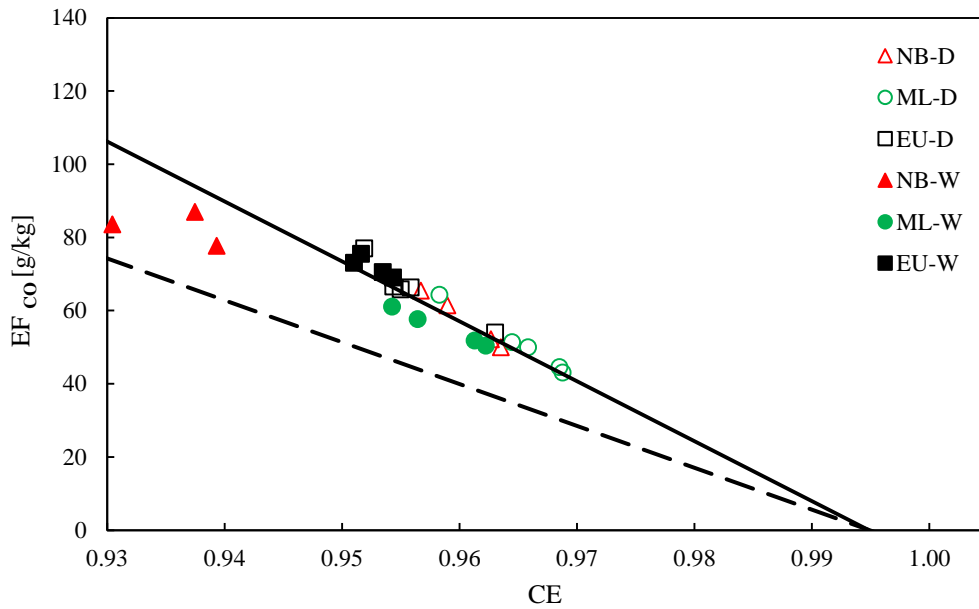


Figure 47 below is such a plot, with the tabulated EF<sub>CO</sub> values against the CE found using Equation (10). Equation (11) was also plotted as a comparison. A linear regression was fitted to the data, providing an equation for EF<sub>CO</sub>,

$$EF_{CO} = 1620.9 - 1637.5 \times CE \quad [g/kg] \quad (15)$$

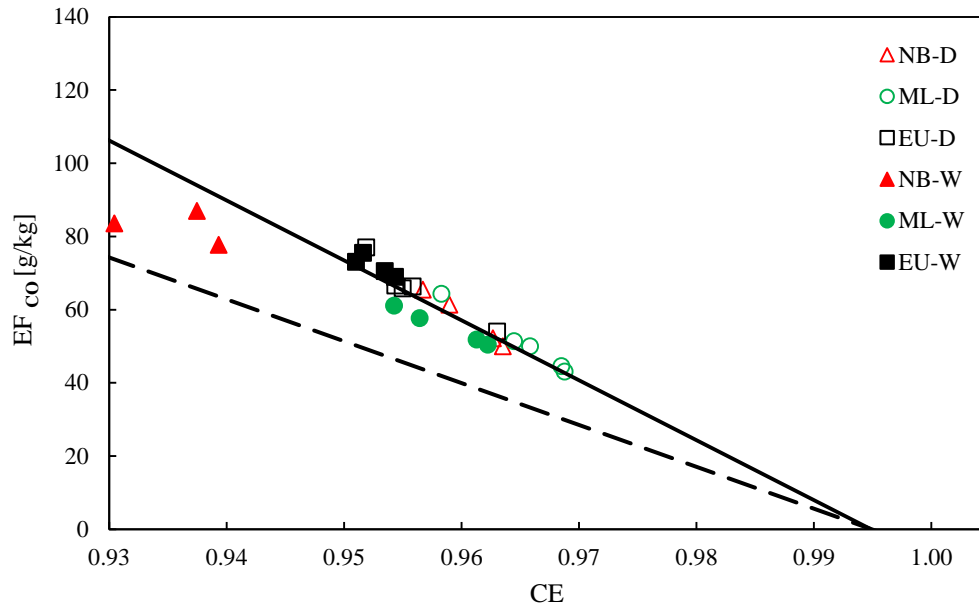


Figure 47: Plot of the CO emission factors against the experimentally derived MCE. The solid line represents a linear regression fit to the experimental data ( $EF_{CO} = 1906.5 - 1904.1 \times MCE$ ;  $R^2 = 0.88$ ). The dashed line is Equation (11)

As the figure shows, the linear regression provides a very good fit to the data, with all points falling within  $\pm 6$  g/kg except for the wet northern bayberry tests ( $R^2 = 0.88$ ). The outlier shown in the plot, NB-W2, was the one test where a majority of the fuel bed was not successfully burned. This caused a change in combustion behavior from flaming to smoldering, in turn leading to a larger than expected production of CO and  $PM_{2.5}$ . Removing the outlier causes the slope of the linear regression to trend towards the correlation provided by [36].

Equation (12) is a correlation for calculating  $PM_{2.5}$  emission factors based on the combustion or modified combustion efficiency [36]. However, unlike the  $EF_{CO}$  correlation, this correlation does not fit the data tabulated for this research. The

correlation itself only appears to be valid for those fuels with very low MC levels and thus typically high CE values.

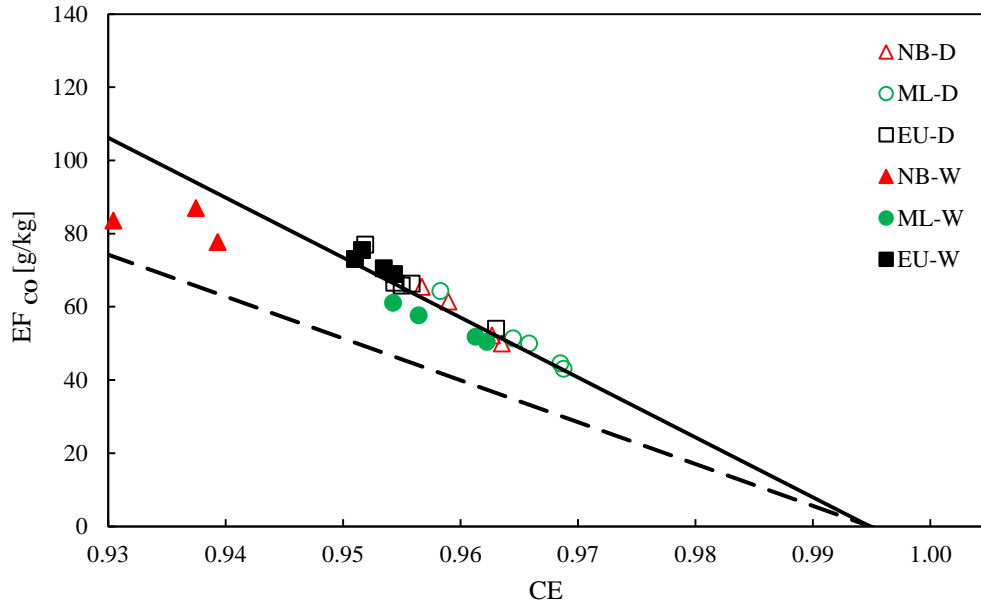


Figure 47, Figure 48 plots the PM<sub>2.5</sub> emission factors along with the EPA correlation. A linear regression was fit to the data, with an R<sup>2</sup> = 0.80.

$$EF_{PM_{2.5}} = 2924.1 - 3048.2 \times CE \quad [g/kg] \quad (16)$$

The levels of PM<sub>2.5</sub> that can be calculated using Equation (12) are very low, as the Figure 48 shows. Using the equation, a combustion efficiency of 0.5 would result in an EF<sub>PM<sub>2.5</sub></sub> of just 34 g/kg. The wet northern bayberry and mountain laurel both produced more PM<sub>2.5</sub> with a combustion efficiency that never remotely approached 0.5. This models seems to fairly accurately predict values with very low moisture content, and thus higher combustion efficiency levels, but the correlation falls apart when the MC increases.



the specific concentration of these oils contained within the leaves, this is purely speculative.

## 5.3 Fire Behavior

The influence of moisture and species type was based on observations made during the experiments. Figure 43 provides a series of column charts that make comparisons easy. The charts show that the moisture content has a noticeable impact on all four parameters presented. However, the degree to which moisture has an impact is fuel specific. It is believed that the pyrophytic nature of the fuels explains this. Eucalyptus had the highest values for spread rate, flame height and peak HRR, for both the dry and wet tests. This was followed by mountain laurel, then northern bayberry. Eucalyptus and mountain laurel are both reported to be highly flammable, so it comes as no surprise that the exhibited fire behavior reflects this.

## 5.4 Fire Radiative Energy

### 5.4.1 Estimating Biomass Consumption

Satellite based fire radiant energy retrievals are widely applied to assess biomass consumed and emissions at regional to global scales [14]. Estimating the amount of biomass consumed during a wildland fire is necessary in order to fully understand the severity of the fire and what post-fire recovery may look like. A proportional relationship between the amount of fire radiative energy released and the biomass consumed has been established for nearly two decades [74]. However, little

research has gone into investigating if variation in fuel moisture, as well as the effects from different species, such as those that are pyrophytic species, change this relationship. Two separate correlations, one stemming from research on pyrophytic fuels [75] and the other on moisture content [14], are provided.

$$BC = (3.025 - 5.32 * W_c)^{-1} * FRE \quad [\text{kg}] \quad (17)$$

where  $W_c$  is the water content (analogous to the MC used in this research), and FRE is the measured fire radiative energy (MJ) [14].

$$BC = 0.248 * FRE + 0.045 \quad [\text{kg}] \quad (18)$$

Equation (18) was developed by burning different species of fuels, both pyrophytic and non-pyrophytic, while varying initial mass. These two empirical equations are plotted along with the experimentally gathered data from this research, shown in Figure 49.

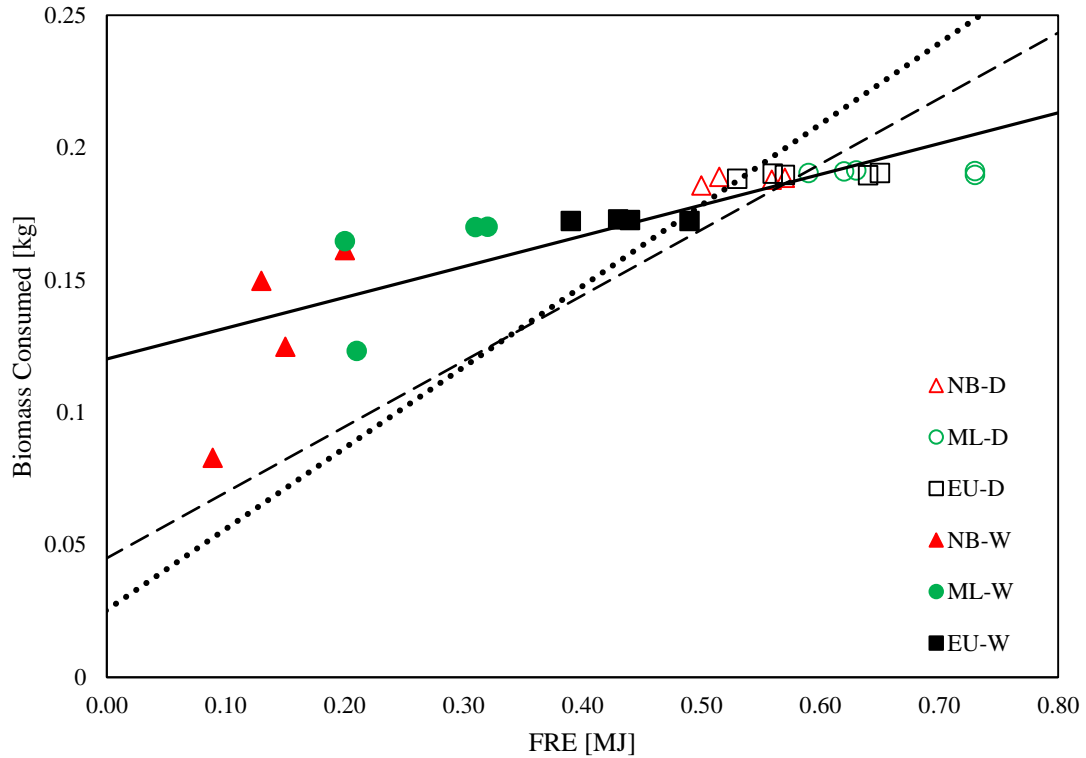


Figure 49: Plot of the measured FRE against the amount of dry biomass consumed. Equation (17) is shown as the dotted black line. Equation (18) is the dashed line. A linear regression, shown as Equation (19) below was fit to the data, shown by the solid line, with an  $R^2=0.71$

Based on the linear regression,

$$BC = 0.1162 * FRE + 0.1202 \quad [\text{kg}] \quad (19)$$

was fitted to the data in Figure 49. This trend being shown still upholds the assumption that the biomass consumed is relatively linearly proportional to the FRE. However, this data suggests that moisture content may have a greater impact on the FRE than previously thought. It is interesting that the different correlations intersect at about the same point, a point on the curve where the experimental fuels were under the driest conditions. As the curve progresses to the left, the moisture content of the fuels increases. The shallower slope indicates that a greater amount of energy is required to consume a relatively small amount of biomass. Ultimately, the assumption that FRE is

linear to the consumption of biomass still appears to be upheld. However, the moisture content of the fuel needs to be accounted for in order to more accurately estimate fuel consumption.

One caveat regarding this conclusion is that large data samples should be collected before more definite conclusions are drawn. This relationship relies on varying biomass to be consumed in order to draw meaningful trends. Because 200 g of unburned fuel was provided for each test, the biomass consumed for each test was relatively the same. A larger array of starting mass needs to be used to solidify this conclusion over scales.

#### 5.4.2 Energy Density

Energy density is used in this paper to describe the amount of stored energy capable of being released during combustion. The calorimetry capabilities of the laboratory allowed for the total energy to be measured, as well as the radiative energy via the overhead radiometer. Dividing these values by the biomass consumed allowed for the total energy density,  $ED_{HRR}$ , and radiative energy density,  $ED_{FRE}$ , to be found. Having these two values allows one to better understand the primary means of heat release during combustion, as well as the influence of moisture and volatile oils on energy output.

Between the three species tested, the difference in total energy density was found to be negligible. This can be seen in the plots shown in Figure 46. This hints to the fact that either these fuels have the same amount of volatile oils in them or that the presence or lack of volatile oils has little significance when burning extremely dry

fuels. However, when moisture is considered, these oils may in fact play a key role in the species' sensitivity to moisture content on combustion. While the amount of total energy decreased for both mountain laurel and northern bayberry when the moisture content was increased to between 0.1 and 0.15, the eucalyptus remained unaffected. This suggests that eucalyptus may actually contain more volatile oils and that these oils might allow the combustion process to easily overcome any heat loss associated with driving the moisture out of the fuel. Unlike the total energy density, the radiative energy density is clearly impacted by the moisture of the fuel. By increasing the MC to between 0.1 and 0.15, the energy density for northern bayberry and mountain laurel decreased by over 50%. The  $ED_{FRE}$  for eucalyptus is also impacted by MC, but by only approximately 20%. This can be seen in the plots shown in Figure 46. These measurements were also visually confirmed by observations. For the higher MC conditions, the flame heights were drastically reduced for mountain laurel and northern bayberry. Due to the reduced flame volume, less energy can be released in the form of radiation. Instead, more energy is released convectively over a longer period of time. This explains why the radiative energy density decreases, but the total energy density is maintained at a relatively constant level.

The radiative fraction,  $\chi_r$ , is used to describe the percentage of heat release due to radiation versus the total energy released. This is easily found by dividing the total energy released by the FRE. Because this radiative measurement is taken overhead in the same IR bands as current remote sensing technologies, applying the radiative fraction to the FRE measurements can provide a coarse but robust estimate of the total

energy released during a wildland without needing to know how much biomass or even area was consumed. Again, the shift in how energy is released under dry fuel conditions versus wet is highlighted by the radiative fraction. Typical values for this are around 12 to 20% [66]. Values from Table 11 reflect this, but only under dry conditions. Higher moisture content levels drop the fraction under 10%. Again, this implies that while the total amount of energy released may be greatly affected by moisture or fuel type, the manner in which the energy released does change. This goes directly against some of the underlying assumptions used during remote sensing.

The fuel combustion factor, CF (kg/MJ), is a metric that describes how much dry biomass is needed to release 1 MJ of FRE when combusted [6], [76]. This is the inverse of the energy density, and was tabulated to allow for comparison with existing data. When the CF is multiplied by the FRE, the total amount of biomass consumed can be estimated. The averaged values of energy density, radiative fraction, and CF are provided in Table 11. Values from literature are also provided for comparison in Table 14. One of the studies gathered data using ground, aerial and satellite-based radiometers during prescribed burns of grassland [52]. Another study did medium scale testing outdoor, using tower-mounted radiometers to image the fuel bed [76]. The third study utilized dozens of small-scale indoor experiments [55], and the fourth study estimated values using a total theoretical combustion energy equation.

Table 14: Literature values for total and radiative energy densities (ED), radiative fraction ( $\chi_r$ ), and fuel combustion factor (CF) to be compared with those shown in Table 11

| <b>Literature</b>              | ED <sub>FRE</sub><br>[MJ/kg] | ED <sub>HRR</sub><br>[MJ/kg] | $\chi_r$  | CF<br>[kg/MJ]                              |
|--------------------------------|------------------------------|------------------------------|---|--|
| [52] Prescribed Burn           | -----                        | -----                        | -----   | 0.261                                      |
| [66] Theoretical Calculation   | -----                        | 20.138                       | $0.17 \pm (0.03)$                                       | -----                                      |
| [77] Medium-Scale Outdoor Test | -----                        | -----                        | -----   | $0.464 \pm (0.018)$<br>$0.368 \pm (0.015)$ |
| [78] Laboratory Study          | 1.29 –<br>4.18               | 17.9 – 22.5                  | $0.121 - 0.124 \pm$<br>$(0.032)$<br>$0.117 \pm (0.024)$ | $0.453 \pm (0.068)$                        |

It appears that literature values best compare to the dry condition test values from this research. This seems reasonable since three of the four studies were either laboratory or theoretically based.

Figure 50 plots the FRE against the total energy released. A linear regression,

$$\text{FRE} = 0.1845 \times Q - 0.3881, \quad [\text{MJ}] \quad (20)$$

was fitted to the data producing Equation (20) with an  $R^2$  of 0.86, which when rearranged, can be used to calculate the total energy produced. In the equation,  $Q$  refers to the total emitted energy. The slope of the line indicates the radiative fraction, roughly 18.5%.

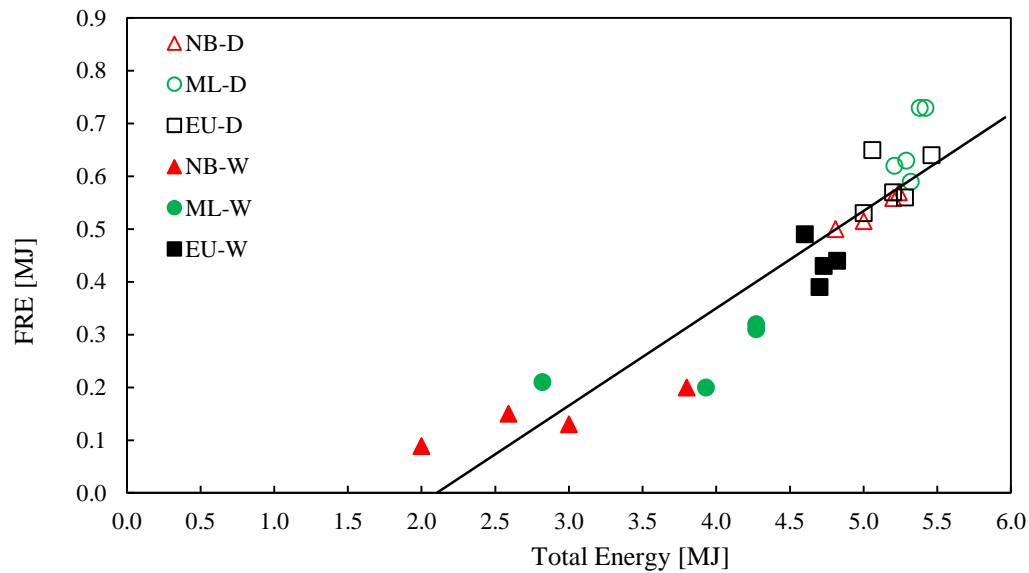


Figure 50: Plot of the radiative energy versus total energy. The radiative fraction can be ascertained from the slope of the applied linear regression.

### 5.4.3 Emission Coefficient

One of the main motivations for gathering FRE data via remote sensing is to ascertain the quantity of combustion products emitted during a wildland fire. In Section 5.2 emission factors, EF (g/kg) based on experimental measurements were presented and discussed. The total amount of a particular effluent can then be determined by using the following equation from [52],

$$E = \text{FRE} * \text{CF} * \text{EF}, \quad [\text{g}] \quad (21)$$

where  $E$  is the total mass of a given effluent, CF is the combustion factor, and EF is the emission factor. However, the use of an intermediate biomass consumption approximation introduces a fairly significant sources of error to the final estimate of total emissions. Instead, the emissions can be directly related to the FRE using the

emission coefficient, EC (g/MJ) [33],[34]. Thus the total emissions can be found using the following:

$$E = \text{FRE} * \text{EC} \quad [\text{g}] \quad (22)$$

The EC values shown in Table 15 were calculated by dividing the total emissions from the different tests by the FRE. Values from literature are provided as comparison ECs. The field measurements are given as range for PM<sub>2.5</sub>, as the lower values represent savanna type ecosystems, with the higher representing boreal forests. The laboratory values were from big sagebrush and ponderosa pine, respectively.

Table 15: Table of emission coefficients, EC, for CO, CO<sub>2</sub>, and PM<sub>2.5</sub>. The ECs were calculated and averaged for all six series of tests. Values from literature are included for comparison.

| <b>Tests</b>                 | EC <sub>CO2</sub><br>[g/MJ]            | EC <sub>CO</sub><br>[MJ/kg]      | EC <sub>PM2.5</sub><br>[MJ/kg]  |
|------------------------------|--|----------------------------------|---------------------------------|
| NB-D                         | 689 ± (20.4)                           | 20.0 ± (1.4)                     | 2.09 ± (0.66)                   |
| ML-D                         | 593 ± (52.6)                           | 14.6 ± (1.6)                     | 1.27 ± (0.35)                   |
| EU-D                         | 642 ± (51.1)                           | 21.2 ± (2.3)                     | 5.16 ± (3.18)                   |
| NB-W                         | 1588 ± (289)                           | 93.5 ± (36.0)                    | 114.0 ± (36.5)                  |
| ML-W                         | 1113 ± (223)                           | 34.8 ± (10.7)                    | 23.2 ± (12.1)                   |
| EU-W                         | 788 ± (81.2)                           | 28.5 ± (2.1)                     | 4.06 ± (0.30)                   |
| <b>Literature</b>            | EC <sub>CO2</sub><br>[g/MJ]            | EC <sub>CO</sub><br>[MJ/kg]      | EC <sub>PM2.5</sub><br>[MJ/kg]  |
| [34] Field Measurements      | -----                                  | -----                            | 2.7 ± (0.3) – 14.4 ± (0.8)      |
| [55] Laboratory Measurements | 813.63 ± (141.03)<br>758.29 ± (175.82) | 28.33 ± (5.49)<br>33.71 ± (1.79) | 13.24 ± (5.88)<br>5.24 ± (4.11) |

While all of the other emission-type factors that have been discussed compared fairly well to existing literature, the calculated emission coefficients compare very well. The table further solidifies the fact that when fuels are completely dried, the emissions are not very different, meaning the volatility of the fuels may not directly influence emissions. However, when moisture content is introduced, there are significant differences. And as previously discussed, this is where the volatility of the species may become important, as those oils may help the leaves overcome the heat losses due to water vaporization. According to the  $EC_{CO_2}$  (Figure 45), the amount of  $CO_2$  actually increases when the fuels have a higher MC. This goes against what would be expected and the total amounts of  $CO_2$  that were directly measured using the gas analyzers. This is because a large amount of  $CO_2$  was still produced during wet tests. However, since the amount of FRE decreased fairly significantly, dividing the total amount of  $CO_2$  by a smaller FRE caused the reported EC to be larger than the dry tests. However, when taking the total energy into consideration, this large increase in the  $EC_{CO_2}$  is not seen.

Plotting the total species production versus the FRE revealed two relationships, one between  $CO_2$  and FRE, and the other between  $PM_{2.5}$  and FRE. Although the carbon monoxide did not produce a usable trend, Figure A1 is still very telling of emissions behavior. The key to this plot is that the overall carbon monoxide production is for the most part constant.

Figure 51 is the plot of the total carbon dioxide versus the FRE. The linear regression applied to the data,

$$E_{CO_2} = 319.44 * FRE + 188.85, \quad [g] \quad (23)$$

fits the data extremely well, with an  $R^2$  of 0.88. This trend shows that as the moisture content decreases, the total  $\text{CO}_2$ , as well as FRE, will increase linearly. Similar to this, Figure 52 provides an exponential fit to the data,

$$E_{\text{PM}_{2.5}} = 19.803e^{-4.576 \cdot \text{FRE}}, \quad [g] \quad (24)$$

describing how that when the moisture content decreases, the amount of PM produced decreases exponentially with increasing FRE ( $R^2 = 0.74$ ).

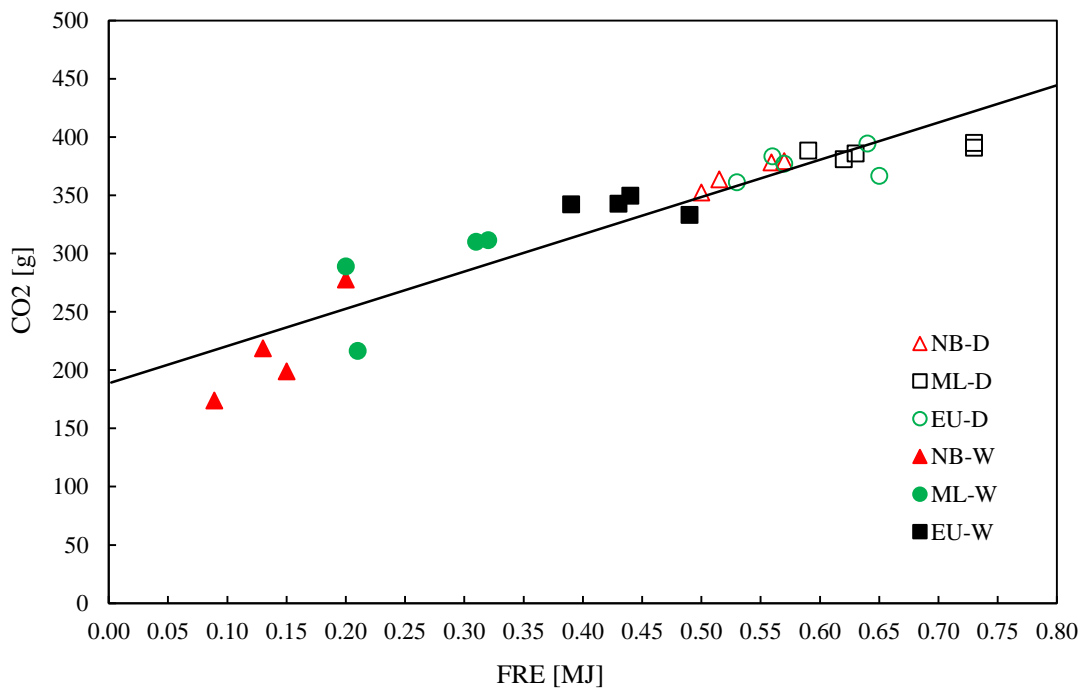


Figure 51: Plot of the total  $\text{CO}_2$  produced against the FRE. A linear regression, Equation (23), with an  $R^2=0.88$  was applied to the data

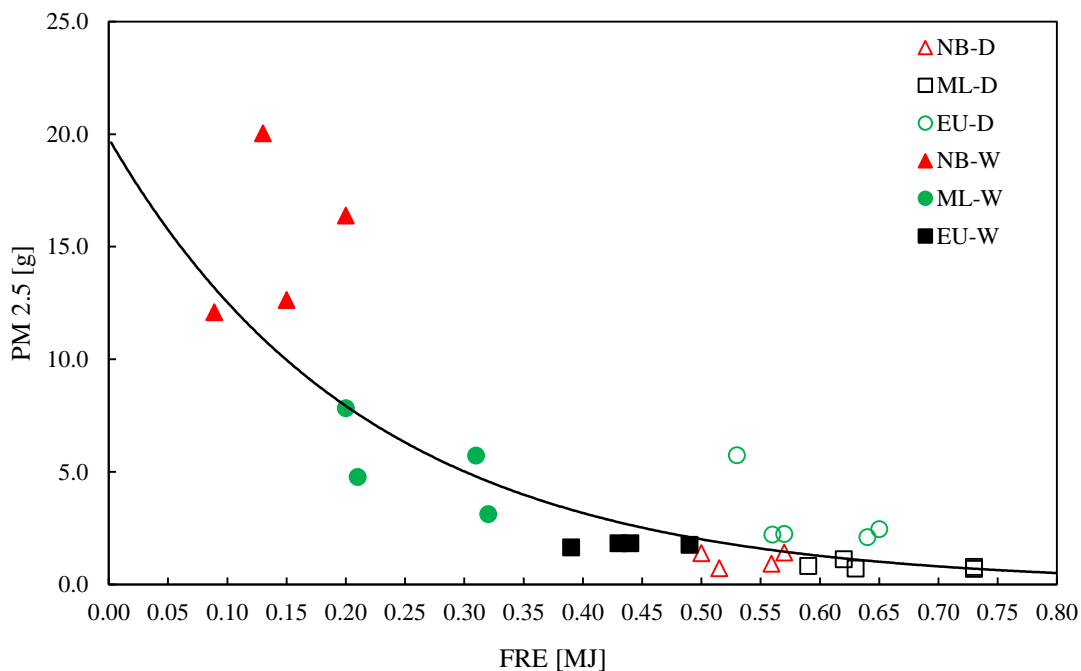


Figure 52: Plot of the total PM<sub>2.5</sub> produced against the FRE. An exponential regression, Equation (23), with an R<sup>2</sup>=0.74 was applied to the data

All three of these plots showing the emissions against the FRE highlight that having a fixed, linear coefficient that relates the FRE to the total emissions produced may not be completely representative of reality. For CO<sub>2</sub> production, this linear assumption may in fact work well. However, if PM<sub>2.5</sub> does behave exponentially, then an integer coefficient could vastly underestimate particulate emissions when at higher moisture levels.

## 6. Conclusion

Twenty-six laboratory experiments were conducted on three species of pyrophytic vegetation, with the goal of understanding the influence of moisture content and volatile oils on emissions and radiant energy release during wildland fires. The basis for this need is that there are certain underlying assumptions regarding radiant energy and emissions that may in fact be impacted by moisture and fuel type. This has vast implications for the field of remote sensing, where wildland fires are tracked via radiant energy measurements and correlations are drawn between these measurements and the mass of fuel consumed and combustion products released.

The primary question tackled in this study was whether moisture content and volatile oils affect biomass consumption and radiant emissions, and if so, whether they do so linearly. This study showed that this relationship is still linear for fully-dried samples, however current relationships do not adequately account for the effects fuel moisture in pyrophytic species. Our findings show that pyrophytic fuels with increased moisture content require more energy to be consumed than in other cases. This occurs despite the presence of volatile oils that were initially thought to encourage combustion.

The experiments revealed that under very dry conditions, there is very little delineation in emissions and energy release for fuels that are hypothesized to have high amounts of volatile compounds. In essence, as long as other parameters like fuel shape, bulk density, orientation, etc. remain consistent, a very dry fuel with no volatile compounds can be expected to release a similar amount of energy as a fuel with a high concentration of these compounds. However, when moisture content begins to

increase, volatile oils certainly do have an impact. At the limited MC levels tested, fuels with higher amounts of volatile substances continued to burn unimpeded with little influence on overall emissions and FRE, regardless of the moisture content. However, those fuels with lower levels of volatile compounds are certainly affected by the presence of water. It is thought the oils provide additional fuel that is easily ignited, allowing the water contained within the foliage to be more quickly drawn out.

The emission factors calculated, as well as the measured FRE, are bulk values, meaning they are not time dependent. Within each group of tests, the burn time could vary fairly substantially. However, as long as the fuel bed burned completely, without changing combustion regimes (flaming to smoldering), the total time of burning was irrelevant. This was because longer burn times meant smaller flames and less heat release. The result is that lower emissions and energy are given off at a single instant, but integrated over the entire span of the test, the total values were equivalent. However, the instantaneous release of emissions and energy is important to consider in regards to remote sensing. If there are concerns over the immediate impact of the emissions on local health and visibility, knowing what regime the fire is burning in (flaming or smoldering) and emissions associated with that regime are important.

The emission factors that were developed, although very fuel specific, can be used to build fuel inventories for various ecosystems. The New Jersey Pine Barrens has areas where mountain laurel is very thick. Understanding how a fire would spread through that region, and the type of emissions and energy emitted during the fire would be extremely useful. California has also experienced many large fires involving

eucalyptus. Having a better understanding of the emissions and energy released will help to address public safety as well as environmental concerns.

In the future, more tests at increased moisture content levels are needed. Based on preliminary tests, a MC of 0.2 was the upper bound for continued flame propagation at laboratory scale with our apparatus. Varying external heating or fuel bed sizes (mass, packing, dimensions, etc.) would be beneficial as well. This would provide more data points that would likely make the biomass consumed versus FRE correlation more robust.

## Appendix A: Supplementary Tables and Figures

Table A1: CE,  $EF_{CO}$ , and  $EF_{PM_{2.5}}$  values calculated using Equations (10), (11), and (12), based on the experimentally determined MCE

| Test | MCE                | CE   | $EF_{CO}$<br>[g/kg] | $EF_{PM_{2.5}}$<br>[g/kg] |
|------|--------------------|------|---------------------|---------------------------|
| NB-D | $0.97 \pm (0.003)$ | 0.96 | 20.8                | 3.58                      |
| ML-D | $0.98 \pm (0.004)$ | 0.96 | 16.2                | 3.26                      |
| EU-D | $0.97 \pm (0.004)$ | 0.95 | 25.2                | 3.87                      |
| NB-W | $0.95 \pm (0.01)$  | 0.93 | 50.5                | 5.59                      |
| ML-W | $0.97 \pm (0.003)$ | 0.95 | 22.7                | 3.70                      |
| EU-W | $0.96 \pm (0.001)$ | 0.95 | 28.6                | 4.10                      |

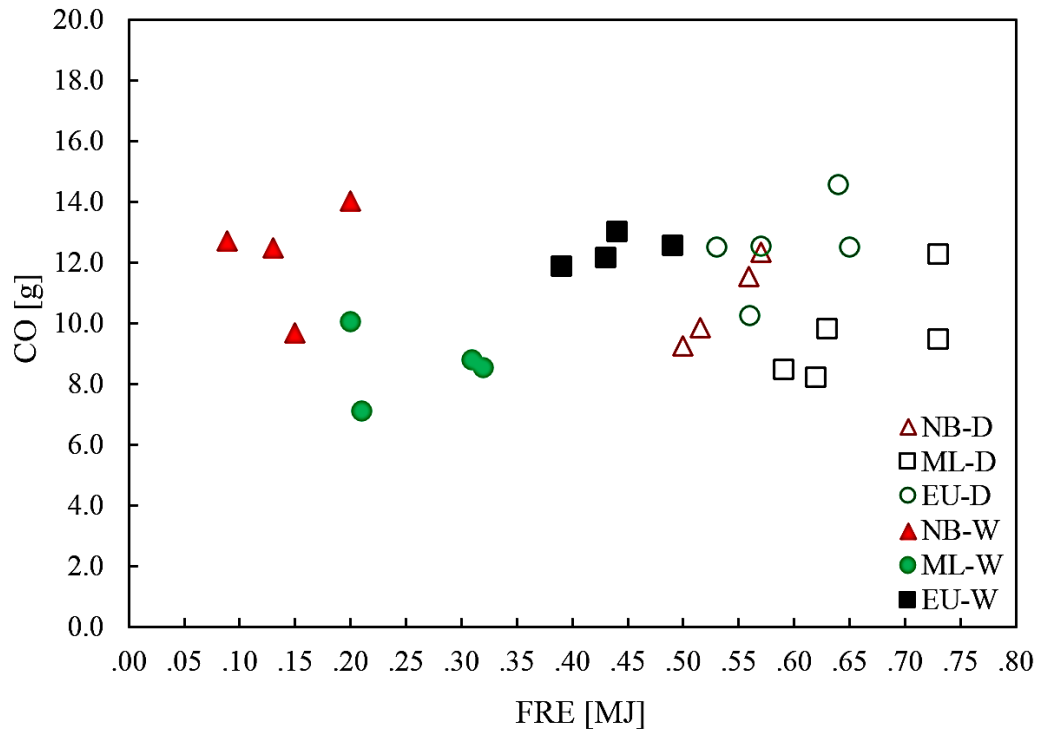


Figure A1: Plot of the total carbon monoxide production versus the FRE.

Table A2: Emission factor, energy density, and MCE values for all of the tests

| <b>Test</b>  | EF <sub>CO2</sub> | EF <sub>CO</sub> | EF <sub>PM2.5</sub> | ED <sub>FRE</sub> | ED <sub>HRR</sub> | MCE   |
|--------------|-------------------|------------------|---------------------|-------------------|-------------------|-------|
|              | [g/kg]            | [g/kg]           | [g/kg]              | [MJ/kg]           | [MJ/kg]           |       |
| <b>NB-D1</b> | 2014              | 61.4             | 5.0                 | 2.98              | 27.7              | 0.970 |
| <b>NB-D2</b> | 1925              | 52.2             | 3.8                 | 2.73              | 26.4              | 0.974 |
| <b>NB-D3</b> | 2012              | 65.5             | 7.6                 | 3.00              | 27.8              | 0.968 |
| <b>NB-D4</b> | 1898              | 50.0             | 7.5                 | 2.70              | 25.9              | 0.974 |
| <b>ML-D1</b> | 2061              | 50.0             | 4.1                 | 3.84              | 28.4              | 0.976 |
| <b>ML-D2</b> | 2067              | 64.3             | 3.6                 | 3.81              | 28.4              | 0.970 |
| <b>ML-D3</b> | 1994              | 43.1             | 5.9                 | 3.24              | 27.3              | 0.979 |
| <b>ML-D4</b> | 2040              | 44.6             | 4.3                 | 3.09              | 28.0              | 0.979 |
| <b>ML-D5</b> | 2017              | 51.4             | 3.7                 | 3.31              | 27.7              | 0.975 |
| <b>EU-D1</b> | 2081              | 77.0             | 11.1                | 3.40              | 28.8              | 0.964 |
| <b>EU-D2</b> | 2016              | 54.0             | 11.7                | 2.97              | 27.8              | 0.974 |
| <b>EU-D3</b> | 1927              | 65.8             | 12.9                | 3.39              | 26.6              | 0.967 |
| <b>EU-D4</b> | 1988              | 66.3             | 11.9                | 2.99              | 27.4              | 0.968 |
| <b>EU-D5</b> | 1919              | 66.6             | 30.5                | 2.84              | 26.5              | 0.966 |
| <b>NB-W1</b> | 1461              | 83.6             | 133.9               | 0.92              | 20.3              | 0.946 |
| <b>NB-W2</b> | 2099              | 153.6            | 145.8               | 1.30              | 29.6              | 0.932 |
| <b>NB-W3</b> | 1594              | 77.7             | 101.2               | 1.27              | 22.1              | 0.954 |
| <b>NB-W4</b> | 1723              | 87.0             | 101.6               | 1.23              | 23.9              | 0.952 |
| <b>ML-W1</b> | 1825              | 51.8             | 33.7                | 1.82              | 25.2              | 0.972 |

|              |      |      |      |      |      |       |
|--------------|------|------|------|------|------|-------|
| <b>ML-W2</b> | 1759 | 57.7 | 38.7 | 1.85 | 24.3 | 0.968 |
| <b>ML-W3</b> | 1831 | 50.4 | 18.4 | 1.90 | 25.2 | 0.973 |
| <b>ML-W4</b> | 1755 | 61.1 | 47.6 | 1.25 | 24.1 | 0.966 |
| <b>EU-W1</b> | 1934 | 73.1 | 10.3 | 2.83 | 26.9 | 0.964 |
| <b>EU-W2</b> | 1983 | 70.5 | 10.6 | 2.48 | 27.4 | 0.966 |
| <b>EU-W3</b> | 2027 | 75.5 | 10.6 | 2.57 | 28.1 | 0.964 |
| <b>EU-W4</b> | 1986 | 69.0 | 9.6  | 2.25 | 27.4 | 0.966 |

Table A3: Emission coefficients, spread rates, flame height, and peak HRR values for all of the tests

| <b>Test</b>  | EC <sub>CO2</sub><br>[g/MJ] | EC <sub>CO</sub><br>[g/MJ] | EC <sub>PM2.5</sub><br>[g/MJ] | Spread<br>Rate<br>[cm/s] | Flame<br>Height<br>[cm] | Peak<br>HRR<br>[kW] |
|--------------|-----------------------------|----------------------------|-------------------------------|--------------------------|-------------------------|---------------------|
| <b>NB-D1</b> | 677                         | 20.6                       | 1.7                           | 0.36                     | 29.4                    | 34.53               |
| <b>NB-D2</b> | 707                         | 19.2                       | 1.4                           | 0.26                     | 24.7                    | 29.17               |
| <b>NB-D3</b> | 666                         | 21.7                       | 2.5                           | 0.25                     | 21.3                    | 24.25               |
| <b>NB-D4</b> | 705                         | 18.6                       | 2.8                           | 0.30                     | 25.5                    | 27.88               |
| <b>ML-D1</b> | 536                         | 13.0                       | 1.1                           | 0.40                     | 35.2                    | 37.76               |
| <b>ML-D2</b> | 541                         | 16.8                       | 0.9                           | 0.45                     | 33.5                    | 38.96               |
| <b>ML-D3</b> | 615                         | 13.3                       | 1.8                           | 0.50                     | 32.2                    | 44.84               |
| <b>ML-D4</b> | 658                         | 14.4                       | 1.4                           | 0.48                     | 30.5                    | 42.15               |
| <b>ML-D5</b> | 613                         | 15.6                       | 1.1                           | 0.40                     | 31.6                    | 35.86               |

|              |      |       |       |      |      |       |
|--------------|------|-------|-------|------|------|-------|
| <b>EU-D1</b> | 617  | 22.8  | 3.3   | 0.42 | 30.7 | 39.83 |
| <b>EU-D2</b> | 685  | 18.3  | 4.0   | 0.39 | 27.3 | 36.82 |
| <b>EU-D3</b> | 564  | 19.3  | 3.8   | 0.72 | 44.5 | 61.96 |
| <b>EU-D4</b> | 662  | 22.1  | 3.9   | 0.76 | 46.1 | 59.52 |
| <b>EU-D5</b> | 682  | 23.7  | 10.8  | 0.68 | 46.8 | 55.01 |
| <b>NB-W1</b> | 1682 | 96.3  | 154.2 | 0.12 | 15.1 | 10.97 |
| <b>NB-W2</b> | 1955 | 143.0 | 135.8 | 0.10 | 18.4 | 10.93 |
| <b>NB-W3</b> | 1327 | 64.7  | 84.2  | 0.12 | 17.2 | 8.85  |
| <b>NB-W4</b> | 1389 | 70.2  | 81.9  | 0.14 | 14.7 | 8.82  |
| <b>ML-W1</b> | 1001 | 28.4  | 21.1  | 0.14 | 13.6 | 17.35 |
| <b>ML-W2</b> | 1032 | 33.8  | 22.7  | 0.09 | 12.0 | 12.47 |
| <b>ML-W3</b> | 974  | 26.8  | 9.8   | 0.18 | 14.6 | 18.67 |
| <b>ML-W4</b> | 1445 | 50.3  | 39.2  | 0.10 | 12.8 | 12.01 |
| <b>EU-W1</b> | 680  | 25.7  | 3.6   | 0.54 | 43.2 | 40.97 |
| <b>EU-W2</b> | 797  | 28.3  | 4.3   | 0.49 | 53.4 | 43.07 |
| <b>EU-W3</b> | 795  | 29.6  | 4.2   | 0.52 | 44.0 | 42.87 |
| <b>EU-W4</b> | 878  | 30.5  | 4.2   | 0.48 | 38.4 | 36.86 |

## Bibliography

- [1] K. L. Clark, N. Skowronski, and M. Gallagher, “The Fire Research Program at the Silas Little Experimental Forest , New Lisbon , New Jersey,” in *USDA Forest Service experimental forests and ranges research for the long term*, New Yor, NY, 2014, pp. 515–534.
- [2] S. J. Husari and K. S. McKelvey, “Fire-Management Policies and Programs,” in *Sierra Nevada Ecosystem Project, Final Report to Congress, Assessments and Scientific Basis for Management Options*, vol. II, Davis, CA, 1996, pp. 1101–1117.
- [3] S. E. Caton, H. S. Raquel, D. J. Gorham, A. Zhou, and M. J. Gollner, “Review of pathways for building re spread in the wildland urban interface part 1: exposure conditions,” *Fire Technol.*, pp. 1–45, 2016.
- [4] P. A. Werth, B. E. Potter, C. B. Clements, M. A. Finney, S. L. Goodrick, M. E. Alexander, M. G. Cruz, A. Jason, and S. S. Mcallister, “Synthesis of Knowledge of Extreme Fire Behavior : Volume I for Fire Managers,” Portland, OR, 2011.
- [5] L. Lentile, Z. Holden, A. M. S. Smith, M. J. Falkowski, A. T. Hudak, P. Morgan, S. A. Lewis, P. E. Gessler, and N. C. Benson, “Remote sensing techniques to assess active fire characteristics and post-fire effects and post-fire effects,” *Int. J. Wildl. Fire*, vol. 15, pp. 319–345, 2006.
- [6] E. Ellicott, E. Vermote, L. Giglio, and G. Roberts, “Estimating biomass consumed from fire using MODIS FRE,” *Geophys. Res. Lett.*, vol. 36, pp. 1–5, 2009.
- [7] S. K. Akagi, R. J. Yokelson, C. Wiedinmyer, M. J. Alvarado, J. S. Reid, T. Karl, and J. D. Crouse, “Emission factors for open and domestic biomass burning for use in atmospheric models,” *Atmos. Chem. Phys.*, vol. 11, pp. 4039–4072, 2011.
- [8] B. J. Harvey, “Human-caused climate change is now a key driver of forest fire activity in the western United States,” *Proc. Natl. Acad. Sci.*, vol. 113, no. 42, pp. 11649–11650, 2016.
- [9] S. P. Urbanski, “Combustion efficiency and emission factors for wildfire-season fires in mixed conifer forests of the northern Rocky Mountains, US,” *Atmos. Chem. Phys.*, vol. 13, no. 14, pp. 7241–7262, 2013.
- [10] P. E. Schwarze, J. Ø, and M. La, “Particulate matter properties and health effects : consistency of epidemiological and toxicological studies,” *Hum. Exp. Toxicol.*, vol. 25, pp. 559–579, 2006.
- [11] E. Ellicott, M. Gollner, N. May, R. Kremens, and W. Schroeder, “Examination of pyrophytic plant combustion and the relationship between fuel moisture , energy released , and emissions .,” p. 3.

- [12] M. A. Possell and T. L. Bell, “The influence of fuel moisture content on the combustion of Eucalyptus foliage,” *Int. J. Wildl. Fire*, no. 22, pp. 343–352, 2013.
- [13] T. H. Fletcher, B. M. Pickett, S. G. Smith, G. S. Spittle, M. M. Woodhouse, and E. Haake, “Effects of Moisture on Ignition Behavior of Moist California Chaparral and Utah Leaves,” *Combust. Sci. Technol.*, vol. 179, pp. 1183–1203, 2007.
- [14] A. M. S. Smith, W. T. Tinkham, D. P. Roy, L. Boschetti, R. L. Kremens, S. S. Kumar, A. M. Sparks, and M. J. Falkowski, “Quantification of fuel moisture effects on biomass consumed derived from fire radiative energy retrievals,” *Geophys. Res. Lett.*, vol. 40, no. 23, pp. 6298–6302, 2013.
- [15] R. T. T. Forman, Ed., *Pine Barrens: Ecosystem and Landscape*. New Brunswick, NJ: Rutgers University Press, 1998.
- [16] R. W. Mutch, “Wildland Fires and Ecosystems--A Hypothesis,” *Ecology*, vol. 51, no. 6, pp. 1046–1051, 1970.
- [17] M. . A. . Arthur, R. D. Paratley, and B. . A. . Blankenship, “Single and Repeated Fires Affect Survival and Regeneration of Woody and Herbaceous Species in an Oak-Pine Forest,” *J. Torrey Bot. Soc.*, vol. 125, no. 3, pp. 225–236, 1998.
- [18] G. Rein, “Smoldering Combustion,” in *SFPE Handbook of Fire Protection Engineering*, 5th ed., NFPA, 2016, pp. 581–603.
- [19] A. L. W. Chen, H. Moosmuller, J. C. Chow, J. G. Watson, R. A. Susott, R. E. Babbitt, C. E. Wold, E. N. Lincoln, and W. M. Hao, “Emissions from Laboratory Combustion of Wildland Fuels: Emission Factors and Source Profiles,” *Environ. Sci. Technol.*, vol. 41, no. 12, pp. 4317–4325, 2007.
- [20] I. R. Burling, R. J. Yokelson, D. W. T. Griffith, T. J. Johnson, P. Veres, J. M. Roberts, C. Warneke, S. P. Urbanski, J. Reardon, D. R. Weise, W. M. Hao, and J. De Gouw, “Laboratory measurements of trace gas emissions from biomass burning of fuel types from the southeastern and southwestern United States,” *Atmos. Chem. Phys.*, vol. 10, no. 22, pp. 11115–11130, 2010.
- [21] T. Lee, A. P. Sullivan, L. Mack, J. L. Jimenez, S. M. Kreidenweis, T. B. Onasch, D. R. Worsnop, W. Malm, C. E. Wold, W. M. Hao, and J. L. Collett, “Chemical Smoke Marker Emissions During Flaming and Smoldering Phases of Laboratory Open Burning of Wildland Fuels,” *Aerosol Sci. Technol.*, vol. 44, no. 9, pp. i–v, 2010.
- [22] R. E. Keane, *Willand fuel fundamentals and Applications*. Springer International Publishing, 2015.
- [23] Interface South, “Quick Guide to Firewise Shrubs,” 2009.
- [24] T. A. Waldrop and P. H. Broseb, “A comparison of fire intensity levels for stand replacement of table mountain pine ( *Pinus pungens* Lamb .),” *For. Ecol.*

- Manage.*, vol. 113, pp. 155–166, 1999.
- [25] D. Close, “Virginia Firescapes.” Communications and Marketing, College of Agriculture and Life Sciences, Virginia Polytechnic Institute and State University, Petersburg, Virginia, 2015.
- [26] H. T. Harvey, H. S. Shellhammer, and R. E. Stecker, *Giant Sequoia Ecology : Fire and Reproduction*, Scientific. Washington, D.C.: U.S. Department of the Interior, National Park Service, 1980.
- [27] J. M. Vose, B. D. Clinto, and W. T. Swank, “Fire, drought, and forest management influences on pine/hardwood exosystems in southern appalachians,” in *12th Conference on Fire and Forest Meteorology*, 1993, pp. 232–238.
- [28] B. Ali, N. A. Al-wabel, S. Shams, A. Ahamad, S. A. Khan, and F. Anwar, “Essential oils used in aromatherapy: A systemic review,” *Asian Pac. J. Trop. Biomed.*, vol. 5, no. 8, pp. 601–611, 2015.
- [29] P. K. Devan and N. V Mahalakshmi, “A study of the performance , emission and combustion characteristics of a compression ignition engine using methyl ester of paradise oil – eucalyptus oil blends,” *Appl. Energy*, vol. 86, no. 5, pp. 675–680, 2009.
- [30] E. Ormeno, B. Cespedes, I. A. Sanchez, A. Velasco-Garcia, J. M. Moreno, C. Fernandez, and V. Baldy, “The relationship between terpenes and flammability of leaf litter,” *For. Ecol. Manage.*, vol. 257, pp. 471–482, 2009.
- [31] K. L. Clark, N. Skowronski, M. Gallagher, and W. Heilman, “Fuel consumption and particulate emissions during fires in the New Jersey Pinelands,” in *Proceedings of 3rd Fire Behavior and Fuels Conference*, 2010.
- [32] R. J. Yokelson, J. G. Goode, D. E. Ward, R. A. Susott, R. E. Babbitt, D. D. Wade, I. Bertschi, D. W. T. Griffith, W. M. Hao, F. Service, K. Air, and N. Carolina, “Emissions of formaldehyde , acetic acid , methanol , and other trace gases from biomass fires in North Carolina measured by airborne Fourier transform infrared spectroscopy were conducted AFrIR data from these,” *J. Geophys. Res.*, vol. 104, pp. 109–125, 1999.
- [33] C. Ichoku and Y. J. Kaufman, “A Method to Derive Smoke Emission Rates From MODIS Fire Radiative Energy Measurements,” *IEEE Trans. Geosci. Remote Sens.*, vol. 43, no. 11, pp. 2636–2649, 2005.
- [34] E. Vermote, E. Ellicott, O. Dubovik, T. Lapyonok, M. Chin, L. Giglio, and G. J. Roberts, “An approach to estimate global biomass burning emissions of organic and black carbon from MODIS fire radiative power,” *J. Geophys. Res.*, vol. 114, no. 18, pp. 1–22, 2009.
- [35] J. Creighton and T. Walkingstick, “The Clean Air Act and Prescribed Fire : What It Means for Arkansas,” *Agriculture and Natural Resources*. University of Arkansas Cooperative Extension Service Printing Services, 2007.

- [36] W. Battye and R. Battye, “Development of Emissions Inventory Methods for Wildland Fire,” Research Triangle Park, North Carolina, 2002.
- [37] J. Peterson and D. E. Ward, “An inventory of particulate matter and air toxic emissions from prescribed fires in the USA for 1989,” 1989.
- [38] N. Birkner and Q. Wang, “How an FTIR Spectrometer Operates.” UC Davis ChemWiki.
- [39] I. R. Burling, R. J. Yokelson, D. W. T. Griffith, T. J. Johnson, P. Veres, J. M. Roberts, C. Warneke, S. P. Urbanski, J. Reardon, D. R. Weise, W. M. Hao, and J. De Gouw, “Laboratory measurements of trace gas emissions from biomass burning of fuel types from the southeastern and southwestern United States,” *Atmos. Chem. Phys.*, vol. 10, no. 22, pp. 11115–11130, 2010.
- [40] J. B. Kinney and R. H. Staley, “Applications of Spectroscopy, Photoacoustic,” *Annu. Rev. Mater. Sci.*, no. 12, pp. 295–321, 1982.
- [41] L. W. a Chen, H. Moosmuller, W. P. Arnott, J. C. Chow, and J. G. Watson, “Particle emissions from laboratory combustion of wildland fuels: In situ optical and mass measurements,” *Geophys. Res. Lett.*, vol. 33, no. 4, p. L04803, 2006.
- [42] S. Thomas and N. S. Haider, “A Study on Basics of a Gas Analyzer,” *Int. J. Adv. Res. Electr. Electron. Instrum. Eng.*, vol. 2, no. 12, pp. 6016–6025, 2013.
- [43] M. D. Wheeler, S. M. Newman, A. J. Orr-ewing, and M. N. R. Ashfold, “Cavity ring-down spectroscopy,” *J. Chem. Soc., Faraday Trans*, vol. 94, no. 3, pp. 337–351, 1998.
- [44] T. Strand, B. Gullett, S. Urbanski, S. O. Neill, B. Potter, O. Aurell, A. Holder, N. Larkin, M. Moore, and M. Rorig, “Grassland and forest understorey biomass emissions from prescribed fires in the southeastern United States – RxCADRE 2012,” *Int. J. Wildl. Fire*, vol. 25, pp. 102–113, 2016.
- [45] L. R. Mazzoleni, B. Zielinska, and H. Moosmüller, “Emissions of levoglucosan, methoxy phenols, and organic acids from prescribed burns, laboratory combustion of wildland fuels, and residential wood combustion,” *Environ. Sci. Technol.*, vol. 41, no. 7, pp. 2115–2122, 2007.
- [46] “Airborne particles: continuous monitoring.” Department of Science, Information Technology and Innovation, Queensland, 2017.
- [47] R. J. Yokelson, I. R. Burling, S. P. Urbanski, E. L. Atlas, K. Adachi, P. R. Buseck, C. Wiedinmyer, S. K. Akagi, D. W. Toohey, and C. E. Wold, “Trace gas and particle emissions from open biomass burning in Mexico,” *Atmos. Chem. Phys.*, vol. 11, pp. 6787–6808, 2011.
- [48] R. J. Yokelson, I. R. Burling, J. B. Gilman, C. Warneke, C. E. Stockwell, J. De Gouw, S. K. Akagi, S. P. Urbanski, P. Veres, J. M. Roberts, W. C. Kuster, J. Reardon, D. W. T. Griffith, T. J. Johnson, S. Hosseini, J. W. Miller, D. R. Cocker, H. Jung, and D. R. Weise, “Coupling field and laboratory

- measurements to estimate the emission factors of identified and unidentified trace gases for prescribed fires,” *Atmos. Chem. Phys.*, vol. 13, no. 1, pp. 89–116, 2013.
- [49] W. M. Jolly, “Sensitivity of a surface fire spread model and associated fire behaviour fuel models to changes in live fuel moisture,” *Int. J. Wildl. Fire*, vol. 16, pp. 503–509, 2007.
- [50] D. C. Lutes and R. E. Keane, “Fuel Load ( FL ) Sampling Method,” 2006.
- [51] R. L. Kremens, A. M. S. Smith, and M. B. Dickinson, “Fire metrology: current and future directions in physics-based methods,” *Fire Ecol.*, vol. 6, no. 1, pp. 13–35, 2010.
- [52] W. Schroeder, E. Ellicott, C. Ichoku, L. Ellison, M. B. Dickinson, R. D. Ottmar, C. Clements, D. Hall, V. Ambrosia, and R. Kremens, “Remote Sensing of Environment Integrated active fire retrievals and biomass burning emissions using complementary near-coincident ground , airborne and spaceborne sensor data,” *Remote Sens. Environ.*, vol. 140, pp. 719–730, 2014.
- [53] B. Leblon, L. Bourgeau-chavez, and J. San-miguel-ayanz, “Use of Remote Sensing in Wildfire Management,” in *Sustainable Development - Authoritative and Leading Edge Content for Environmental Management*, Rijeka, Croatia: InTech, 2012, pp. 55–82.
- [54] “Remote Sensing / Infrared Resources,” 2015.
- [55] P. H. Freeborn, M. J. Wooster, W. M. Hao, C. A. Ryan, B. L. Nordgren, S. P. Baker, and C. Ichoku, “Relationships between energy release, fuel mass loss, and trace gas an aerosol emissions during laboratory biomass fires,” *J. Geophys. Res.*, vol. 113, pp. 1–17, 2008.
- [56] R. T. T. Forman and R. E. Boerner, “Fire Frequency and the Pine Barrens of New Jersey,” *Bull. Torrey Bot. Club*, vol. 108, no. 1, pp. 34–50, 1981.
- [57] B. Foereid, J. Lehmann, C. Wurster, and M. Bird, “Presence of Black Carbon in Soil due to Forest Fire in the New Jersey Pine Barrens,” *J. Earth Sci. Eng.*, vol. 5, pp. 91–97, 2015.
- [58] “MOUNTAIN LAUREL WILDFLOWERS, PINE BARRENS, NEW JERSEY,” 2011. [Online]. Available: <http://njphotographs.photoshelter.com/image/I0000F6CgQ8TPFrc>.
- [59] S. Hiwale, *Sustainable Horticulture in Semiarid Dry Lands*. Springer India, 2015.
- [60] “Catoctin Mountain: Trees and Shrubs,” *National Park Service*. [Online]. Available: <https://www.nps.gov/cato/learn/nature/treesandshrubs.htm>.
- [61] A. Young, “Geisel Library from the Forest,” 2010. [Online]. Available: <https://www.flickr.com/photos/alexyoung34/4501039357/in/photostream/>.
- [62] S. A. Matthews, “Effect of drying temperature on fuel moisture content

- measurements,” *Int. J. Wildl. Fire*, no. 19, pp. 800–802, 2010.
- [63] J. L. Dupuy, J. Marechal, and D. Morvan, “Fires from a cylindrical forest fuel burner : Combustion dynamics and flame properties Fires from a cylindrical forest fuel burner : combustion dynamics and flame properties,” *Combust. Flame*, vol. 135, pp. 65–76, 2003.
- [64] J. P. White, E. D. Link, A. C. Trouve, P. B. Sunderland, and A. W. Marshall, “A general calorimetry framework for measurement of combustion efficiency in a suppressed turbulent line fire.”
- [65] M. L. McNamara, C. W. Noonan, and T. J. Ward, “Correction factor for continuous monitoring of wood smoke fine particulate matter,” *Aerosol Air Quality Res.*, vol. 11, no. 3, pp. 315–322, 2011.
- [66] R. L. Kremens, M. B. Dickinson, and A. S. Bova, “Radiant flux density, energy density and fuel consumption in mixed-oak forest surface fires,” *Int. J. Wildl. Fire*, vol. 21, pp. 722–730, 2012.
- [67] M. J. Gollner, F. A. Williams, and A. S. Rangwala, “Upward flame spread over corrugated cardboard,” *Combust. Flame*, vol. 158, no. 7, pp. 1404–1412, 2011.
- [68] R. C. Kellison, R. Lea, and P. Marsh, “Introduction of Eucalyptus spp. into the United States with Special Emphasis on the Southern United States,” *Int. J. For. Res.*, pp. 1–9, 2013.
- [69] H. R. Delcourt, D. C. West, and P. A. Delcourt, “Forests of the Southeastern United States : Quantitative Maps for Aboveground Woody Biomass , Carbon , and Dominance of Major Tree Taxa,” *Ecology*, vol. 62, no. 4, pp. 879–887, 1981.
- [70] L. Morawska, Z. D. Ristovski, and J. Marsh, “Quantification of Particle Number and Mass Emission Factors from Combustion of Queensland Trees,” *Environ. Sci. Technol.*, vol. 40, no. 18, pp. 5696–5703, 2006.
- [71] T. E. L. Smith, E. L. Young, D. W. T. Griffith, and É. Guérette, “New emission factors for Australian vegetation fires measured using open-path Fourier transform infrared spectroscopy – Part 1 : Methods and Australian temperate forest fires,” *Atmos. Chem. Phys.*, vol. 14, pp. 11313–11333, 2014.
- [72] D. F. Hurst, D. W. T. Griffith, and G. . Cook, “Trace gas emission from biomass burning in Australia,” in *Biomass Burning and Global Change*, 1996, pp. 787–794.
- [73] P. M. Fernandes and M. G. Cruz, “Plant flammability experiments offer limited insight into vegetation – fire dynamics interactions,” *New Phytol.*, no. 194, pp. 606–609, 2012.
- [74] M. J. Wooster, “Small-scale experimental testing of fire radiative energy for quantifying mass combusted in natural vegetation fires,” *Geophys. Res. Lett.*, vol. 29, no. 21, pp. 21–24, 2002.

- [75] E. Ellicott, M. Gollner, N. May, and W. Schroeder, "Examination of pyrophytic plant combustion and the relationship between fuel moisture , energy released , and emissions . • Plants which have adapted to tolerate and even promote fire . pyrophytes ”."
- [76] M. J. Wooster, G. Roberts, G. L. W. Perry, and Y. J. Kaufman, "Retrieval of biomass combustion rates and totals from fire radiative power observations : FRP derivation and calibration relationships between biomass consumption and fire radiative energy release," *J. Geophys. Res.*, vol. 110, pp. 1–24, 2005.
- [77] M. J. Wooster, G. Roberts, G. L. W. Perry, and Y. J. Kaufman, "Retrieval of biomass combustion rates and totals from fire radiative power observations : FRP derivation and calibration relationships between biomass consumption and fire radiative energy release," vol. 110, pp. 1–24, 2005.
- [78] P. H. Freeborn, M. J. Wooster, W. M. Hao, C. A. Ryan, B. L. Nordgren, S. P. Baker, and C. Ichoku, "Relationships between energy release, fuel mass loss, and trace gas an aerosol emissions during laboratory biomass fires," *J. Geophys. Res. Atmos.*, vol. 113, no. 1, pp. 1–17, 2008.